

São Paulo State University
School of Natural Sciences and Engineering

Ruhan Carlos Ponce de Oliveira

**Numerical investigation of fluid flows using
finite element method combined with
characteristic-based split scheme**

Ilha Solteira

2020



UNIVERSIDADE ESTADUAL PAULISTA
“JÚLIO DE MESQUITA FILHO”
Câmpus de Ilha Solteira

MECHANICAL ENGINEERING GRADUATE PROGRAM

Ruhan Carlos Ponce de Oliveira

**Numerical investigation of fluid flows using
finite element method combined with
characteristic-based split scheme**

Dissertation submitted to the School of Natural Sciences and Engineering of the São Paulo State University (UNESP) in partial fulfillment of the requirements for the degree of Master of Sciences in Mechanical Engineering. Field of Thermal Sciences.

Prof. Dra. Elaine Maria Cardoso
Supervisor

Prof. Dr. Emanuel Rocha Woiski
Co-supervisor

Ilha Solteira

2020

FICHA CATALOGRÁFICA

Desenvolvido pelo Serviço Técnico de Biblioteca e Documentação

O48n Oliveira, Ruhan Carlos Ponce de.
Numerical investigation of fluid flows using finite element method combined with characteristic-based split scheme / Ruhan Carlos Ponce de Oliveira. -- Ilha Solteira: [s.n.], 2020
156 f. : il.

Dissertação (mestrado) - Universidade Estadual Paulista. Faculdade de Engenharia de Ilha Solteira. Área de conhecimento: Ciências Térmicas, 2020

Orientador: Elaine Maria Cardoso

Coorientador: Emanuel Rocha Woiski

Inclui bibliografia

1. Characteristic-based split. 2. Python. 3. Element-by-element approach. 4. Parallel programming.

CERTIFICADO DE APROVAÇÃO

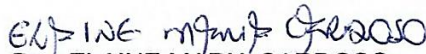
TÍTULO DA DISSERTAÇÃO: Numerical investigation of fluid flows using finite element method combined with characteristic-based split scheme

AUTOR: RUHAN CARLOS PONCE DE OLIVEIRA

ORIENTADORA: ELAINE MARIA CARDOSO

COORIENTADOR: EMANUEL ROCHA WOISKI

Aprovado como parte das exigências para obtenção do Título de Mestre em ENGENHARIA MECÂNICA, área: Ciências Térmicas pela Comissão Examinadora:



Profa. Dra. ELAINE MARIA CARDOSO

Coordenadoria de Curso de Engenharia Aeronáutica / Câmpus Experimental de São João da Boa Vista - UNESP



Prof. Dr. JOAO BATISTA CAMPOS SILVA

Departamento de Engenharia Mecânica / Faculdade de Engenharia de Ilha Solteira - UNESP



Prof. Dr. ROGÉRIO GONÇALVES DOS SANTOS

Departamento de Energia / Universidade Estadual de Campinas - UNICAMP

Ilha Solteira, 23 de março de 2020

Dedicated to: all constituted by my Ohana.

Em um sistema no qual o conhecimento é criminalizado, torno-me traficante de informação.

ACKNOWLEDGEMENTS

I thank God for all the incredible people who have passed or are still in my life, because it was through them, the difficulties faced, that I shaped my personality and grounded who I am today.

To my base on earth, my family, my Robertos, Rosimeiri, Rayane, and Guilhermina, know father, mother, "tato", and even Dona Nega, affectionate names that can not represent the immense love I feel for each of them. These are responsible for building a critical, righteous man who loves what he does.

The second family, my friends, more than that, are all a family that I chose to walk with me. Peterson, Sofia, Lucas, Beatriz and Fernando, names that were daily helping me in this trajectory.

At UNESP, because at this university I found the greatest minds in my small world, who fed my hunger for knowledge, taught me, built me from undergraduate to master's degree. In the lectures given at this university, which I had the privilege of presenting, they strengthened my choice to be a knowledge facilitator, a teacher, a friend, a builder of critical minds both technically and humanly.

Especially from this university, I thank Professor Woiski, who has been with me since my early days of undergraduate. To Professor João Batista Campos Silva, eternal JBC, for the immense mathematical knowledge and, of course, the one who administers and guides me, Professor Elaine.

This study was financed in part by the Coordenação de Aperfeiçoamento de Pessoal de Nível Superior - Brasil (CAPES) - Finance Code 001

Each of these constitute my *Ohana*.

ABSTRACT

This work presents the fundamentals of transport phenomena, some equations of thermodynamic state, the weak formulation of the finite element method applied to the flow and some methods for solving the various fields of analysis of the flow, the turbulence in incompressible and compressible flows, the combustion as reactive flow in a premixed homogeneous mixture. A technical review of several chosen references addressing aspects of the numerical solution, the turbulent model, the turbulence-combustion integration (TCI), the premixture and the choice of fuel and oxidizer, including a table so that you can analyze the complex relationship between all these aspects in publications checked. The main objective of this work is to develop a theoretical and numerical analysis of incompressible and compressible turbulent flows for several domains, developing a framework base to be integrated into the simulation of reactive flows in rocket engines in the future. The equations of continuity, momentum, energy and conservation of chemical species are discretized using the Galerkin finite element method combined with the CBS (Characteristic Based-Split) stabilization scheme, to obtain the fluid dynamic and thermal effects of the process. The combustion process and flame front behavior was only analyzed theoretically and for this, the Flamelet-Progress Variable method was employed. For the modeling of chemical kinetics, the software Cantera® is applied, which uses the GRI-3.0, a mechanism that contains 325 reactions and includes 53 chemical species as a product of combustion. For this, a premixed mixture of methane and oxygen was considered. A framework was developed in Python with the algebraic system resulting from the temporal and spatial discretization of finite elements with the application of Object Oriented Programming (OOP) and local parallelism through process control. For the temporal and transient resolution, the completely explicit Euler scheme was applied, while the Element-by-Element (EbE) method was used to obtain the spatial behavior, based on the Biconjugated Gradient method for solving linear systems, reducing computational costs. and memory space associated with not using sparse arrays. For consistency analysis of the framework, results are presented for several reference flows in the literature.

Keywords: Characteristic-based split. Python. Element-by-Element approach. Parallel programming.

RESUMO

No presente trabalho são apresentados os fundamentos de fenômenos de transporte, algumas equações de estado termodinâmico, a formulação fraca do método dos elementos finitos aplicado à escoamento e alguns métodos para resolução dos diversos campos de análise deste, a turbulência em escoamentos incompressíveis e compressíveis, a combustão como escoamento reativo em uma mistura homogênea pré-misturada. Procede-se então à apresentação em forma resumida de uma revisão técnica de várias referências escolhidas abordando aspectos da solução numérica, do modelo turbulento, da integração turbulência-combustão (TCI), da pré-mistura e da escolha do combustível e comburente, incluindo ainda uma tabela para que possa analisar a complexa relação entre todos esses aspectos nas publicações verificadas. O principal objetivo neste trabalho é desenvolver uma análise teórica e numérica de escoamentos incompressíveis e compressíveis turbulentos para diversos domínios, desenvolvendo um *framework* base para futuramente ser integrado a simulação de escoamentos reativos em motores à foguetes. As equações de continuidade, momentum, energia e conservação de espécies químicas são discretizadas aplicando o método de elementos finitos de Galerkin combinado o esquema de estabilização CBS (Characteristic Based-Split), para se obter os efeitos fluidodinâmicos e térmicos do processo. O processo de combustão e comportamento da frente de chama foi analisado somente teoricamente e para isso foi empregado o método de *Flamelet-Progress Variable*. Para a modelagem da cinética química é aplicado o software Cantera®, o que utiliza o GRI-3.0, mecanismo que contém 325 reações e inclui 53 espécies químicas como produto da combustão. Para isso, foi considerado uma mistura pré-misturada de metano e oxigênio. Um *framework* foi desenvolvido em Python com o sistema algébrico resultante da discretização temporal e espacial de elementos finitos com aplicação de uma Programação Orientada à Objetos (POO) e paralelismo local por meio de controle de processos. Para a resolução temporal e transiente foi aplicado o esquema de Euler completamente explícito, já para a obtenção do comportamento espacial foi empregado o método de Elemento por Elemento (EbE), baseado no método de Gradiente Biconjugado para resolução de sistemas lineares, reduzindo os custos computacionais e espaço de memória associados a não utilização de matrizes esparsas. Para análise de consistência do framework é apresentado resultados para diversos escoamentos de referência da literatura.

Palavras-chave: *Characteristic-based split*. Python. Método elemento por elemento. Programação paralela.

LIST OF FIGURES

Figure 1 – Global rocket launches during the period 2012 to 2017.	18
Figure 2 – Block diagram of the submodule structure for the problem.	25
Figure 3 – Compared small scale analysed by different methodologies.	31
Figure 4 – Scheme of laminar (left) and turbulent (right) premixed flames.	32
Figure 5 – Contours of instantaneous flame boundaries in turbulent flame in a injector.	32
Figure 6 – Scheme of characteristic-Galerkin procedure.	35
Figure 7 – Output numbering default in 8-node hexahedral isoparametric element produced by FVM and FEM.	46
Figure 8 – Output numbering default for 4-node tetrahedral isoparametric ele- ment by Gmsh® mesh generation.	46
Figure 9 – Global scheme of parallelism methodology for CBS method in flow.	47
Figure 10 – Mutual nodes in parallel process.	49
Figure 11 – SpeedUp test for distincting grids.	50
Figure 12 – Scheme of geometry and boundary conditions apply over cavity.	52
Figure 13 – Streamlines behavior for Re 100.	53
Figure 14 – 3D mid-plane centerline distributing for Re 100 for.	54
Figure 15 – Streamlines behavior for Re 400.	55
Figure 16 – 3D mid-plane centerline distributing for Re 400.	56
Figure 17 – Streamlines behavior for Re 1000.	57
Figure 18 – 3D mid-plane centerline distributing for Re 1000.	58
Figure 19 – Representation conditions on thermal-driven cavity.	59
Figure 20 – Validation mid-plane temperature for Re 100.	60
Figure 21 – Validation mid-plane temperature for Re 400.	60
Figure 22 – Temperature distributing for Re 400.	61
Figure 23 – Temperature distribution in the central plane for different Reynolds.	61
Figure 24 – Geometry of square channel.	62
Figure 25 – Boundary conditions for straight channel flow.	62
Figure 26 – Velocity profile in steady state center plane 3D fully developed channel flow for $Re = 100$	64
Figure 27 – Combustion chamber, injector and nozzle geometries.	65
Figure 28 – Release temperature for adiabatic flame.	66
Figure 29 – Release temperature combustion process.	66
Figure 30 – Mass fraction com conditions of flame fixed.	67
Figure 31 – Speed field near the injector.	68
Figure 32 – Profiles for distinct y position near injector.	69

Figure 33 – Main directions and infinitesimal control volume.	93
Figure 34 – Characteristic times of turbulent flows.	120
Figure 35 – Two-dimensional scheme of the function description \mathbb{G} as a function of position.	131

LIST OF TABLES

Table 3 – Machine architecture for computational simulation.	50
Table 4 – Parameters of mesh non-uniformity.	63
Table 5 – Characteristic combustion chamber and injector dimensions.	64
Table 6 – Nominal conditions operating.	65
Table 7 – Parameters of mesh non-uniformity for chamber combustion flow with LES.	68
Table 8 – Table of study of art’s overview.	81
Table 9 – Cubic equations of state.	152
Table 10 – Constants of the Lee-Kesler model.	156

ABBREVIATIONS

FEM	Finite Element Method
CBS	Characteristic-Based Split
EbE	Element by Element method
TCI	Turbulent-Combustion Integration
OOP	Object Oriented Programming
BiCGM	Biconjugate Gradients Method
FVM	Finite Volume Method
FDM	Finite Difference Method
LES	Large Eddy Simulation
CAA	Computational Aeroacoustic
RANS	Reynolds-Averaged Navier-Stokes
AUSM	Advection Upstream Splitting Method
DNS	Direct Numeric Simulation
DES	Detached Eddy Simulation
JST	Jameson-Schmidt-Turkel
FSD	Flame Surface Density
TFM	Thickened Flame Model
LEM	Linear Eddy Model
FDF	Filtered Density Function
TGM	Taylor-Galerkin Method
GGM	Generalized Galerkin Method
CGM	Galerkin Characteristic Method
RK	Redlich-Kwong
RKS	Redlich-Kwong-Soave
PR	Peng-Robinson
LK	Lee-Kesler
vdW	van der Waals

SYMBOLS

ρ	Density	$[kg/m^3]$
u_i	Three dimensional velocity field	$[m/s]$
p	Pressure	$[Pa]$
T	Temperature	$[K]$
δ_{ij}	Kronecker delta	$[-]$
Y_k	Mass fractions	$[-]$
N	Number of species in the reacting mixture	$[un]$
$f_{k,j}$	Volume force acting on species k in direction j	$[N/kg]$
μ	Dynamic viscosity	$[kg/(m \cdot s)]$
D_k	Diffusion coefficient of species k (mass diffusivity)	$[m^2/s]$
$V_{k,i}$	i-component of the diffusion velocity V_k of species k	$[m/s]$
$\dot{\omega}_k$	Reaction rate of species k	$[kg/(m^3 \cdot s)]$
τ_{ij}	Shear stress	$[Pa]$
$\dot{\omega}_T$	Heat release due to combustion	$[W/m^3]$
$D_{T,i}$	Thermal diffusion coefficient	$[kg/(m \cdot s)]$
R	Gas constant	$[J/(kg \cdot K)]$
l_p	Planck-mean absorption length	$[m]$
σ_{SB}	Stefan-Boltzmann constant	$[W/(m^2 \cdot K^4)]$
ϵ_{em}	Surface Emissivity	$[-]$
ϵ_{abs}	Surface Absorption	$[-]$
L	Surface thickness	$[m]$
$\Delta h_{f,k}^0$	Enthalpy of formation species k	$[J/kg]$
V_i^k	Correction velocity i-component	$[m/s]$
S_{ij}	Mean stress tensor	$[Pa]$
\mathbf{S}_v	rate of volumetric deformation	$[Pa]$
\mathbf{S}^d	rate of deviant deformation	$[Pa]$
ν_t	Kinematic viscosity turbulent	$[m^2/s]$
β	Artificial compressibility	$[-]$
\square^{sgs}	Subgrid closure model	$[-]$
$\tilde{\square}$	Filtered variable	$[-]$
\square'	Fluctuating component of variable	$[-]$
W_k	Molar weight	$[g/mol]$
Sc_{kt}	Turbulent Schmidt number for species k	$[-]$
$U_{s,i}$	Effect of shock in i-th Momentum component	$[kg/(m^2 \cdot s^2)]$
$\hat{\square}$	Nodal values	$[-]$
$\bar{\Delta}$	Characteristic length of the mesh	$[m]$

\square_u	Unburned variable	$[-]$
T_a	Adiabatic Temperature	$[K]$
κ	Volumetric viscosity coefficient	$[Pa \cdot s]$

CONTENTS

1	INTRODUCTION	17
1.1	Study of the Art	19
2	METHODOLOGY	25
2.1	Mathematical Model	26
3	NUMERICAL MODEL	35
3.1	General CBS	35
3.2	Temporal Discretization of the Momentum Equation	37
3.3	Space Discretization	38
3.4	Artificial Compression in Transient Problems	41
4	PROGRAMMING ASPECT	44
5	CONSISTENCY ANALYSIS	49
5.1	SpeedUp Test	49
5.2	Lid-driven Cavity Flow	51
5.3	Thermal Lid-driven Cavity	59
5.4	Flow in Channel of Square Cross Section	62
5.5	Combustion Chamber	64
5.5.1	Combustion	65
5.5.2	Cold Flow in a Chamber Combustion	67
6	CONCLUSION	70
	REFERENCES	72
	A – STUDY OF ART’S OVERVIEW	81
	B – GENERIC MATHEMATICAL MODEL	91
	C – TRANSPORT EQUATION AND REYNOLDS DECOM- POSITION	117
	D – TURBULENT COMPRESSIBLE FLOW	121
	E – REACTIVE FLOWS - COMBUSTION	129
	F – MATHEMATICAL DETAILING	137
	G – THERMODYNAMIC STATE EQUATIONS	151

1 INTRODUCTION

From Tehran (in November 1943), passing through Yalta (February 1945) and arriving in Potsdam (July 1945), the three great allies (United States, Great Britain and Soviet Union) poured in the revenue of a weak alliance almost exclusively sustained in the fight against Hitler. It concealed, however, the emergence of the antagonism that would lead international society to other systemic parameters [...] SARAIVA, LESSA, and ROCHA, 2007.

According to SARAIVA, LESSA, and ROCHA (2007), the antagonism displayed by the two superpowers that emerged after the Second World War (1939 - 1945), the Soviet Union and the United States, due to the confrontation of ideologies, generated tensions in the international globe relations . In this period, known as the Cold War, also has emerged a great advance in the technological field. Marked mainly by the arms and aerospace races, the production of new technologies and investments in advanced studies have become the hallmarks of the hegemony of the superpowers. As a consequence, aerospace research centers have emerged in several parts of the world, distributed in ten countries/consortia¹: The United States, the USSR², the European Aerospace Consortium, Japan, China, India, Israel, Brazil, and North Korea I.-S. CHANG, 2000.

In the Cold War on October 4, 1957 the man reached the space for the first time, by means of an artificial satellite placed in orbit by the USSR, with the Sputnik launch vehicle (SL-1) using liquid propellant as fuel ANDERSON JR, 2015.

I.-S. CHANG (2000) conducted a study about the World launches after the Sputnik feat, from 1957 to 1998. The largest number of releases were by the United States and the USSR, with 1125 and 2560 launches, and success rates of 87.5% and 93.5%, respectively. The other countries with the most significant aerospace technology were the European Consortium and Japan with 107 and 52 launches and success rates of 89.9% and 86.7%, respectively.

The aeronautics and aerospace needs of that period brought the technological advances in other sectors such as communication, geolocation, electhronics, material science and many others. There has been a growth in the number of space agencies: DLR³ (Germany), ESA⁴ (Europe), UK Space (UK), Roscosmos (URSS) and NASA⁵ (United States) ISECG, 2013.

Figure 1 depicts the launches between 2012 and 2017. Russia, the United States and China together hold about 80% of them.

¹ Alliances for development of joint research in aerospace.

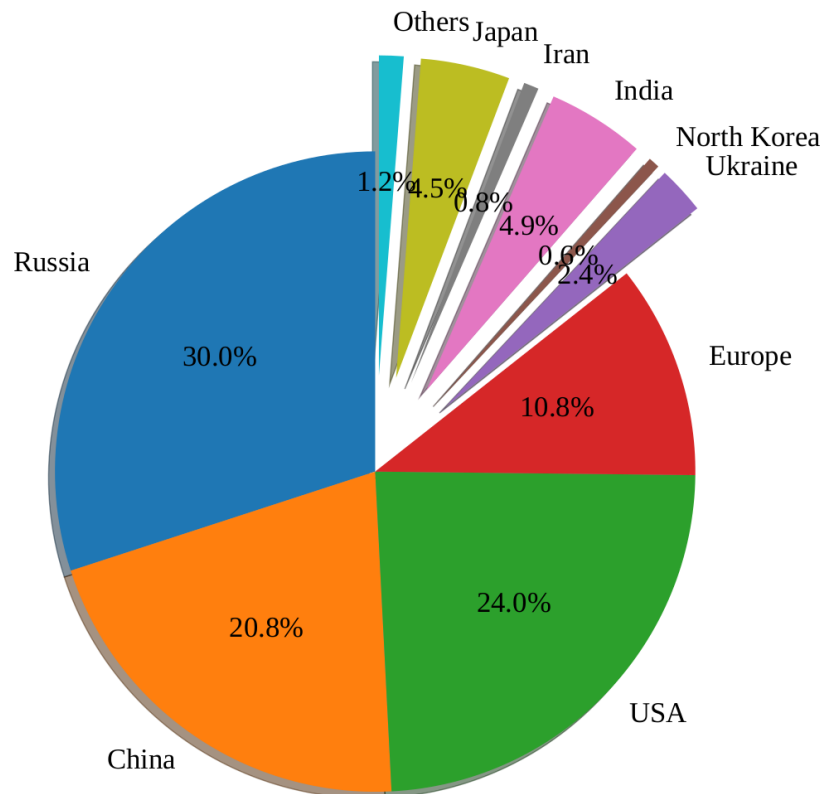
² Union of Soviet Socialist Republics

³ Deutsches Zentrum für Luft-und Raumfahrt (DRL)

⁴ European Space Agency (ESA)

⁵ National Aeronautics and Space Administration (NASA)

Figure 1 – Global rocket launches during the period 2012 to 2017.



Source – Prepared by the author with data presented by HUOT (2017).

In the national scenario, the Brazilian Space Agency (AEB) is responsible for the programs and development of technology in the aerospace sector, along other agencies related to national security. Following the relationship between Brazil and China, the Agreement for the Expansion of Sino-Brazilian Research, in the Aerospace Segment⁶, was signed with intention of increasing the Brazilian performance in the sector. Due to its strategic position, the national territory hosts most of the world's satellite launches, with savings of 20% or more in launch cost⁷.

During 2016, Brazil promoted the release of the VSB-30 V11 launch vehicle, product of joint efforts among the Brazilian Air Force (FAB), Department of Aerospace Science and Technology (DCTA) and AEB⁸. In the same year, the same vehicle was launched, but using a propellant developed by DCTA. The launches took place at the Woomera Launch Center - WIR (Woomera Instrumented Range), located in Australia⁹, what shows

⁶ <http://www.aeb.gov.br/acordo-ampliaca-esquisa-sino-Brazilian-in-segment-aerospace/>

⁷ <https://www.cnbc.com/2018/02/23/rocket-builders-looking-to-brazil-for-equatorial-launch-site.html>

⁸ <http://www.fab.mil.br/noticias/mostra/28667/ESPA%C3%87O%20-%20Foguete%20suborbital%20%C3%A9%20lan%C3%A7ado%20pela%20FAB%20no%20Maranh%C3%A3o>

⁹ <http://www.fab.mil.br/noticias/mostra/25901/ESPA%C3%87O%20-%20Foguete%20com%20propulsor%20desenvolvido%20pelo%20DCTA%20%C3%A9%20lan%C3%A7ado%20na%20Austr%C3%A1lia>

the development of Brazil in this sector.

With respect to the subsystems of a launch vehicle, I.-S. CHANG, 2000 studied the failure frequency with respect to each component. The propulsion subsystem accounted for 62.3% of launch failures in the world between 1983 and 1988, 50% for the United States, 71.4% for USSR and 83.3% for Europe. In Brazil it is even more alarming, because the propulsion system was responsible for 100% of the failures that occurred in the launches. In this way, it seems necessary a continuous advancement in technologies and studies applied to the aerospace propulsion subsystem, in order to develop methods of prediction and simulations to identify possible failures long before they occur.

SUTTON and BIBLARZ (2001), studying the propulsion of aerospace vehicles, stated the high complexity of that subsystem requiring careful design and large production costs. Within the propulsion system, the combustion chamber, which is responsible for the production of the gases for thrust to accomplish the mission of the vehicle, still presents challenges in the modeling of the flow through it mainly due to three factors: combustion details WANG, 2016; interference of the turbulence on the process MAESTRO et al., 2016; and, representation of the real conditions of the atmosphere CHEN and MATHIAS, 2002 due to the high altitudes reached by the prototypes.

In this research project the main objective is to develop a numerical analysis of a transient compressible flow with turbulent combustion of homogeneous mixture in a convergent-divergent nozzle with known geometry. FEM¹⁰ with CBS¹¹ scheme for stabilization, a suitable thermo-chemical model for a premixed combustion and a novel LES¹² subgrid closure model will be employed, coded in a modular way. The integration turbulent-combustion will be characterized by the Flamelet/Progress Variable, as well as the analysis of the behavior of the flame front, as presented by LIANG, FISHER, and Y. M. CHANG (1986).

1.1 Study of the Art

As for the discretization method

In the most of the references analyzed, the FVM¹³ has been used with the help of some softwares such as Ansys CFX® MÜHLBAUER et al., 2012, FLUENT® CAO et al., 2015, FIRE® code DEKENA and PETERS, 1999, AVBP® MARTIN et al., 2006, NTMIX-3D® BOGER et al., 1998. A few works have used the FDM¹⁴ such as MARTIN et al. (2006) and there LES/CAA¹⁵ coupling analysis with the existing AVSP® code. Must be mentioned the theoretical work of OEFELEIN (2015) and ALBAYRAK and POLIFKE

¹⁰ Finite Element Method

¹¹ Characteristic-Based Split

¹² Large Eddy Simulation

¹³ Finite Volume Method

¹⁴ Finite Difference Method

¹⁵ Computational Aeroacoustic

(2017), the latter for laminar flow. Note that it has not being possible to determine the kind of numerical solution method presented by Y. LIU et al. (2012), HUO and YANG (2017) and A. N. LIPATNIKOV et al. (2017).

Among the several methods of discretization, is extremely difficult to identify the most suitable method. In the books by CHUNG (2002) and HIRSCH (1994), for example, although they use all three methods for the same combustion problem, there is no comparison between them under the same conditions, especially, for problems with available experimental data in the literature.

It has been verified that the FVM was a preferred initial choice for solving flow problems due to its robust way to deal with the inherent non-linearities present in the Navier-Stokes equations, which were not easily solved by using the classical Galerkin approach of the FEM due to stability problems, and, therefore, FEM was initially applied only to conductive problems. With respect to the FDM, its reduced utilization is associated with its difficult application to situations with complex geometries and with unstructured meshes.

One of the most contrasting differences between the FVM and FEM is the conservativeness property. Considered a good property to respect when solving flow problems, the FVM includes this property by construction, both locally and globally FERZIGER and PERIĆ, 2002. On the contrary, the FEM yields only global conservation of the equations – the local conservation is not guaranteed when considering the internal product of the equation by the weight function CONNOR and BREBBIA, 1976.

Also FEM uses the weak formulation of the equations then yielding the disappearance of the derivatives of higher order during the integration process, leading to an easier modeling and, consequently, programming, if compared with the FVM, which uses the strong formulation of the conservation equations.

Therefore, FEM was assessed as more suitable for the analysis of the problem proposed in this scope. However, due to the instabilities caused by the pure Galerkin method, it is necessary to employ a proper stabilizer method, and the CBS or Taylor-Galerkin method has been found to be adequate. Moreover, due to the robustness of the CBS method, it can be applied for both incompressible and compressible problems with the same general formulation ZIENKIEWICZ, TAYLOR, and NITHIARASU, 2014.

As for the turbulence model

Although most of the references analyzed employed the LES methodology with the kinetic energy subgrid (SGS) closure method, SCHLIMPERT et al. (2016) and MÜHLBAUER et al. (2012) used the RANS¹⁶ methodology, the last with the closing model $\kappa - \epsilon$. In the work of SCHLIMPERT et al. (2016), the low-dissipation AUSM¹⁷

¹⁶ Reynolds-averaged Navier–Stokes

¹⁷ Advection Upstream Splitting Method

was applied to the spatial discretization of the advective terms and for discretization in time a third-order Runge-Kutta scheme. The DNS¹⁸ method was selected by BOGER et al. (1998), A. N. LIPATNIKOV et al. (2017) and Y. LIU et al. (2012). In particular DOMINGO et al. (2005) compared results between DNS and LES, whereas POTTURI, PATTON, and EDWARDS (2017) used the hybrid model of LES/RANS with the least squares closure model NAGHIAN, LASHKARBOLOK, and JABBARI, 2017.

Since the accuracy of a method is related to its ability to discretize the behavior of the smaller, or Komolgorov, scales, the different methodologies for turbulence analysis are distinguished by this aspect. Therefore, the methodologies may be classified in descending order of accuracy by DNS, LES and RANS.

However, the discretization ability of the smaller scales is directly linked to the computational cost, resulting in the non-applicability of the DNS methodology for the present work. From the analyzed works that apply DNS, as a way to counteract the excessive computational cost they have employed some simplifications for the problem, such as isotropic turbulence and homogeneity BOGER et al., 1998 or statistically planar turbulence Y. LIU et al., 2012; A. N. LIPATNIKOV et al., 2017.

An alternative to DNS is the LES methodology, which obtains the average flow through an analysis of both the small and large vortices, evaluating with some precision the energy contained in the flow. In this methodology the small scales are not simulated as in the DNS. Once, they influence the rest of the flow, this influence occurs in a passive way, such that the larger vortices usually contain greater energy values, which increase their importance in the simulation. In short, the success of the LES methodology is obtained by the fact that the energy and other information of the flow travels from the direction of the largest to the smallest vortex scales, a phenomenon known as the energy cascade, but almost never in the opposite direction DAVIDSON, 2004.

The RANS model provides results for the average flows with engineering precision employing moderate cost of computing. As a comparison, it is about 1% to 10% of the cost employed in LES, the latter requiring a much more refined mesh. However, for anisotropic vortex flow situations, the mean quantities are less satisfactory with RANS. In addition, LES provides instability in the data that is indispensable for modeling a chaotic flow as is the case of real turbulence, but cannot be used for symmetric flows in space FRÖHLICH and TERZI, 2008.

Considering the strengths of RANS and LES methodologies, it was natural for some authors to combine both to ally the computational speed of one with the applicability and reliability of the other through hybrid models POTTURI, PATTON, and EDWARDS, 2017 as it is the case of THAKUR et al. (2012) with DES¹⁹, a hybrid model used in FVM for axissymmetric flow. NGUYEN, POPOV, and SIRIGNANO (2017) used the same

¹⁸ Direct Numerical Simulation

¹⁹ Detached Eddy Simulation

DES, also for axisymmetric flows with chemical multispecies, but with FDM associated to a variation of the classical JST²⁰ method.

Finally, the applicability of each methodology must be consistent with the level of accuracy and computational cost that should be previously established for each problem. With this in mind, and taking into account the strengths presented, the LES methodology will be used in the present work. In addition, both LES and RANS, because of the application of the filters and averages to the modeling, demand some way of closing the system of equations. The novel closure that will be proposed in the present work is a variation of the subgrid scale model involving the concept of turbulent kinetic energy OEFELEIN, 2015; FOSTER and MILLER, 2015; MAESTRO et al., 2016.

As for the turbulence-chemical integration

Due to its simplicity and ease of implementation, the G-Equation model that detects the flame front was employed in the great majority of works analyzed SCHLIMPERT et al., 2016; NOGENMYR et al., 2008; ALBAYRAK and POLIFKE, 2017; DEKENA and PETERS, 1999; LAGENESTE and PITSCH, 2002. The works of A. N. LIPATNIKOV et al. (2017), BOGER et al. (1998), DOMINGO et al. (2005) employ the Flame Surface Density (FSD) model. The Thickened Flame model MARTIN et al., 2006; ANGELBERGER, VEYNANTE, and EGOLFOPOULOS, 2000. MERK et al. (2018) used Linear Eddy Model (LEM), whereas FLEMMING, SADIKI, and JANICKA (2007) worked with Flamelet Model; Steady Flamelet Model BUI, SCHRÖDER, and MEINKE, 2008; MÜHLBAUER et al. (2012) and CECERE et al. (2011) applied Flamelet/Progress Variable. OEFELEIN (2015) compared the models Laminar Flamelet Model LADEINDE and LOU, 2017, Transported Probability Density Function FERRARO, GE, and PFITZNER, 2015 and LEM BILGER, 2011, whereas HUO and YANG (2017) compared Flamelet Model and Flamelet/Progress Variable and ZONG, RIBERT, and YANG (2008) compared Conserved Scalar Approach and Direct-closure Approach.

Despite the progress in turbulent combustion, a truly predictive, universal, multi-regime and multi-application model is still undefined. The main models analyzed in this literature review are the Flamelet models – including Steady Flamelet Model, Flamelet/Progress Variable and Unsteady Flamelet/Progress Variable Model PITSCH and IHME, 2005 – LEM and Filtered Density Function (FDF) Y. LIU et al., 2012, all them employing the LES methodology.

The Flamelet models, which are limited by the reduction in the number of chemical species, do not produce good results for flows of pure substances. Still, the simplest Flamelet model is the Steady Flamelet, in which the turbulent combustion can be characterized by the chemical kinetics of some reaction GLASSMAN and YETTER, 2008. To circumvent

²⁰ Jameson–Schmidt–Turchiello

such limitations of the model, one has the most robust model of Flamelet/Progress Variable, to be discussed in the present work.

For LEM, molecular diffusion is considered directly along some directions within the flow. However the strong multidimensional nature of the flames and the turbulent convection of the sub-grid scale acting on the level-set function of mapping of the flame front, which limits the characterization of the flame, do not easily justify that procedure FOSTER and MILLER, 2015.

In the FDF model with LES the source terms of the level-set transport equation are naturally closed, which limits the performance due to modeling difficulties of the filtered conditional diffusion, or the filtered conditional dissipation in the reactive flows. In fact, there may be substantial differences in behavior within different places in the domain, between regions of high and low variance of turbulent small scale closure FOSTER and MILLER, 2015.

In the Flamelet models, the LES transport equations for the fraction of the filtered mixture and/or progress variables can converge to their exact equations; however, combustion will always be dictated by a suitable flamelet library, not by the solution of the detailed coupled chemistry. As a way to bypass such limitation some authors have used the opensource GRI 3.0 (also called GRI-Mech 3.0) library MAESTRO et al., 2016; HUO and YANG, 2017; ANGELBERGER, VEYNANTE, and EGOLFOPOULOS, 2000, that aggregates 325 reactions and 53 chemical species²¹ for methane-oxygen combustion.

For this work, the Flamelet/Progress Variable model will be used in conjunction with Cantera® – a Python developed library – that includes GRI 3.0.

As for the premixed mixture

Most references used homogeneous premixed mixture prior to combustion. However, non-premixed combustion was also detected in the works by OEFLEIN (2015), MÜHLBAUER et al. (2012), HUO and YANG (2017), FLEMMING, SADIKI, and JANICKA (2007), and BUI, SCHRÖDER, and MEINKE (2008). Finally, DEKENA and PETERS (1999) and A. N. LIPATNIKOV et al. (2017) worked with partially premixed blends.

As for fuel and oxidizer

Most of the references used methane as fuel and molecular oxygen as oxidizer. POTTURI, PATTON, and EDWARDS (2017), MARTIN et al. (2006), ANGELBERGER, VEYNANTE, and EGOLFOPOULOS (2000) and Y. LIU et al. (2012) worked with the propane/oxygen ratio. CAO et al. (2015) and HUO and YANG (2017) applied hydrogen to molecular oxygen. Some laborers chose more elaborate mixtures of fuel, such as the

²¹ <http://combustion.berkeley.edu/gri-mech/version30/text30.html>

hydrogen-nitrogen mixture with molecular oxygen in BUI, SCHRÖDER, and MEINKE (2008) and FLEMMING, SADIKI, and JANICKA (2007) and the mixture of dilute nitrogen in methane-hydrogen with application of oxygen as oxidizer MÜHLBAUER et al. (2012). Finally, DEKENA and PETERS (1999) analyzed the behavior of gasoline-air mixture during the combustion process.

As for the code development

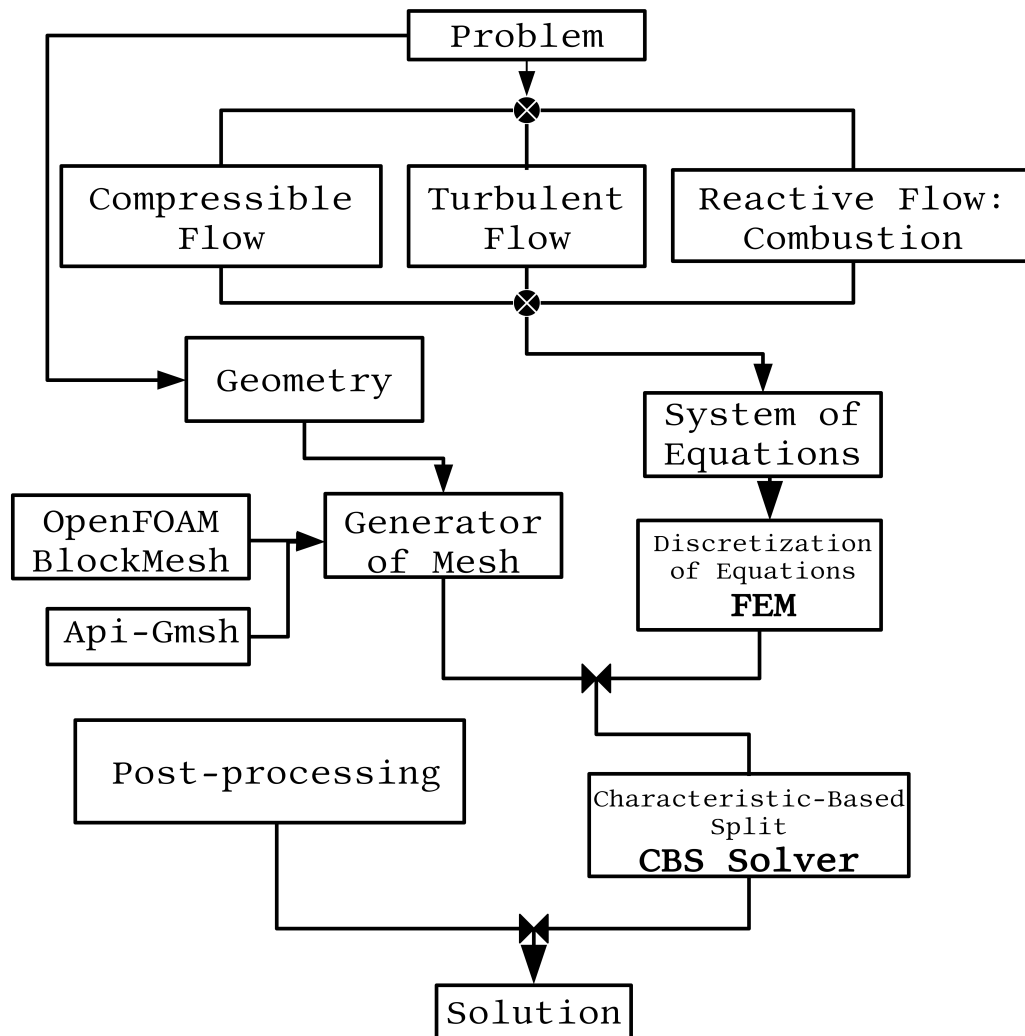
In all the references analyzed, even those in which the use of some kind of commercial or open source software in the various aspects of transport phenomena was informed, the authors omitted or somehow trivialized the solution methodology employed, as well as the choice of some important physical parameters involved directly in solving the specific problem, making it impossible to further analyze in detail or even to reconstruct their procedures.

A complete schematic analysis of these references can be seen in Appendix A.

2 METHODOLOGY

The analysis and modeling of highly complex problems require their breakdown into a set of submodules, which although interconnected, can be modified or suppressed according to the hypotheses underlying each problem. A block diagram with submodules can be seen in Figure 2.

Figure 2 – Block diagram of the submodule structure for the problem.



Source – Prepared by the author.

From problem statements, in a specific geometrical situation, the system of equations to be solved was produced. Linked directly to the flow and geometry, the boundary and initial conditions were set.

After establishing the system of equations and the conditions of the problem, the discretization was carried out applying FEM. The FEM and the programming language Python were proposed from the start, due to its ease of programming coupled with the

modern methods of stabilization of the Galerkin method, such as the one used in this project, CBS, with which better results are obtained when compared to other methods of stabilization ZIENKIEWICZ, TAYLOR, and NITHIARASU, 2014.

As for the mesh generation, the BlockMesh *toolbox* of the software OpenFOAM was applied, due to its practicability and efficiency for simple geometries. In order to compare different mesh generators and to verify the robustness of the developed framework, Gmsh was also used for the generation of both structured and unstructured meshes.

As for the post-processing, the open-source visualization software Paraview was chosen, since it provides practicality in the manipulation of complex geometries and it has large amounts of tools for better analysis of the results.

In the following sections, all the methods and strategies used to solve the problem will be presented in detail, concerning the main global aspects.

2.1 Mathematical Model

The proposed problem is the characterization of the flame front and the effects generated by a turbulent compressible premixed combustion. For this, after the definition of the geometry and the coordinate system, the system of transport equations to be solved was obtained.

For the LES methodology, a spatial filter of Favré was applied and a model of subgrid closure was developed. For the subgrid terms an isotropic flow was assumed.

For the combustion modeling, a premixed mixture of GCH_4/GO_2 was selected, and the flamelet/progress variable method was used to characterize the flame front. Following, the system of transport equations as well as the other hypotheses employed in the present work are set POINSOT and VEYNANTE, 2005:

$$\frac{\partial \rho}{\partial t} + \frac{\partial(\rho u_i)}{\partial x_i} = 0 \quad (1)$$

$$\frac{\partial(\rho u_i)}{\partial t} + \frac{\partial}{\partial x_j} [\rho u_i u_j + p \delta_{ij} - \tau_{ij}] - \rho g_i = \rho \sum_{k=1}^N Y_k f_{k,i} \quad (2)$$

$$\frac{\partial(\rho Y_k)}{\partial t} + \frac{\partial}{\partial x_i} [(\rho u_i + \rho V_{k,i}) Y_k] = \dot{\omega}_k, \quad \text{for } k = 1, \dots, N$$

by definition:

$$\sum_{k=1}^N Y_k V_{k,i} = 0 \quad \text{and} \quad \sum_{k=1}^N \dot{\omega}_k = 0$$

From these definitions, one has to locally analyze the mass fraction Y_k for each specie, since mass is not globally preserved. With this, there is a need to add a correction

speed WILLIAMS, 1985, resulting in

$$\frac{\partial(\rho Y_k)}{\partial t} + \frac{\partial}{\partial x_i} [(\rho u_i + \rho V_i^c) Y_k + \rho V_{k,i} Y_k] = \dot{\omega}_k \quad (3)$$

where

$$V_i^c = \sum_{k=1}^N D_k \frac{\partial Y_k}{\partial x_i}$$

Applying Fick's Law, the last term on the left hand side is:

$$V_{k,i} Y_k = -D_k \frac{\partial Y_k}{\partial x_i}$$

The total energy conservation equation is

$$\frac{\partial(\rho E)}{\partial t} + \frac{\partial}{\partial x_j} [\rho u_j E + u_j p - u_i \tau_{ij} + q_j] = \dot{\omega}_T + \rho \sum_{k=1}^N Y_k f_{k,i} (u_i + V_{k,i}) \quad (4)$$

where

$$\dot{\omega}_T = - \sum_{k=1}^N \Delta h_{f,k}^0 \dot{\omega}_k \quad (5)$$

$$q_i = \underbrace{-k \frac{\partial T}{\partial x_i}}_{\text{Conduction}} + \underbrace{\sum_k \rho V_{k,i} Y_k h_k}_{\text{Mass Diffusion}} + \underbrace{RT \sum_k \frac{D_{T,k}}{T} \frac{\partial T}{\partial x_i}}_{\text{Soret effect}} + \underbrace{q_{R_i}}_{\text{Radiation}} \quad (6)$$

The Dufour effect is an induced heat flow caused by the concentration gradient. These effects represent examples of couplings between two vector field flows. The cross-phenomenological coefficients relate the Dufour and Soret effects DEMIREL, 2007. Heat and mass transport give rise to the Soret effect, which is the mass diffusion due to heat transfer, and the Dufour effect, which is the heat transport due to mass diffusion.

It is not obvious that the cross-transport effects are unimportant in ignition stability because it will be found that changes in diffusion coefficients or Lewis numbers by amounts on the order of 10% can be significant, and Soret effects typically may reach 10% of those of the ordinary diffusion processes. Analysis has shown that there are conditions, Soret and Lewis numbers, under which may even change the character of the instability, but for usual flames, including mixtures containing hydrogen (for which the effect might be anticipated to be greatest), its only influence appears to be a relatively small quantitative modification to the stability boundaries WILLIAMS, 1985.

Rewriting the complete heat flow equation. taking into account the Dufour effect, results

$$q_i = \underbrace{-k \frac{\partial T}{\partial x_i}}_{\text{Conduction}} + \underbrace{\sum_k \rho V_{k,i} Y_k h_k}_{\text{Mass Diffusion}} + \underbrace{\bar{R}T \sum_j \sum_k \frac{x_k D_{T,j}}{M_j D_{jk}} (V_{j,i} - V_{k,i})}_{\text{Dufour Effect}} + \underbrace{q_{R_i}}_{\text{Radiation}} \quad (7)$$

In many problems, the only significant effects of radiation are those concerning radiant transfer to and from solid surfaces WILLIAMS, 1985. With this, the effects of radiation was taken into consideration only near the wall regions, such that the normal component from the surface is

$$q_R \cdot \vec{n} = \epsilon \sigma_{SB} T^4 \quad (8)$$

where $\epsilon_{em} = 4L/l_p$ is the engineering emissivity. Absorbance is generally given by WILLIAMS, 1985

$$\epsilon_{abs} = 1 - e^{-4L/l_p} \quad (9)$$

Disregarding the effects of body forces between species, the system of PDE for the instantaneous variables becomes:

$$\frac{\partial \rho}{\partial t} + \frac{\partial(\rho u_i)}{\partial x_i} = 0 \quad (10a)$$

$$\frac{\partial(\rho u_i)}{\partial t} + \frac{\partial}{\partial x_j} [\rho u_i u_j + p \delta_{ij} - \tau_{ij}] - \rho g_i = 0 \quad (10b)$$

$$\frac{\partial(\rho Y_k)}{\partial t} + \frac{\partial}{\partial x_i} [\rho (u_i + V_i^c) Y_k + \rho V_{k,i} Y_k] = \dot{\omega}_k \quad (10c)$$

$$\frac{\partial(\rho E)}{\partial t} + \frac{\partial}{\partial x_j} [\rho u_j E + u_j p - u_i \tau_{ij} + q_j] = \dot{\omega}_T \quad (10d)$$

Following, the equations for LES will be obtained. Setting Favre Filter as

$$\tilde{f} = \frac{\overline{\rho f}}{\bar{\rho}}; \quad (11a)$$

any variable f can be written as:

$$f = \tilde{f} + f'. \quad (11b)$$

As a consequence of the definition:

$$f' = f - \tilde{f} \longrightarrow \overline{\rho f'} = \overline{\rho f} - \overline{\rho \tilde{f}} = \bar{\rho} \tilde{f} - \bar{\rho} \tilde{f} = 0. \quad (11c)$$

By LES methodology, variables can be filtered in the spectral space or physical space. The filtered amount is defined by POINSOT and VEYNANTE, 2005:

$$\tilde{f}(x) = \int_{\Omega} f(x') F(x - x') dx' \quad (12)$$

where F may be one of the LES filters: Cut-off filter, or Box filter, or Gaussian filter. These filters are described in sequence.

The Cut-off filter in spectral space is defined by

$$F(k) = \begin{cases} 1 & \text{if } k \leq \kappa_c = \pi/\bar{\Delta} \\ 0 & \text{otherwise} \end{cases} \quad (13)$$

The Box filter in physical space is defined as:

$$F(\mathbf{x}) = \begin{cases} 1/\bar{\Delta}^3 & \text{if } |x_i| \leq \Delta/2, i = 1, 2, 3 \\ 0 & \text{otherwise} \end{cases} \quad (14)$$

The Gaussian filter in physical space is defined in the form:

$$F(\mathbf{x}) = \left(\frac{6}{\pi\Delta^2}\right)^{3/2} \exp\left[-\frac{6}{\Delta^2}(x_1^2 + x_2^2 + x_3^2)\right] \quad (15)$$

Applying the Favre filter, the system of equations for LES is the following:

$$\frac{\partial \bar{\rho}}{\partial t} + \frac{\partial}{\partial x_j} (\bar{\rho} \tilde{u}_i) = 0 \quad (16)$$

$$\frac{\partial}{\partial t} (\bar{\rho} \tilde{u}_i) + \frac{\partial}{\partial x_j} [\bar{\rho} \tilde{u}_i \tilde{u}_j + \tau_{ij}^{sgs} + \bar{p} \delta_{ij} - \bar{\tau}_{ij}] - \bar{\rho} \tilde{g}_i = 0 \quad (17)$$

$$\frac{\partial (\bar{\rho} \tilde{Y}_k)}{\partial t} + \frac{\partial}{\partial x_i} \left[\bar{\rho} (\tilde{u}_i + \tilde{V}_i^c) \tilde{Y}_k + \bar{\rho} \widetilde{V_{k,i} Y_k} + Y_{k,i}^{sgs} \right] = \bar{\omega}_k \quad (18)$$

$$\frac{\partial (\bar{\rho} \tilde{E})}{\partial t} + \frac{\partial}{\partial x_j} [\bar{\rho} \tilde{u}_j \tilde{E} + \tilde{u}_j \bar{p} - \tilde{u}_i \bar{\tau}_{ij} + H_j^{sgs} + \sigma_j^{sgs} + \bar{q}_j] = \bar{\omega}_T \quad (19)$$

where

$$\bar{q}_i = -\bar{k} \frac{\partial \tilde{T}}{\partial x_i} + \bar{\rho} \sum_k \tilde{h}_k \widetilde{V_{k,i} Y_k} + \bar{R} \frac{\partial \tilde{T}}{\partial x_i} \sum_k \overline{D_{T,k}} + \bar{q}_{R_i} + q_{i,sgs} \quad (20)$$

with the variables that need closure modeled by using the turbulent viscosity approach, as follow:

$$\bar{\tau}_{ij} = 2\mu(\tilde{T}) \left(\tilde{S}_{ij} - \frac{1}{3} \tilde{S}_{kk} \delta_{ij} \right)$$

$$\tau_{ij}^{sgs} = -2\bar{\rho} \nu_t \left(\tilde{S}_{ij} - \frac{1}{3} \tilde{S}_{kk} \delta_{ij} \right) + \frac{2}{3} \bar{\rho} k^{sgs} \delta_{ij}$$

$$\bar{p} = \bar{\rho} \tilde{R} \tilde{T} + \bar{\rho} R_u T^{sgs}$$

$$T^{sgs} = \sum_{k=1}^{N_s} \frac{(\tilde{Y}_k \tilde{T} - \tilde{Y}_k \tilde{T})}{W_k}$$

$$Y_{k,i}^{sgs} = -\frac{\bar{\rho} \nu_t}{Sc_{kt}} \frac{\partial \tilde{Y}_k}{\partial x_i} - \sum_{k=1}^N \frac{\bar{\rho} \nu_t}{Sc_{kt}} \frac{\partial \tilde{Y}_k}{\partial x_i}$$

$$\begin{aligned}\widetilde{V_{k,i}Y_k} &= -\rho D_k \frac{\partial \widetilde{Y_k}}{\partial x_i} \approx -\bar{\rho} \overline{D_k} \frac{\partial \widetilde{Y_k}}{\partial x_i} \\ \widetilde{E} &= \tilde{e} + \frac{1}{2} \widetilde{u_k u_k} \\ &= \tilde{e} + \frac{1}{2} \widetilde{u_k u_k} + \frac{1}{2} (\widetilde{u_k u_k} - \widetilde{u_k u_k}) \\ &= \tilde{e} + \frac{1}{2} \widetilde{u_k u_k} + k^{sgs} \\ \tilde{e} &= \sum_{k=1}^{N_s} \widetilde{Y_k} \Delta h_{f,k}^0 + \sum_{k=1}^{N_s} \widetilde{Y_k} \int_{T_0}^{\widetilde{T}} c_{V,k}(T) dT + \sum_{k=1}^{N_s} E_k^{sgs} \\ H_i^{sgs} + \sigma_i^{sgs} &= -(\bar{\rho} \nu_t + \mu) \frac{\partial k^{sgs}}{\partial x_i} - \frac{\bar{\rho} \nu_t c_p}{Pr_t} \frac{\partial \widetilde{T}}{\partial x_i} + \widetilde{u_j \tau_{ij}^{sgs}} \\ q_{sgs} &= -\sum_k \overline{h_k} \frac{\bar{\rho} \overline{D_k}}{Sc_t} \frac{\partial^2 \widetilde{Y_k}}{\partial x_i^2}\end{aligned}$$

According to Smagorinsky the turbulent viscosity ν_t is modelled as SCHIESTEL (2008)

$$\nu_t = C_\nu \overline{\Delta}^2 |\overline{\mathbf{S}}| \quad (21)$$

Assuming, the conditions of high Reynolds numbers, isotropic flow and considering that $\overline{\Delta}/\eta \gg 1$, where the cutoff wavenumber κ_c is defined by $\kappa_c = \pi/\overline{\Delta}$ POPE, 2000, thus $\kappa_c \eta \ll 1$. In this way, since the exponential of the spectral distribution of the flow can be ignored,

$$E^*(\kappa) = \alpha \epsilon^{\frac{2}{3}} \kappa^{-\frac{5}{3}} \quad (22)$$

The turbulent viscosity can be obtained by applying the closed spectral theory of KRAICHNAN (1976) applied to isotropic flows:

$$\nu_t = 0.441 \alpha^{\frac{3}{2}} \sqrt{\frac{E^*(\kappa_c)}{\kappa_c}} \quad (23)$$

where α is Kolmogorov constant ($\alpha \approx 1.5$).

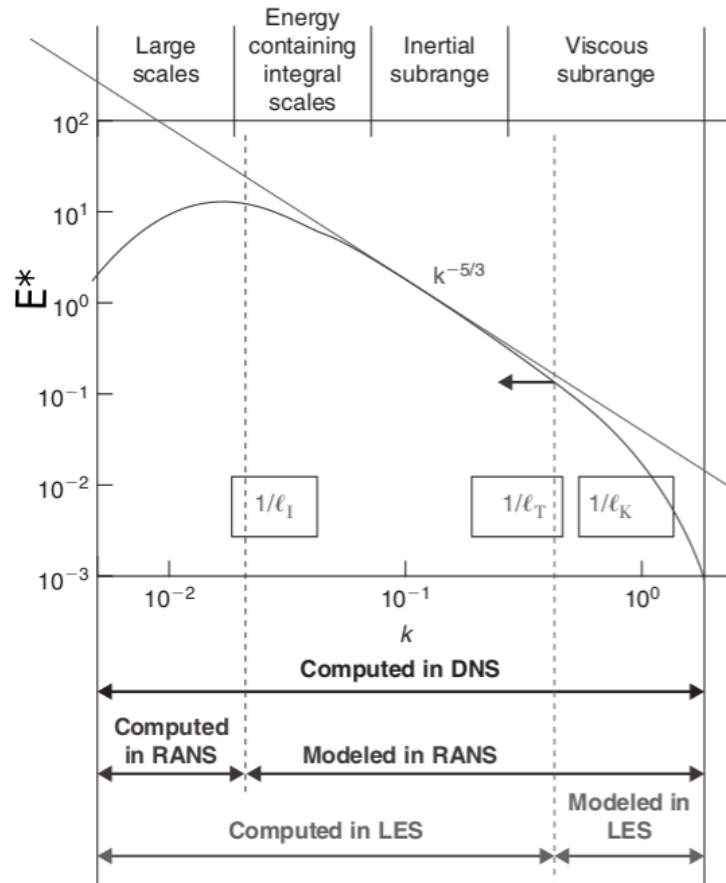
The dissipation rate can be approximated by $\epsilon^{sgs} \approx \epsilon = 0.931 \frac{(k^{sgs})^{3/2}}{\overline{\Delta}}$ GÉN, 2009. Therefore, equalling equations 21 and 23 the subgrid kinetic energy becomes

$$k^{sgs} = 22.5523 |\overline{\mathbf{S}}|^2 C_\nu^2 \overline{\Delta}^2 \quad (24)$$

This novel model of the subgrid kinetic energy proposed in this work differs from the method presented by GÉN (2009) and LIN (2010) and POPE (2000) with the purpose of avoiding the addition of one more transport equation, this way, reducing the computational cost and the complexity of the system of equations.

The application of the LES methodology implies directly in minimally refined mesh for convergence. Thus, one way to verify this refining is by applying the concept of spectral distribution, which is addressed in Figure 3 and explained in Section D. As shown in Figure 3, in LES, if the mesh is sufficiently refined, 80% of the energy spectrum is simulated, while the small vortices or viscous subgrid effects are modeled.

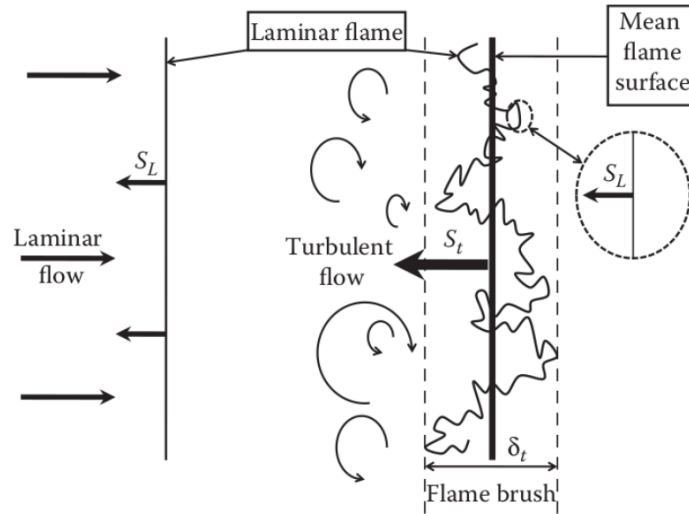
Figure 3 – Compared small scale analysed by different methodologies.



Source – Adapted by the author from HIRSCH (2007).

Analyzing from the point of view of combustion, laminar combustion generates a stable and well defined flame front, in contrast turbulence generate perturbations in the fire flame front appearing as a flame brush as shown in Figure 4.

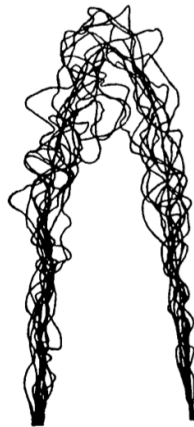
Figure 4 – Scheme of laminar (left) and turbulent (right) premixed flames.



Source – A. LIPATNIKOV (2013).

As shown in Figure 5, the characterization of the turbulent flame front might become such more complex, for example, in the case when the combustion presents the contour of a turbulent flame in a injector. The detection of the flame front or reaction front is developed by scanning some chemical species, thus, the phenomenon of turbulence, distorts the flame front, which makes it difficult to map.

Figure 5 – Contours of instantaneous flame boundaries in turbulent flame in a injector.



Source – GLASSMAN and YETTER (2008).

Turbulent premixed flame front was characterized by the Flamelet/ Progress Variable model, presented in detail in Appendix E. With this, CECERE et al. (2011), the proposal of this method is the resolution of two additional transport equations for the non-normalized progress variable \tilde{G}_ζ and for the squared variable \tilde{G}_ζ^2 . For more details of the progress variable definition and its normalization see Section E. Thus, the variance of the progress variable is given by $\tilde{G}_{\zeta_v} = \tilde{G}_\zeta^2 - \tilde{G}_\zeta^2$.

CECERE et al. (2011) also stated that the progress variable might be any scalar that characterizes the flame (mass fraction of the species, temperature, etc.), but this must be a monotonic function of the spatial coordinates. It is still suggested in that work, for a methane/oxygen mixture, that the progress variable be a combination of the CO_2 and CO species. This way, the mass fraction will be used as a progress variable with the following correlation

$$\mathbb{G} = \tilde{Y}_{CO_2} + \tilde{Y}_{CO} \quad (25)$$

The normalization of the progress function is given by

$$\zeta = \frac{\mathbb{G}(\vec{x}) - \mathbb{G}^u(\vec{x})}{\mathbb{G}^b(\vec{x}) - \mathbb{G}^u(\vec{x})} \quad (26)$$

where \square^u represents the unburnt gases, similarly, \square^b the flared gases.

Thus, additional non-normalized transport equations are:

$$\frac{\partial \bar{\rho} \tilde{\mathbb{G}}_\zeta}{\partial t} + \frac{\partial}{\partial x_j} (\bar{\rho} \tilde{u}_j \tilde{\mathbb{G}}_\zeta) = \frac{\partial}{\partial x_k} \left(\bar{\rho} \alpha_{\mathbb{G}_\zeta} \frac{\partial \tilde{\mathbb{G}}_\zeta}{\partial x_k} \right) + \bar{\rho} \tilde{\omega}_{\mathbb{G}_\zeta} + \frac{\partial f_{\zeta k}}{\partial x_k} \quad (27)$$

and

$$\frac{\partial \bar{\rho} \tilde{\mathbb{G}}_\zeta^2}{\partial t} + \frac{\partial}{\partial x_j} (\bar{\rho} \tilde{u}_j \tilde{\mathbb{G}}_\zeta^2) = \frac{\partial}{\partial x_k} (\bar{\rho} \alpha_{\mathbb{G}_\zeta} \tilde{\mathbb{G}}_\zeta^2) + \frac{\partial f_{\zeta^2 k}}{\partial x_k} - 2\bar{\rho} \tilde{X}_{\mathbb{G}_\zeta} + 2\bar{\rho} \tilde{\omega}_{\mathbb{G}_\zeta} \tilde{\mathbb{G}}_\zeta \quad (28)$$

where

$$f_{\zeta k} = \bar{\rho} \alpha_{\mathbb{G}_\zeta}^t \frac{\partial \tilde{\mathbb{G}}_\zeta}{\partial x_k}$$

and

$$\alpha_{\mathbb{G}_\zeta}^t = C_{\mathbb{G}_\zeta} \bar{\Delta}^2 |\mathbf{S}| S_{ij}$$

Although for the constant $C_{\mathbb{G}_\zeta}$ GERMANO et al. (1991) propose a dynamic calculation, in the present work it is proposed that the calculation be performed taking into account the subgrid kinetic energy, see Section D. For further details seek also Section E, such that

$$C_{\mathbb{G}_\zeta}(x, t) = -0.4655 \frac{k^{sgs \frac{3}{2}}}{\bar{\Delta}^3 |\mathbf{S}| S_{ij}^2} \quad (29)$$

The proposal of the equations 24 and 29 is reducing the turbulence control parameters, so the only external parameter to be controlled is the Smagorinsky constant, together with the analytical closure of the transport equations.

The closure of the balance equation of progress variable becomes

$$f_{\zeta^2 k} = \bar{\rho} \alpha_{\mathbb{G}_\zeta}^t \frac{\partial \widetilde{\mathbb{G}_\zeta^2}}{\partial x_k}$$

$$\bar{\rho} \widetilde{X}_{\mathbb{G}_\zeta} = \bar{\rho} D |\nabla \widetilde{\mathbb{G}_\zeta}|^2 + \bar{s}_{X_{\mathbb{G}_\zeta}}$$

By VEYNANTE and VERVISCH (2002) if a linear relaxation of the fluctuations generated by micromixing is postulated, then

$$\bar{s}_{X_{\mathbb{G}_\zeta}} = \frac{\bar{\rho} \widetilde{\mathbb{G}_{\zeta v}}}{\tau_t}$$

Following DOMINGO et al. (2005) the turbulent Schmidt number is assumed to be 0.7.

For full details of the turbulent equation see Appendix F.

3 NUMERICAL MODEL

CBS scheme was originally introduced for a solution in the fully explicit form, later it was extended to the semi-implicit form and could be applied for both compressible and incompressible flows. From the outset, it has been realized that the explicit solution to the fully incompressible fluid dynamics equations using the CBS scheme is possible, provided an artificial compressibility method is employed. The solution of transient problems with CBS was achieved using a two-step time-staging approach. Recently, the method was extended to solve problems of viscoelastic flow NITHIARASU, CODINA, and ZIENKIEWICZ, 2006.

3.1 General CBS

Consider the transport equation of any scalar ϕ

$$\frac{\partial \phi(\vec{x}, t)}{\partial t} + \vec{u} \cdot \nabla \phi - \nabla \cdot (k_\phi \nabla \phi) = S_\phi \quad (30)$$

For coordinates along the characteristic line so that

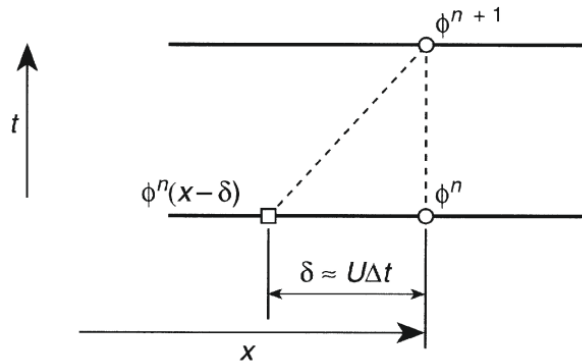
$$dx' = dx - udt \quad (31)$$

Equation 30 can be rewritten as and considering the terms $n+1/2$ being approximated by terms n , one gets:

$$\frac{d\phi(x', t)}{dt} - \nabla \cdot (k_\phi \nabla \phi) = S_\phi \quad (32)$$

Where it is implied, now, that one is in a mobile coordinate system. Suppose, the one-dimensional case, as illustrated in the Figure 6, and that in the time interval a shift $\delta = u\Delta t$ in x occurred.

Figure 6 – Scheme of characteristic-Galerkin procedure.



Source – ZIENKIEWICZ, TAYLOR, and NITHIARASU (2014).

The time discretization of the one-dimensional equation leads to:

$$\frac{\phi^{n+1} - \phi_{x-\delta}^n}{\Delta t} \approx \theta [\nabla \cdot (k_\phi \nabla \phi) + S_\phi]^{n+1} + (1 - \theta) [\nabla \cdot (k_\phi \nabla \phi) + S_\phi]_{x-\delta}^n \quad (33)$$

The problem is that the terms at time n are in different positions than the terms $n + 1$, a consequence of being in a mobile coordinate system. However, by Taylor series expansion, the terms in the position $x - \delta$ can be transformed to the x position, that is,

$$\phi_{x-\delta}^n \approx \phi_x^n - \delta \frac{\partial \phi_x^n}{\partial x} + \frac{\delta^2}{2} \frac{\partial^2 \phi_x^n}{\partial x^2} + O(\Delta t^3) \quad (34a)$$

$$(1-\theta) \left[\frac{\partial}{\partial x} \left(k_\phi \frac{\partial \phi}{\partial x} \right) \right]_{x-\delta}^n \approx (1-\theta) \left[\frac{\partial}{\partial x} \left(k_\phi \frac{\partial \phi}{\partial x} \right) \right]^n - (1-\theta) \delta \frac{\partial}{\partial x} \left[\frac{\partial}{\partial x} \left(k_\phi \frac{\partial \phi}{\partial x} \right) \right]^n + O(\Delta t^2) \quad (34b)$$

$$(1 - \theta) (S_\phi)_{x-\delta}^n \approx (1 - \theta) S_\phi^n - (1 - \theta) \delta \frac{\partial S_\phi^n}{\partial x} + O(\Delta t^2) \quad (34c)$$

Thus, the Equation 33 can be rewritten as

$$\begin{aligned} \phi^{(n+1)} = & \phi_x^n - u \Delta t \frac{\partial \phi_x^n}{\partial x} + \frac{\Delta t^2}{2} u \frac{\partial}{\partial x} \left(u \frac{\partial \phi_x^n}{\partial x} \right) + \theta \Delta t \left[\frac{\partial}{\partial x} \left(k_\phi \frac{\partial \phi}{\partial x} + S_\phi \right) \right]^{(n+1)} + (35) \\ & + (1 - \theta) \Delta t \left[\frac{\partial}{\partial x} \left(k_\phi \frac{\partial \phi}{\partial x} \right) \right]^n - (1 - \theta) \Delta t^2 u \frac{\partial}{\partial x} \left[\frac{\partial}{\partial x} \left(k_\phi \frac{\partial \phi}{\partial x} \right) \right]^n + \\ & + (1 - \theta) \Delta t S_\phi^n - (1 - \theta) \Delta t^2 u \frac{\partial S_\phi^n}{\partial x} \end{aligned}$$

for $\theta = 0.5$

$$\begin{aligned} \phi^{(n+1)} = & \phi_x^n - u \Delta t \frac{\partial \phi_x^n}{\partial x} + \frac{\Delta t^2}{2} u \frac{\partial}{\partial x} \left(u \frac{\partial \phi_x^n}{\partial x} \right) + \frac{\Delta t}{2} \left[\frac{\partial}{\partial x} \left(k_\phi \frac{\partial \phi}{\partial x} + S_\phi \right) \right]^{(n+1)} + (36) \\ & + \frac{\Delta t}{2} \left[\frac{\partial}{\partial x} \left(k_\phi \frac{\partial \phi}{\partial x} \right) \right]^n - \frac{\Delta t^2}{2} u \frac{\partial}{\partial x} \left[\frac{\partial}{\partial x} \left(k_\phi \frac{\partial \phi}{\partial x} \right) \right]^n + \\ & + \frac{\Delta t}{2} S_\phi^n - \frac{\Delta t^2}{2} u \frac{\partial S_\phi^n}{\partial x} \end{aligned}$$

Whereas

$$(\square)^{\left(n+\frac{1}{2}\right)} = \frac{1}{2} (\square)^n + \frac{1}{2} (\square)^{(n+1)} \quad (37)$$

thus

$$\phi^{(n+1)} = \phi_x^n - \Delta t \left[u \frac{\partial \phi_x^n}{\partial x} - \frac{\partial}{\partial x} \left(k_\phi \frac{\partial \phi}{\partial x} \right)^{\left(n+\frac{1}{2}\right)} - S_\phi^{\left(n+\frac{1}{2}\right)} \right] + \quad (38)$$

$$+ \Delta t \left\{ \frac{\Delta t}{2} u \frac{\partial}{\partial x} \left(u \frac{\partial \phi_x^n}{\partial x} \right) - \frac{\Delta t}{2} u \frac{\partial}{\partial x} \left[\frac{\partial}{\partial x} \left(k_\phi \frac{\partial \phi}{\partial x} \right) \right]^n - \frac{\Delta t}{2} u \frac{\partial S_\phi^n}{\partial x} \right\} \quad (39)$$

applying the approximation Equation 37 you get

$$\phi^{(n+1)} = \phi^n - \Delta t \left[u \frac{\partial \phi}{\partial x} - \frac{\partial}{\partial x} \left(k_\phi \frac{\partial \phi}{\partial x} \right) - S_\phi \right]^n + \frac{\Delta t^2}{2} u \frac{\partial}{\partial x} \left[u \frac{\partial \phi}{\partial x} - \frac{\partial}{\partial x} \left(k_\phi \frac{\partial \phi}{\partial x} \right) - S_\phi \right]^n \quad (40)$$

In multidimensions there is

$$\begin{aligned} \phi^{(n+1)} = \phi^n - \Delta t \left[u_j \frac{\partial \phi}{\partial x_j} - \frac{\partial}{\partial x_j} \left(k_\phi \frac{\partial \phi}{\partial x_j} \right) - S_\phi \right]^n + \\ + \frac{\Delta t^2}{2} u_k \frac{\partial}{\partial x_k} \left[u_j \frac{\partial \phi}{\partial x_j} - \frac{\partial}{\partial x_j} \left(k_\phi \frac{\partial \phi}{\partial x_j} \right) - S_\phi \right]^n \end{aligned} \quad (41)$$

or

$$\phi^{(n+1)} = \phi^n - \Delta t [\vec{u} \cdot \nabla \phi - \nabla \cdot (k_\phi \nabla \phi) - S_\phi]^n + \frac{\Delta t^2}{2} \vec{u} \cdot \nabla [\vec{u} \cdot \nabla \phi - \nabla \cdot (k_\phi \nabla \phi) - S_\phi]^n \quad (42)$$

Using a conservative form of the transport equation, the equation resulting from the CBS is

$$\begin{aligned} \phi^{(n+1)} = \phi^n - \Delta t [\nabla \cdot (\vec{u} \phi) - \nabla \cdot (k_\phi \nabla \phi) - S_\phi]^n + \\ + \frac{\Delta t^2}{2} \vec{u} \cdot \nabla [\nabla \cdot (\vec{u} \phi) - \nabla \cdot (k_\phi \nabla \phi) - S_\phi]^n \end{aligned} \quad (43)$$

3.2 Temporal Discretization of the Momentum Equation

Let the Equation 10b be rewritten as

$$\frac{\partial U_i}{\partial t} = - \frac{\partial}{\partial x_j} (u_j U_i) + \frac{\partial \tau_{ij}}{\partial x_j} - \frac{\partial p}{\partial x_i} + \rho g_i \quad (44)$$

where U_i represents the mass flow given by

$$U_i = \rho u_i$$

To apply the CBS to the Equation 10b, similar what has been done for obtention of Equation 42, and introduce introduce the approximations there are two alternatives: Split A and Split B, but in present work it was chosen Split B. Assuming in each split a time increment $\Delta t = t^{n+1} - t^n$.

In the split B, the auxiliary variable ΔU_i^* is also introduced, keeping the known values of $\partial p^n / \partial x_i$, i.e.,

$$\begin{aligned} \Delta U_i^* = \Delta t \left[- \frac{\partial}{\partial x_j} (u_j U_i) + \frac{\partial \tau_{ij}}{\partial x_j} - \frac{\partial p}{\partial x_i} + \rho g_i + \right. \\ \left. + \frac{\Delta t}{2} u_k \frac{\partial}{\partial x_k} \left(\frac{\partial}{\partial x_j} (u_j U_i) + \frac{\partial p}{\partial x_i} - \rho g_i \right) \right]^n \end{aligned} \quad (45)$$

By including the pressure term, this equation gives a better approximation for U_i^* . Now a correction term is given by:

$$\Delta U_i^{**} = -\theta_2 \Delta t \frac{\partial \Delta p}{\partial x_i} \quad (46)$$

Therefore, for $\theta_2 = 0$, no correction (ΔU_i^{**}) will be required. The density variation becomes

$$\Delta \rho = -\Delta t \left[\frac{\partial U_i^n}{\partial x_i} + \theta_1 \frac{\partial \Delta U_i^*}{\partial x_i} - \Delta t \theta_1 \theta_2 \frac{\partial^2 \Delta p}{\partial x_i^2} \right] \quad (47)$$

3.3 Space Discretization

Using spatial approximations by Galerkin FEM, variables are interpolated as ZIENKIEWICZ, TAYLOR, and NITHIARASU, 2014:

$$\begin{aligned} U_i &= N_u \hat{U}_i & \Delta U_i &= N_u \Delta \hat{U}_i & \Delta U_i^* &= N_u \Delta \hat{U}_i^* \\ \Delta U_i^{**} &= N_u \Delta \hat{U}_i^{**} & u_i &= N_u \hat{u}_i & p &= N_p \hat{p} & \rho &= N_\rho \hat{\rho} \end{aligned}$$

where the vectors of node variables and interpolation functions are

$$\begin{aligned} \hat{U}_i &= [\hat{U}_i^1 \ \hat{U}_i^2 \ \dots \ \hat{U}_i^a \ \dots \ \hat{U}_i^m]^T \\ N &= [N^1 \ N^2 \ \dots \ N^a \ \dots \ N^m] \end{aligned}$$

and a is the node number identification, which varies between 1 and m .

The shear stress tensor is defined as

$$\tau_{ij} = 2\mu S_{ij}$$

where the deformation rate is given by,

$$S_{ij} = \frac{1}{2} \left(\frac{\partial u_i}{\partial x_j} + \frac{\partial u_j}{\partial x_i} \right)$$

for incompressible flows, the last term in the deformation rate disappears.

For convenience, the components of the shear strain tensor can be put in matrix form as:

$$\mathbf{S} = [S_{11} \ S_{22} \ S_{33} \ 2S_{12} \ 2S_{23} \ 2S_{31}]^T \quad (48)$$

Thus, for incompressible flow the rate of volumetric deformation is

$$S_v = S_{ii} = S_{11} + S_{22} + S_{33} = 0 \quad (49)$$

The rate of shear strain can be rewritten as

$$\mathbf{S}^d = I_d \mathbf{S} \quad (50)$$

where

$$I_d = \begin{bmatrix} 0 & 0 & 0 & 0 & 0 & 0 \\ 0 & 0 & 0 & 0 & 0 & 0 \\ 0 & 0 & 0 & 0 & 0 & 0 \\ 0 & 0 & 0 & 1 & 0 & 0 \\ 0 & 0 & 0 & 0 & 1 & 0 \\ 0 & 0 & 0 & 0 & 0 & 1 \end{bmatrix} \quad (51)$$

By introducing the concept of the derivation matrix of the velocities and rates of deformation it is shown that the strain tensor can be defined as:

$$\mathbf{S} = S^* \mathbf{u} \quad (52)$$

where

$$\mathbf{u} = [u_1 \quad u_2 \quad u_3]^T$$

Thereby,

$$S^* = \begin{bmatrix} \frac{\partial}{\partial x_1} & 0 & 0 \\ 0 & \frac{\partial}{\partial x_2} & 0 \\ 0 & 0 & \frac{\partial}{\partial x_3} \\ \frac{\partial}{\partial x_2} & \frac{\partial}{\partial x_1} & 0 \\ 0 & \frac{\partial}{\partial x_3} & \frac{\partial}{\partial x_2} \\ \frac{\partial}{\partial x_3} & 0 & \frac{\partial}{\partial x_1} \end{bmatrix} \quad (53)$$

A matrix B is defined as a relation between the rate of deformation and velocities by

$$B = S^* N_u \quad (54)$$

Thus, the solution to ΔU_i^* is

Step 1

$$\begin{aligned} \Delta \hat{U}_i^* = & -\mathbf{M}_u^{(-1)} \Delta t \left[(\mathbf{C}_u \hat{U} + \mathbf{K}_\tau \hat{u} + \mathbf{G}^T \hat{p} - \mathbf{f}) - \right. \\ & \left. - \Delta t \left(\mathbf{K}_u \hat{U} + \mathbf{f}_s + \frac{\Delta t}{2} \mathbf{P} \hat{p} \right) \right]^n \end{aligned} \quad (55)$$

Values with notation $\hat{\square}$ represent the nodal values. The matrices of coefficients in the above equation are:

$$\mathbf{M}_u = \int_{\Omega} N_u^T N_u d\Omega \quad (56a)$$

$$\mathbf{C}_u = \int_{\Omega} N_u^T (\nabla(uN_u)) d\Omega \quad (56b)$$

$$\mathbf{K}_\tau = \int_{\Omega} B^T \mu I_d B d\Omega \quad (56c)$$

$$\mathbf{f} = \int_{\Omega} N_u^T \rho g d\Omega + \int_{\Gamma} N_u^T \bar{t} d\Gamma \quad (56d)$$

$$\mathbf{K}_u = -\frac{1}{2} \int_{\Omega} [\nabla^T(uN_u)]^T [\nabla^T(uN_u)] d\Omega \quad (56e)$$

$$\mathbf{f}_s = -\frac{1}{2} \int_{\Omega} [\nabla^T(uN_u)]^T \rho g d\Omega \quad (56f)$$

In a **Step 2**, the pressure field is obtained from

$$(\mathbf{M}_p + \Delta t^2 \theta_1 \theta_2 \mathbf{H}) \Delta \hat{p} = \Delta t [\mathbf{G} \hat{U} + \theta_1 \mathbf{G} \Delta \hat{U}^* - \mathbf{f}_p]^n \quad (57)$$

and then, the additional correction term defined Eq. (32) is calculated from

Step 3

$$\Delta \hat{U}^{**} = -\mathbf{M}_u^{-1} \Delta t [\theta_2 \mathbf{G}^T \Delta \hat{p}] \quad (58)$$

In a **Step 4** the energy equation is solved. By the approximate functions for energy and temperature inside a finite element:

$$\rho E = N_E \hat{E} \quad \text{and} \quad T = N_T \hat{T} \quad (59)$$

and the discretized equation or algebraic equation for energy is:

$$\begin{aligned} \Delta \hat{E} = & -\mathbf{M}_E^{-1} \Delta t [\mathbf{C}_E \hat{E} + \mathbf{C}_p \hat{p} + \mathbf{K}_T \hat{T} + \mathbf{K}_{\tau E} \hat{u} \\ & + \mathbf{f}_e - \Delta t (\mathbf{K}_{uE} \hat{E} + \mathbf{K}_{up} \hat{p} + \mathbf{f}_{es})]^n \end{aligned} \quad (60)$$

where \hat{E} are the nodal values of ρE and the matrices and vectors are similar to those shown above.

$$\mathbf{M}_E = \int_{\Omega} N_E^T N_E d\Omega$$

$$\begin{aligned}
\mathbf{C}_E &= \int_{\Omega} N_E^T \nabla^T (u N_E) d\Omega \\
\mathbf{C}_P &= \int_{\Omega} N_E^T \nabla^T (u N_p) d\Omega \\
\mathbf{K}_T &= \int_{\Omega} (\nabla N_E)^T k \nabla N_T d\Omega \\
\mathbf{K}_{\tau E} &= \int_{\Omega} B^T \mu u_{\alpha v} I_d B d\Omega \\
\mathbf{K}_{uE} &= -\frac{1}{2} \int_{\Omega} (\nabla^T (u N_E))^T (\nabla N_E) d\Omega \\
\mathbf{f}_e &= \int_{\Gamma} N_E^T n^T (t^d u + k \nabla T) d\Gamma \\
\mathbf{K}_{up} &= -\frac{1}{2} \int_{\Omega} (\nabla^T N_E)^T (\nabla N_p) d\Omega
\end{aligned}$$

The force term \mathbf{f}_{es} contains the source terms. For more details and compressible flows see Section B.

3.4 Artificial Compression in Transient Problems

For transient problems the artificial compressibility method is easily obtained from the CBS structure ZIENKIEWICZ, TAYLOR, and NITHIARASU, 2014. Consider the equation

$$\begin{aligned}
U_i^{n+1} - U_i^n &= \Delta t \left[-\frac{\partial}{\partial x_j} (u_j U_i)^n + \frac{\tau_{ij}^n}{\partial x_j} + (\rho g_i)^n - \right. \\
&\quad \left. - \frac{\Delta U_i^m}{\Delta \tau} \right] - \Delta t \frac{\partial p^{n+\theta_2}}{\partial x_i} + \frac{\Delta t^2}{2} u_k \frac{\partial}{\partial x_k} \left[\frac{\partial}{\partial x_j} (u_j U_i) - \right. \\
&\quad \left. - \frac{\tau_{ij}^n}{\partial x_j} - \rho g_i + \frac{\Delta U_i^m}{\Delta \tau} \right]^n + \frac{\Delta t^2}{2} u_k \frac{\partial}{\partial x_k} \left(\frac{\partial p^{n+\theta_2}}{\partial x_i} \right)
\end{aligned}$$

where ΔU_i^m is the variation of the real time of the variable U_i . This term can be approximated depending on the required accuracy in the transient problem. A second-order accuracy can be obtained by

$$\Delta U_i^m = \frac{3U_i^n - 4U_i^m + U_i^{m-1}}{2} \quad (61)$$

The superscript m refers to the variation of real time. Incorporating the above changes into the CBS formulation, the three semi-discrete steps of the CBS scheme can be written to the **Split A** as:

$$\begin{aligned} \Delta U_i^* = \Delta t & \left[-\frac{\partial}{\partial x_j} (u_j U_i) + \frac{\partial \tau_{ij}}{\partial x_j} + \rho g_i + \right. \\ & \left. + \frac{\Delta t}{2} u_k \frac{\partial}{\partial x_k} \left(\frac{\partial}{\partial x_j} (u_j U_i) - \frac{\tau_{ij}}{\partial x_j} - \rho g_i \right) \right]^n \end{aligned} \quad (62)$$

The correction is obtained by evaluating the pressure increment, thus at the **Step 3**:

$$\begin{aligned} \Delta U_i^{**} = \Delta U_i - \Delta U_i^* = -\Delta t \frac{\partial p^{n+\theta_2}}{\partial x_i} - \\ - \frac{\Delta U_i^m}{\Delta \tau} + \frac{\Delta t^2}{2} u_k \frac{\partial^2 p^n}{\partial x_k \partial x_i} + \frac{\Delta t^2}{2} u_k \frac{\partial}{\partial x_k} \left(\frac{\Delta U_i^m}{\Delta \tau} \right) \end{aligned} \quad (63)$$

Modifying the Equation 10a

$$\Delta \rho = \frac{1}{\beta^2} \Delta p = -\Delta t \frac{\partial U_i^{n+\theta_1}}{\partial x_i} = -\Delta t \left[\frac{\partial U_i^n}{\partial x_i} + \theta_1 \frac{\partial \Delta U_i}{\partial x_i} \right] \quad (64)$$

Substituting ΔU_i by $\Delta U_i^* + \Delta U_i^{**}$ and neglecting third-order or higher order terms yields:

$$\begin{aligned} \frac{1}{\beta^2} \Delta p = -\Delta t & \left[\frac{\partial U_i^n}{\partial x_i} + \theta_1 \frac{\partial \Delta U_i^*}{\partial x_i} - \right. \\ & \left. - \Delta t \theta_1 \left(\frac{\partial^2 p^n}{\partial x_i \partial x_i} + \theta_2 \frac{\partial^2 \Delta p}{\partial x_i \partial x_i} \right) - \theta_1 \frac{\partial}{\partial x_1} \left(\frac{\Delta U_i^m}{\Delta \tau} \right) \right] \end{aligned} \quad (65)$$

the β value may be computed using the relation from ZIENKIEWICZ, TAYLOR, and NITHIARASU, 2014:

$$\beta = \max(\varepsilon, u_{conv}, u_{diff}) \quad (66)$$

where ε is a small constant to ensure that the β does not approach to zero under any situation. u_{conv} and u_{diff} are the convective and diffusive velocities given by

$$u_{conv} = |\mathbf{u}| = \sqrt{u_i u_i} \quad (67a)$$

$$u_{diff} = \frac{\nu}{\Delta} \quad (67b)$$

Thus, the time step limitation for artificial compressibility method may be defined as

$$\Delta t = \frac{\bar{\Delta}}{|\mathbf{u}| + \beta} \quad (68)$$

$\bar{\Delta}$ must be a characteristic length of the mesh, such as the diagonal of the smallest element of the hexagonal mesh.

Combining Step 1 (Equation 63) and Step 3 (Equation 64),

$$\begin{aligned}
 & - \left[\frac{\Delta U_i^m}{\Delta \tau} + \frac{\partial}{\partial x_j} (u_j U_i) + \frac{\partial p}{\partial x_i} - \right. \\
 & \left. - \frac{\partial \tau_{ij}}{\partial x_j} - (\rho g_i) \right]^n + \frac{\Delta t}{2} u_k \frac{\partial}{\partial x_k} \left[\frac{\partial}{\partial x_j} (u_j U_i) - \right. \\
 & \left. - \frac{\partial \tau_{ij}}{\partial x_j} - \rho g_i + \frac{\Delta U_i^m}{\Delta \tau} + \frac{\partial p}{\partial x_i} \right]^n = 0
 \end{aligned} \tag{69}$$

Replacing Step 1 (Equation 63) in Step 2 (Equation 66), neglecting terms of third or higher orders, and rearranging (assuming $\theta_1 = 0.5$ and $\theta_2 = 0$ and permanent pseudo steady-state regime with $\Delta p = 0$), the Equation 51 becomes:

$$\begin{aligned}
 \frac{\partial U_i^n}{\partial x_i} + \frac{\Delta t}{2} \frac{\partial}{\partial x_i} \left[\frac{\partial (u_j U_i)}{\partial x_j} - \frac{\partial \tau_{ij}}{\partial x_j} \rho g + \right. \\
 \left. + \frac{\partial p}{\partial x_i} + \frac{\Delta U_i^m}{\Delta \tau} \right]^n = 0
 \end{aligned} \tag{70}$$

The method presented can be seen in greater detail in the work NITHIARASU, BEVAN, and MURALI, 2012.

4 PROGRAMMING ASPECT

In the present work, a numerical solution of a high-complexity problem, with tenths of transport equations and millions of elements, has been developed, demanding much computational power. Therefore a multicore CPU local homogeneous parallel programming was employed, with the Python *multiprocessing* library.

The Element-by-Element (EbE) is an iterative technique whereby a small dense linear system for each element is solved in a block-parallel scheme, and the residues are dealt with methods such as the Conjugate Gradient Method (CGM) or Bi-Conjugate Gradient Method (BiCGM). The EbE technique generates smaller matrices, increasing processing speed and lowering RAM usage, without the need for clusters or workstations to solve problems with very refined meshes. For the present work, the EbE technique with the BiCGM method was employed, using homogeneous programming with multiprocessing.

In order to exemplify the application of the EbE¹ method, the solution of the transient compressible Navier-Stokes equations was structured as following. Considering the element system and applying *Split B* in fully explicit form, the steps 1 and 2 became.

Step 1

$$\underbrace{\mathbf{M}_u}_{LHS} \Delta \hat{U}_i^* = \underbrace{\Delta t \left[(\mathbf{C}_u \hat{U} + \mathbf{K}_\tau \hat{u} + \mathbf{G}^T \hat{p} - \mathbf{f}) - \Delta t \left(\mathbf{K}_u \hat{U} + \mathbf{f}_s + \frac{1}{2} \mathbf{P} \hat{p} \right) \right]}_{RHS}^n \quad (71)$$

Step 2

$$\underbrace{\mathbf{M}_\rho}_{LHS} \Delta \hat{\rho} = \underbrace{\Delta t \left[\mathbf{G} \hat{U} + \theta_1 \mathbf{G} \Delta \hat{U}^* - \mathbf{f}_\rho \right]}_{RHS}^n \quad (72)$$

The EbE is an iterative technique whereby the linear system for each element is solved, and the residues are dealt with methods such as Conjugate Gradient Method (CGM) or Biconjugate Gradient Method (BiCGM). Systems of equations, such as 71 and 72, are examples of linear systems to be solved, where LHS² contains the unknowns and RHS³ contains known variables of the linear systems.

For the present work the EbE technique with the BiCGM method was employed, using homogeneous programming with multiprocessing. The EbE technique generates smaller matrices, increasing processing speed and lowering RAM memory usage.

For further details regarding the complete construction of the CBS method see Section B.

¹ Element-by-Element

² Left Hand Side

³ Right Hand Side

Thus, taking into account the general linear system:

$$M\Delta\phi = F \quad (73)$$

the following pseudocode demonstrates the parallelism methodology applied in the EbE technique.

The application process EbE is simple, being composed initially by dividing the elements for a number of predetermined processes. A residual is defined as the difference between the RHS and LHS of the linear system. Locally, in each element it is taken into account the effects of node connectivity. Finally, an initial error is calculated and it is started an iterative process to minimize this error until a pre-established tolerance is reached.

INIT

```

for u ∈ DoF do #Dof Iteration
  [
    r(u) ← 0
    D(u) ← 0
  ]
  # Multiprocessing on CPU
  for p in 0 to process do #Serial loop
    for e ∈ Ξ(c) do #EbE iteration
      [
        #Ξ(c) → Elements slice for each color
        re ← re + Fe - MeΔφe
        De ← De + diag(Me)
      ]
    for u ∈ DoF do #Dof Iteration
      [
        D(u) ← 1/D(u)
        r̄(u) ← r(u)
        d(u) ← D(u) · r(u)
        d̄(u) ← D(u) · r̄(u)
        q(u) ← 0
        q̄(u) ← 0
      ]
    δ ← 0 #Error
    for u ∈ DoF do #Dof Iteration
      [
        δ ← δ + r(u) · d(u) #Global error DoF
      ]
    while δ > tolerancy do #host loop
      for p in 0 to processes do
        [
          #Slice Elements for Processes...
          for e ∈ Ξ(c) do #EbE iteration
            [
              qe ← qe + Me · de
              q̄e ← q̄e + Me · d̄e
            ]
            α ← 0
            for u ∈ DoF do #Dof Iteration
              [
                α ← α + d̄(u) · q(u)
              ]
            for u ∈ DoF do #Dof Iteration
              [
                Δφ(u) ← Δφ(u) + δ/α · d(u)
                r(u) ← r(u) - δ/α · q(u)
                r̄(u) ← r̄(u) - δ/α · q̄(u)
              ]
            #Update iteration
            δ̄ ← δ; δ ← 0
            for u ∈ DoF do #Dof Iteration
              [
                δ ← δ + r(u) · D(u) · r̄(u)
              ]
            α ← δ/δ̄
            for u ∈ DoF do #Dof Iteration
              [
                d(u) ← D(u) · r(u) + α · d̄(u)
                d̄(u) ← D(u) · r̄(u) + α · d̄(u)
                q(u) ← 0
                q̄(u) ← 0
              ]
        ]
      ]
  ]

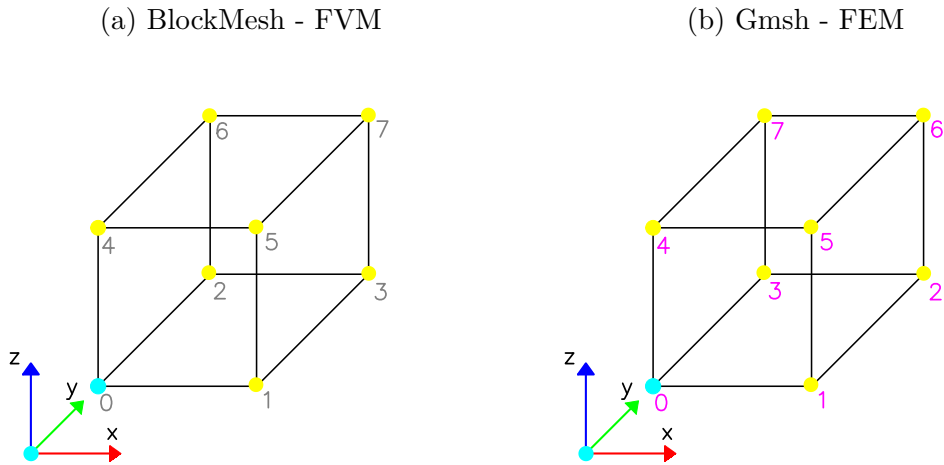
```

After having defined the geometry the next step was to chose a suitable mesh generator, the BlockMesh toolbox, from OpenFOAM software. For that, information gathering filter libraries had to be developed concerning the connectivity of the nodes, coordinates of the points and the boundary elements, collected in files in the *MakeToOpenFOAM*⁴ folder. With the mesh information generated by BlockMesh, it was necessary to restructure

⁴ <https://github.com/ruhanponce/Numerical-Investigation-CBS.git>

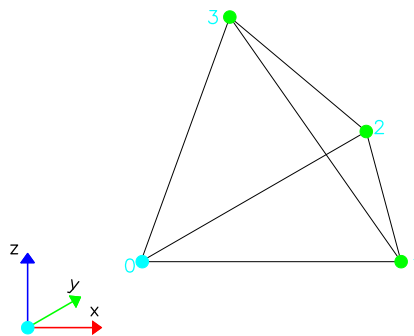
the numbering scheme of the assembly matrix, since the toolbox was originally designed for FVM, as shown in Figure 7, for hexahedral elements. In Figure 8 is shown a four node tetrahedral element for Gmsh generator mesh.

Figure 7 – Output numbering default in 8-node hexahedral isoparametric element produced by FVM and FEM.



Source – Prepared by author adapted from GREENSHIELDS (2017) (7a) and GEYZAINE and REMACLE (2019) (7b).

Figure 8 – Output numbering default for 4-node tetrahedral isoparametric element by Gmsh® mesh generation.



Source – Prepared by author adapted from GEYZAINE and REMACLE (2019).

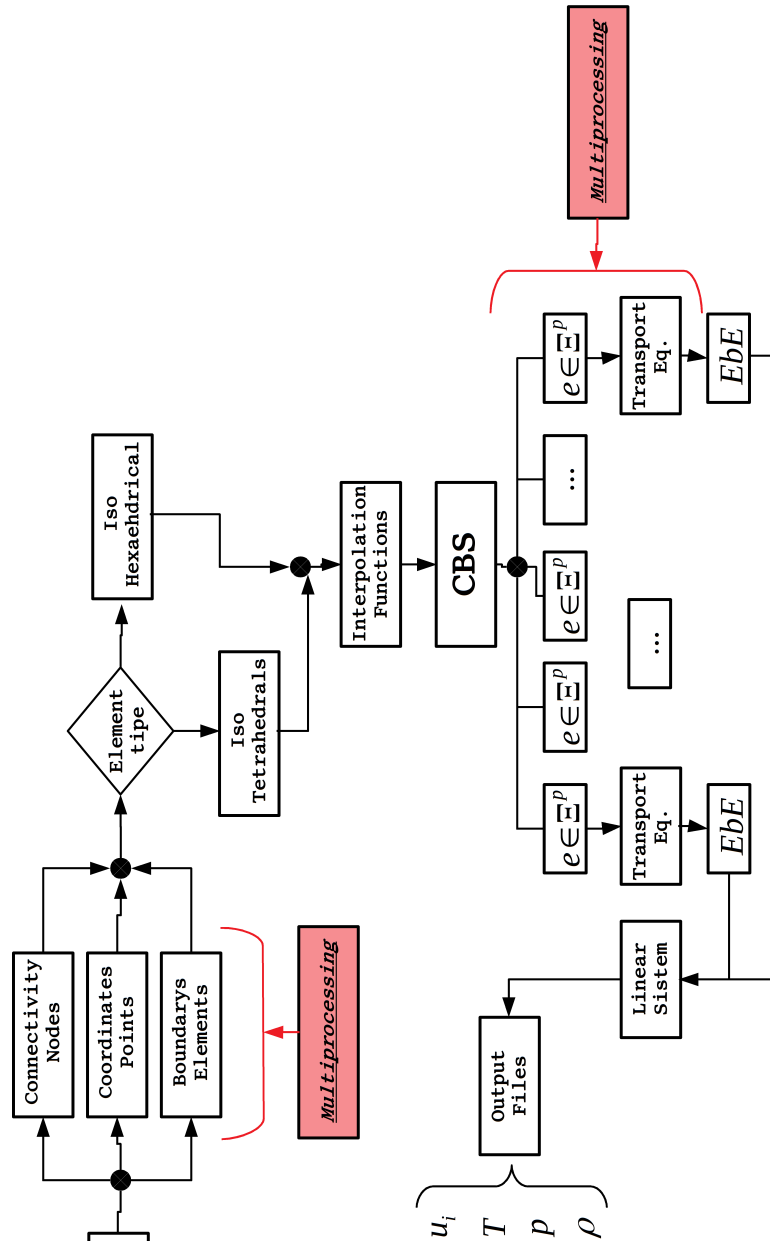
For the relocation procedure, the numbering of any element associated to the respective interpolations functions must produced a positive Jacobian determinant. Beginning from the first node at the first element all element nodes were tested for the sign of the Jacobian. In the negative case, the node being tested was exchanged by next one and so successively until all nodes of the element were subjected to scrutiny. This process was repeated until ensuring all elements with positive determinants. The whole procedure can be analysed in the code named *meshFV2FE.py*⁵.

⁵ <https://github.com/ruhanponce/Numerical-Investigation-CBS.git>

After the renumbering and reconstruction of the assembly matrix, the files in the folder **MakeToOpenFOAM** were loaded in parallel into memory with the help of the *Modin-Pandas* Python library.

The overall construction of the problem is characterized in Figure 9.

Figure 9 – Global scheme of parallelism methodology for CBS method in flow.



Source – Prepared by the author.

For the time being this framework is capable of processing only homogeneous meshes, either totally hexahedral or tetrahedral isoparametric elements, with linear interpolation functions.

After applying the CBS scheme, the domain was divided into blocks of partially common nodes of elements such that a number of blocks were attributed to a process to be run in parallel with all other processes.

Aiming at developing an useful parallelized framework for simulation of any turbulent incompressible and compressible reactive flows, it was necessary to simulate the most diverse types of flows to validate both the computational and the mathematical aspects. In the present work, the methodologies were tested in simpler incompressible non-reactive and reactive flows, which are benchmarks in the literature, in order to proceed with a solid and consistent solver. The results of these validations will be presented in the next section.

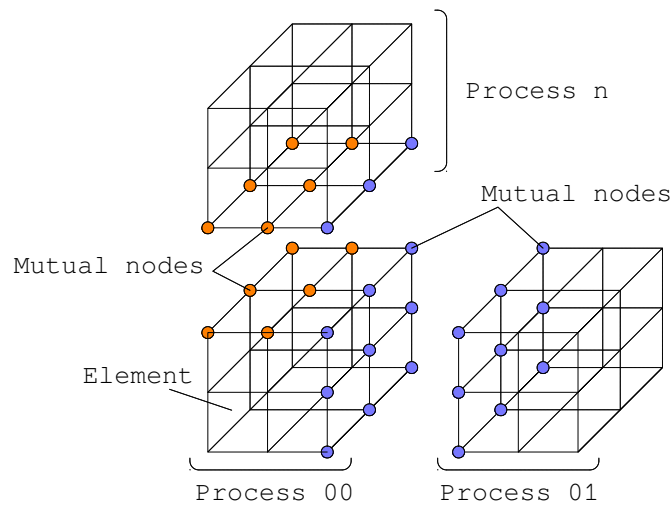
5 CONSISTENCY ANALYSIS

In this chapter several classic examples from the literature that have been simulated to validate the developed CBS-FEM parallel framework, for both incompressible and compressible reactive and non-reactive flows are described. In all simulations an explicit Euler scheme was applied for the time discretization, while for the spatial discretization, the CBS-FEM.

5.1 SpeedUp Test

For the development of a parallelized framework, the main obstacle might be the overhead incurred by the information sending and receiving between processes, represented by the mapping of the element blocks into several processes, see Figure 10.

Figure 10 – Mutual nodes in parallel process.



Source – Prepared by author.

Thus, the strategy used is that all element blocks would be evaluated separately and in parallel and the return of the information would be collected in serial way, such that the value of each common node would be the arithmetic average. Another point observed is that slicing the elements of the domain maintaining the symmetry of the problem, in relationship to the number of processes, a somewhat faster convergence could be observed.

In order to determine the relationship between the number of processes and the mesh size for one specific problem and a specific workstation several tests were performed, named *speedUp* tests. The chosen problem was the reconstruction of the assembly matrix

and the selected workstation is described in Table 3. The baseline for comparison was the entire process performed serially.

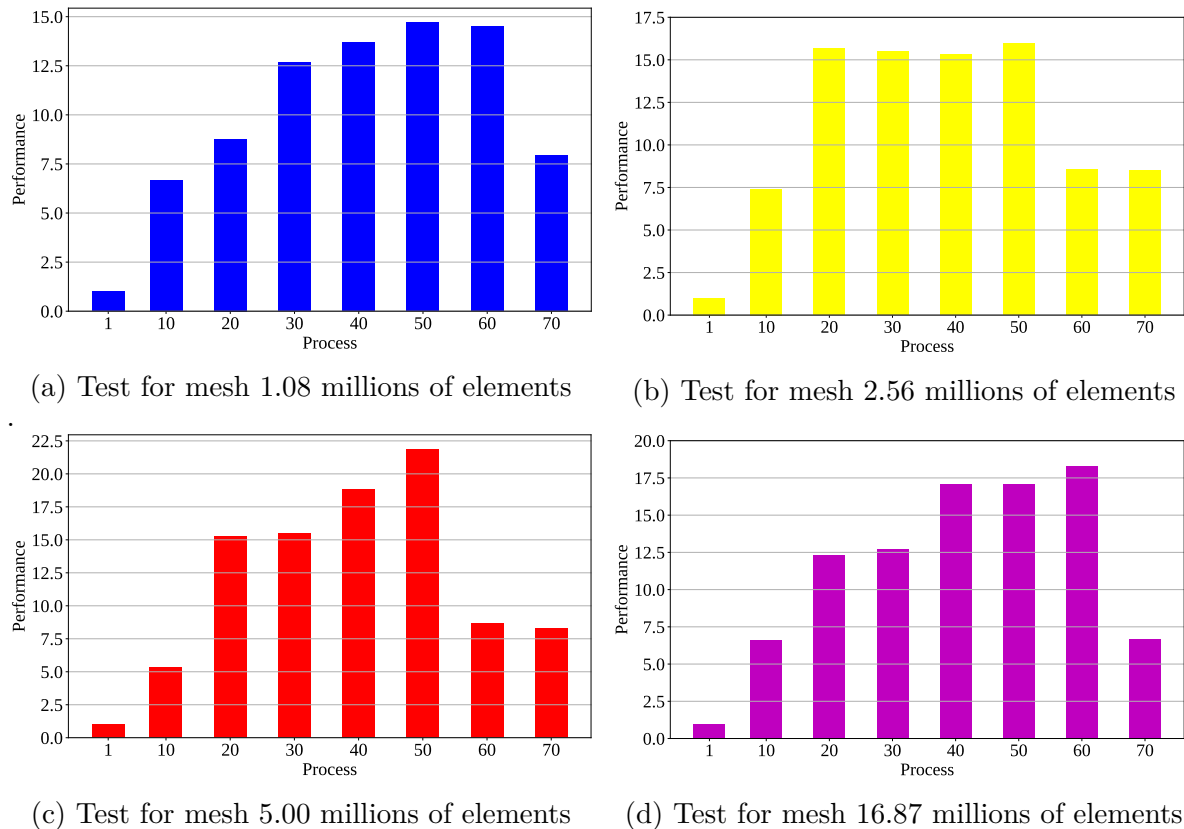
Table 3 – Machine architecture for computational simulation.

Host	X10DAi
CPU	Intel Xeon E5-2660 v4 (56) @ 3.200GHz
RAM	128 GB - DDR4@2800

Source – Prepared by author.

The tests were performed measuring the wall clock time for different homogeneous and uniform structured meshes, modifying only the number of elements, resulting in the data presented in the Figure 11.

Figure 11 – SpeedUp test for distinting grids.



Source – Prepared by author.

These figures 11b and 11c show that large overhead with 60 processes and more for 2.56 and 5.00 millions of elements whereas for 1.08 million (Figure 11a) and 16.87 million (Figure 11d).

These figures 11b and 11c show that large overhead with 60 processes and more for 2.56 and 5.00 millions of elements whereas for 1.08 million (Figure 11a) and 16.87 million (Figure 11d). However, by increasing the number of elements, performance improvements

are achieved, obtaining up to 22 times faster processing speeds. With that, it is constant for all the analyzed cases, guaranteeing high performance for 50 processes, resulting in great processing efficiency of the developed code.

An observation regarding the parallelism and python should be made; according to LANARO (2013) and the present work, the performance of multiprocessing and multithreading are different, being the Python multithreading fundamentally used for I/O while multiprocessing is actually applied for data processing. At this point, as optimized and parallelized libraries for I/O were used, multithreading was not used in the present work.

It can be seen that with the application of EbE, the non utilization of sparse matrices reflected in reductions of up to 70 %, in preliminary tests, together with the necessary RAM reduction

5.2 Lid-driven Cavity Flow

Lid-driven cavity flow is a classic two-dimensional and three-dimensional benchmark for incompressible flows WONG and BAKER, 2002. Thus, in order to validate the developed solver, the methodology was applied to analyze an isothermal flow by applying several structured and uniform meshes of varying dimensions, for the following Reynolds numbers: 100, 400 and 1000. To this, the CBS method was applied, together to concept of artificial compressibility, see Section B. This strategy was chosen because, according to KIRIS, HOUSMAN, and KWAK (2006), artificial compressibility is used for direct temporal resolution methods, not requiring predictor-corrective methods, and thereby minimizing the computational cost and the stability of direct temporal integration methods. Unlike the solution of a Poisson equation, which to obtain better stability must be applied together to implicit integration methods. Thus, when using artificial compressibility, together to Euler's temporal integration method, there is no need to use Step 3 of the methodology presented by ZIENKIEWICZ, TAYLOR, and NITHIARASU (2014) and seen in Section B, therefore; its application results in a slower convergence process and without significant improvements in the final results. Thus, from the concept of artificial compressibility, $\epsilon = 0.1$ was considered for all simulations performed.

Figure 12, characterizes the initial and boundary conditions presented in the problem in question. As a boundary condition for pressure, the condition of null normal gradient was used.

Thus, for incompressible cases, the time step applied for temporal integration was taking into account

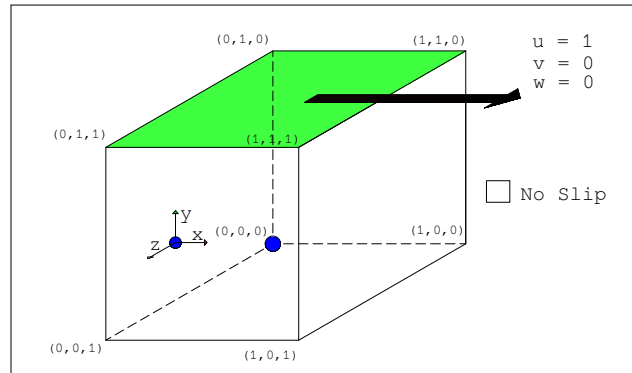
$$\Delta t = \frac{\bar{\Delta}}{|\mathbf{u}| + \beta} \quad (74)$$

$\bar{\Delta}$ being a characteristic length of the mesh, for which was used the diagonal of the smallest element of the hexagonal mesh.

The code developed for isothermal and incompressible flows was named *icoFlow* and for quantify the discrepancy in relation to the analysis performed by WONG and BAKER (2002), for a standard relative error, was adopted the norm L_∞ ¹ considering the velocity profiles at the middle planes inside the cavity.

The convergence criterion was a relative error of quantities, such as: speeds, temperature and pressure, in the order of 10^{-4} , criterion also used by ZIENKIEWICZ, TAYLOR, and NITHIARASU (2014).

Figure 12 – Scheme of geometry and boundary conditions apply over cavity.



Source – Prepared by author.

For the simulation, the chose fluid was air², modeled as perfect gas, under standard conditions of temperature and pressure ($T = 298.15 K$ and $p = 101325 Pa$). The results were normalized for comparison with the benchmark WONG and BAKER, 2002, as

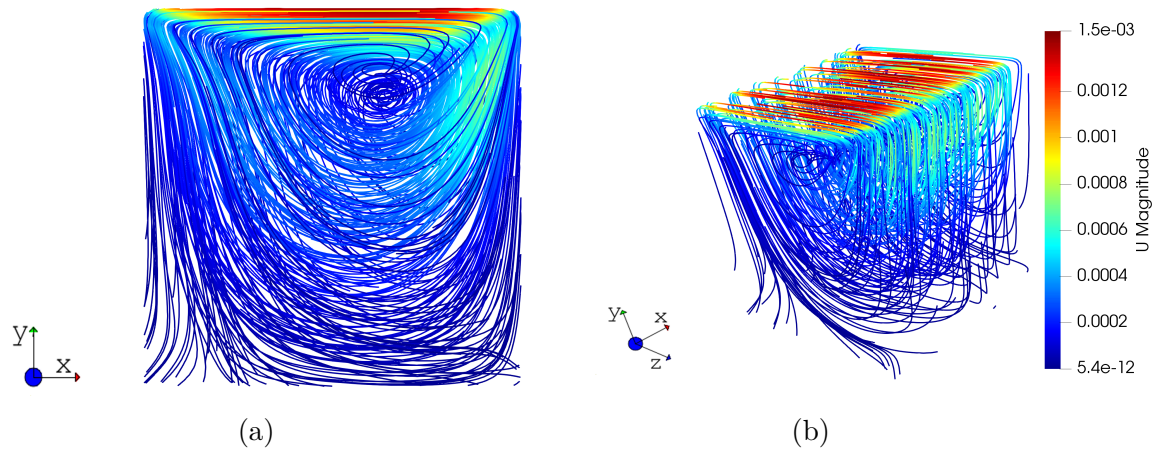
$$u_{j_{normalized}} = \frac{u_j - \min(u_j)}{\max(u_j) - \min(u_j)} \quad (75)$$

The first condition analyzed was for $Re = 100$, for that, it was considered a uniform structured mesh with a subdivision in each side of $40 \times 40 \times 40$, resulting 64000 hexahedral elements which corresponds to a topology with 68921 nodes. Figure 13 shows the streamlines obtained for the steady state condition, a) in plane view and b) 3D view.

¹ Chebyshev metric: allow define topology the function space.

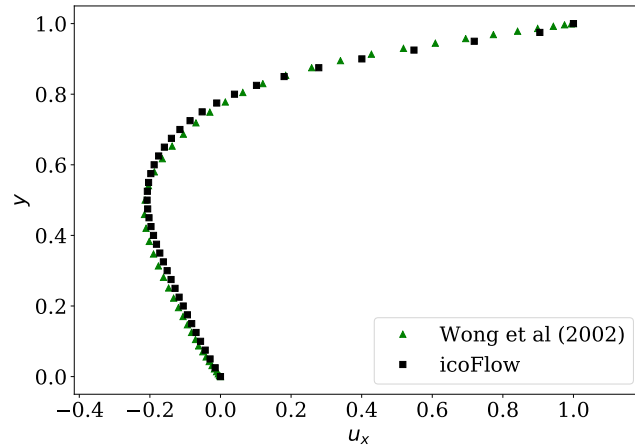
² 3.76 moles of N_2 by O_2 mol

Figure 13 – Streamlines behavior for Re 100.

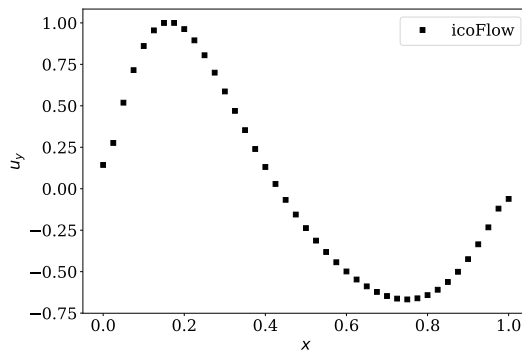


Source – Prepared by author.

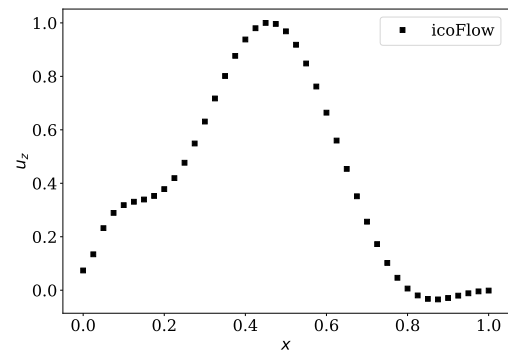
In Figure 13 it is possible to observe the formation of a central recirculation, observing from the point of view of Figure 13b this recirculation extends continuously throughout the center of the cavity. Such phenomenon is observed due to the advection generated in the domain, and for conditions of pure diffusion this phenomenon does not occur. The velocity profiles in x, y and z in each respective central plane of the domain are shown in Figure 14, and compared with WONG and BAKER (2002).

Figure 14 – 3D mid-plane centerline distributing for Re 100 for.

(a) Velocity profile in the x direction



(b) Velocity profil in the y direction



(c) Velocity profile in the z direction

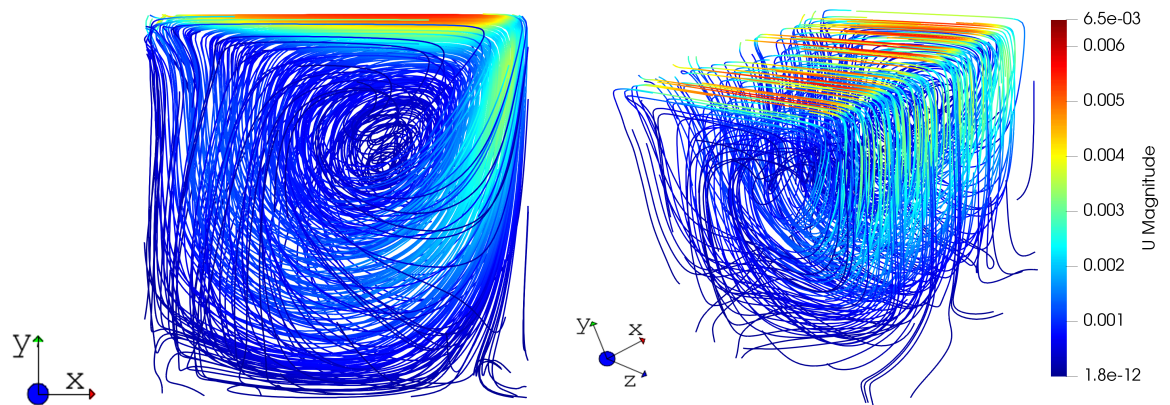
Source – Prepared by author.

With $Re = 100$ and the mesh analyzed, the relative error is of the order 8.70%, for the velocity in the x direction, Figure 14a. For the others directions WONG and BAKER (2002)'s work does not address them.

Regarding the real wall clock time of the process, it was noticed that the permanent regime for the imposed conditions was obtained close to 10 min.

For $Re = 400$ a structured and uniform mesh of $48 \times 48 \times 48$ was generated, obtaining 110592 hexahedral elements resulting in 117649 nodes. The Figure 15 presents the streamlines obtained in permanent regime.

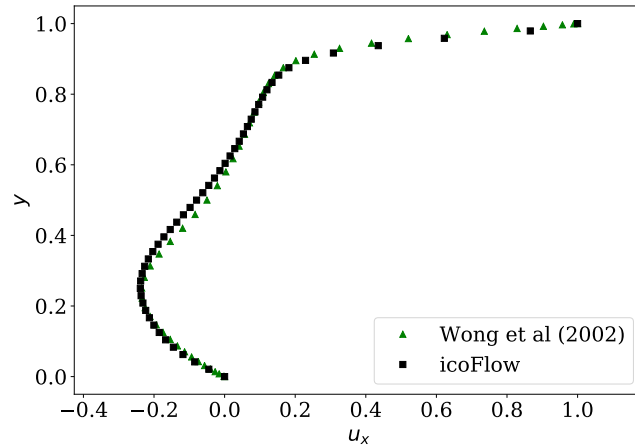
Figure 15 – Streamlines behavior for Re 400.



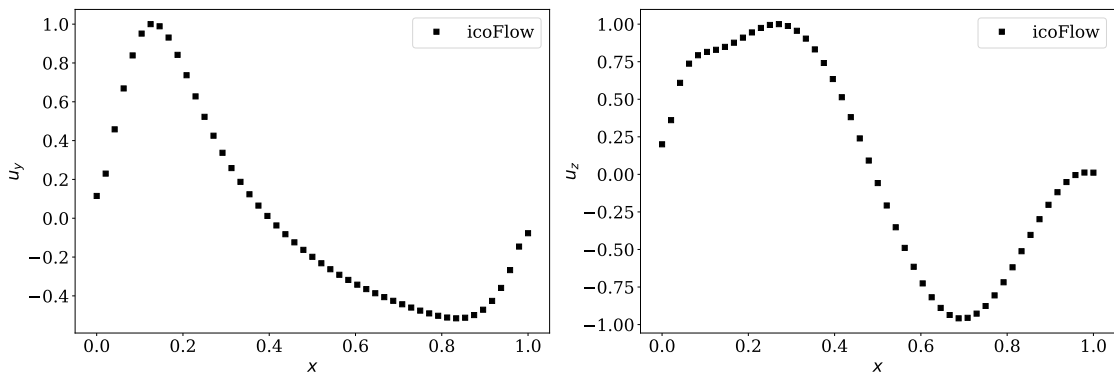
Source – Prepared by author.

The Figures 13 and 15 show the behaviour of the velocity field in domain by the streamlines, with recirculations appearing in the lower corners. In Figure 15, it is possible to verify that the principal vortex tends to the central region of the domain when the Reynolds number is increased. The behavior of velocity profiles is seen in Figure 16.

Figure 16 – 3D mid-plane centerline distributing for Re 400.



(a) Velocity profile in the x direction



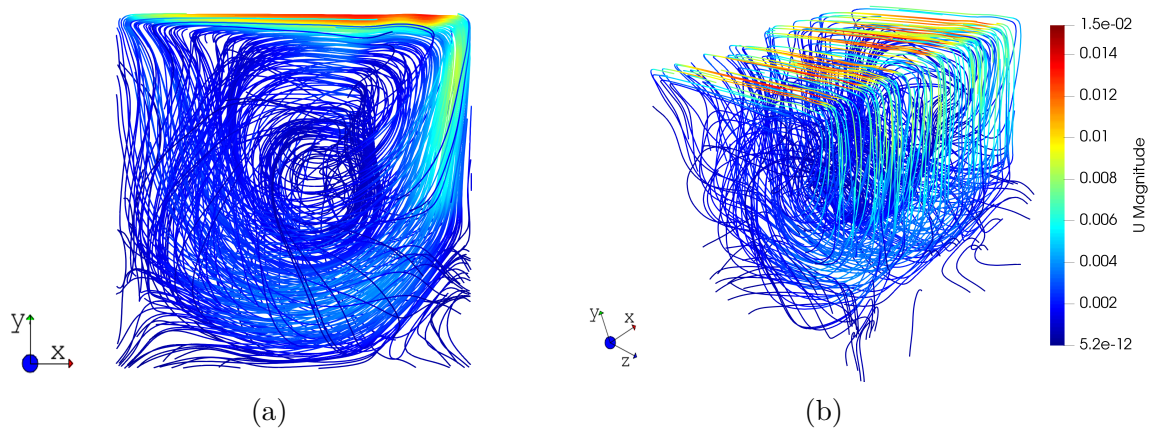
(b) Velocity profile in the y direction

(c) Velocity profile in the z direction

Source – Prepared by author.

For the mesh and the conditions analyzed and comparing with WONG and BAKER (2002), a relative error of 12.01% was obtained. The regime was permanently obtained in about 17 min in terms of wall clock time.

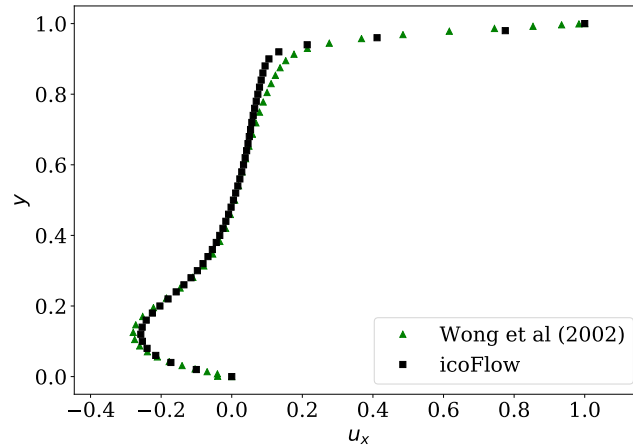
Finally, the last condition analyzed was for $Re = 1000$, applying a uniform structured mesh of $50 \times 50 \times 50$, generating 125000 hexahedral elements with 132651 nodes. According to ZIENKIEWICZ, TAYLOR, and NITHIARASU (2014) for three-dimensional flows, it is not possible to obtain a permanent solution for Reynolds greater than 1000, therefore, for this transition condition, the permanent regime was considered when the relative error of the quantities was in the order of 10^{-3} . Figure 17, the streamlines are represented.

Figure 17 – Streamlines behavior for Re 1000.

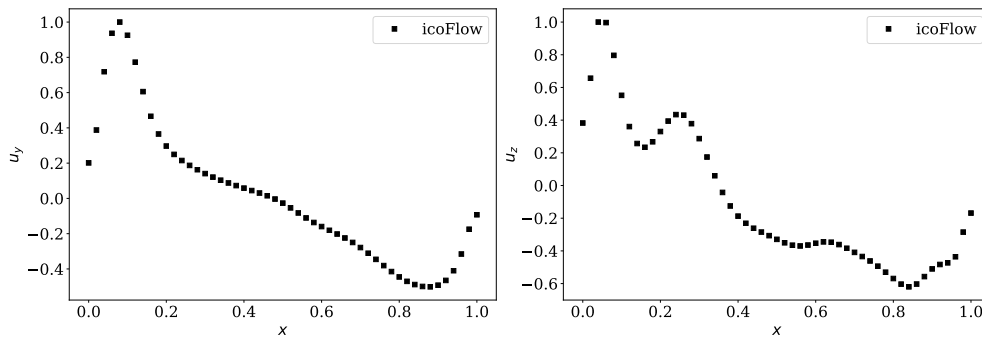
Source – Prepared by author.

Unlike the previous conditions, for $Re = 1000$ the streamlines presented in Figure 17b no longer present the same symmetry, a fact that proves the chaotic behavior for this condition that was observed by ZIENKIEWICZ, TAYLOR, and NITHIARASU (2014).

Figure 18 – 3D mid-plane centerline distributing for Re 1000.



(a) Velocity profile in the x direction



(b) Velocity profile in the y direction (c) Velocity profile in the z direction

Source – Prepared by author.

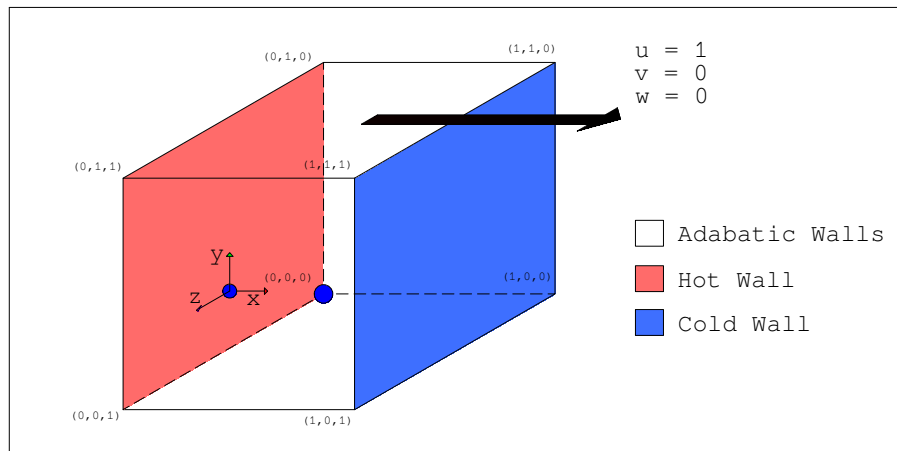
However, comparing with the analysis obtained by WONG and BAKER (2002) a relative error of 13.20% was obtained for velocity in x direction in the central plane. The region that achieved the highest discrepancy in relation to the benchmark was the upper region, corresponding to lid-driven. This region is the most critical, regardless of the number of Reynolds, there are occurrence of great discontinuities in the extremities of sliding wall. This phenomenon was also observed by GELFGAT (2019) and HACHEM et al. (2010) and a way of circumventing this problem is applying a more refined mesh. Therefore, for this problem it is advisable to use meshes greater than 25000 elements, or non-uniform meshes, capable of to capture such discontinuities.

For the lid-driven problem, low relative errors were obtained, which validates the methodology and framework developed for the continuity and momentum equations. A fact that must be observed is that the pressure behavior is not contemplated in the analyzes because the pressure drops were of order of 10^{-6} , and their influence during the period considered was a insignificant phenomenon.

5.3 Thermal Lid-driven Cavity

To validate the energy conservation equation, the thermal and lid-driven cavity problem was used for the Reynolds of 100, 400 and 1000, for which the program named *icoThermFlow* was developed. In this problem, steady state was assumed when the max relative error applying the standard L_∞ to the velocity and temperature was less than 10^{-4} . As a proper benchmark was not found in any of the analyzed references, the same problem in Ansys software was simulate to quantify and "validate" the developed code. The Figure 19 presents the conditions applied to the problem.

Figure 19 – Representation conditions on thermal-driven cavity.



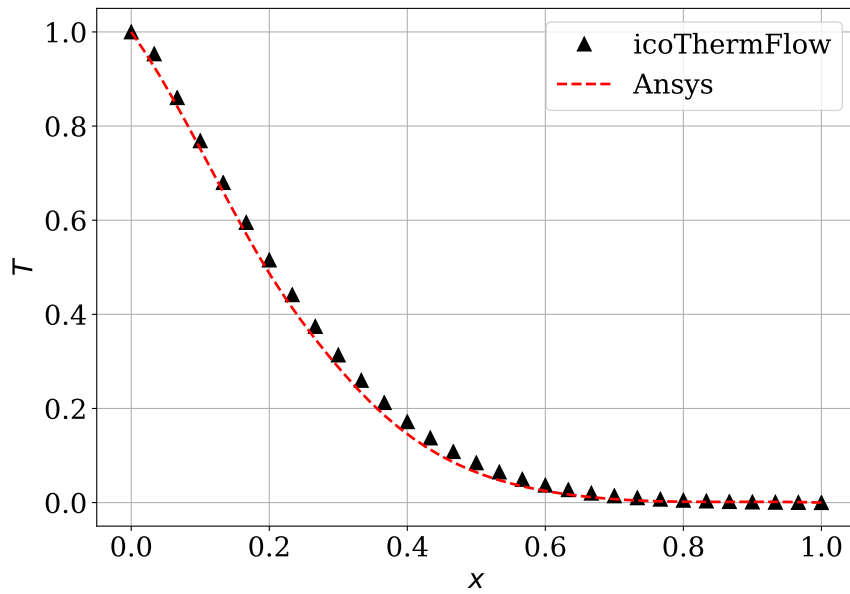
Source – Prepared by author.

In the problem presented in Figure 19 the conditions are presented normalized. However, as in the isothermal lid-driven cavity problem, equations were applied for air in standard conditions as the initial condition in the cavity, and prescribed temperatures of 423.15 K at the heated wall and 300.15 K at the cold wall were applied for all Reynolds numbers. The normalization of temperature is shown in Equation 76.

$$T_{normalized} = \frac{T - \min(T)}{\max(T) - \min(T)} \quad (76)$$

In all the analyzed conditions, a structured, homogeneous and uniform mesh of 30x30x30 was applied, resulting in 27000 hexahedral elements and 29791 nodes. Thus, for $Re = 100$, the behavior of temperature distribution in the central plane of the cavity was analyzed, obtaining the Figure 20.

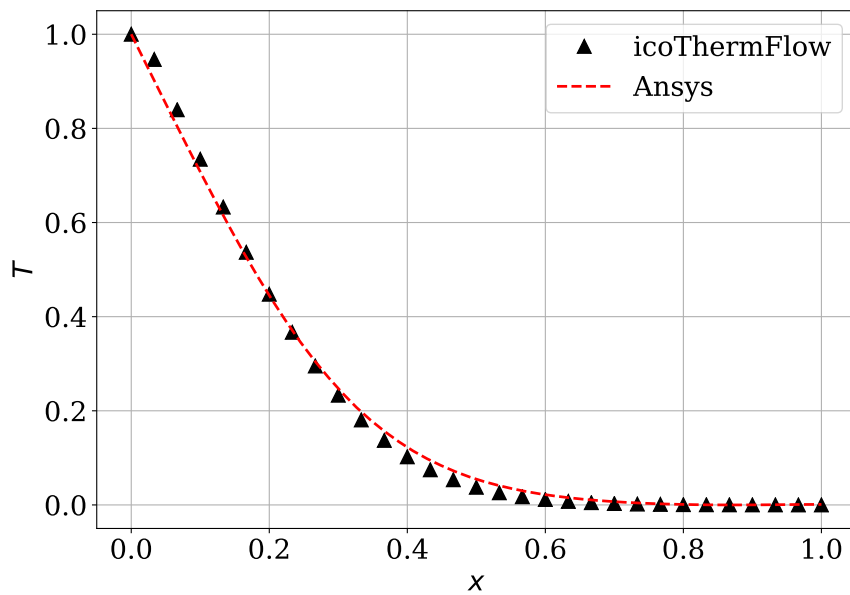
Figure 20 – Validation mid-plane temperature for Re 100.



Source – Prepared by author.

In all the analyzed conditions, a structured, homogeneous and uniform mesh of $30 \times 30 \times 30$ was applied, resulting in 27000 hexahedral elements and 29791 nodes. Thus, for $Re = 100$, the behavior of temperature distribution in the central plane of the cavity was obtained, as seen in Figure 20, for which a discrepancy of 2.83% was evaluated.

Figure 21 – Validation mid-plane temperature for Re 400.

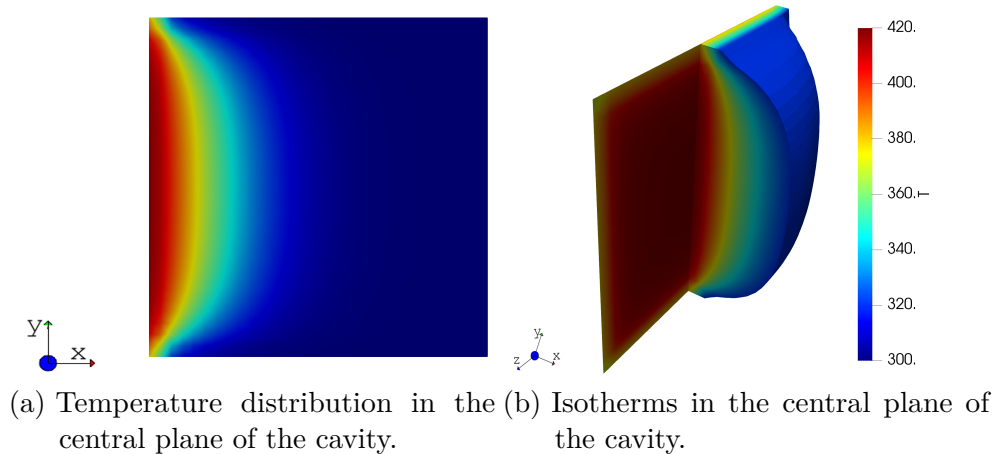


Source – Prepared by author.

In Figure 21 the relative error was 6.68%, and can be seen that the temperature stabilization occurred over a distance, considering the central plane, less than that presented

in Figure 20, characteristic of the increase in Reynolds and consequently forced convection, generating a greater exchange of heat. The three-dimensional behavior of the temperature in the cavity is shown in the Figure 22.

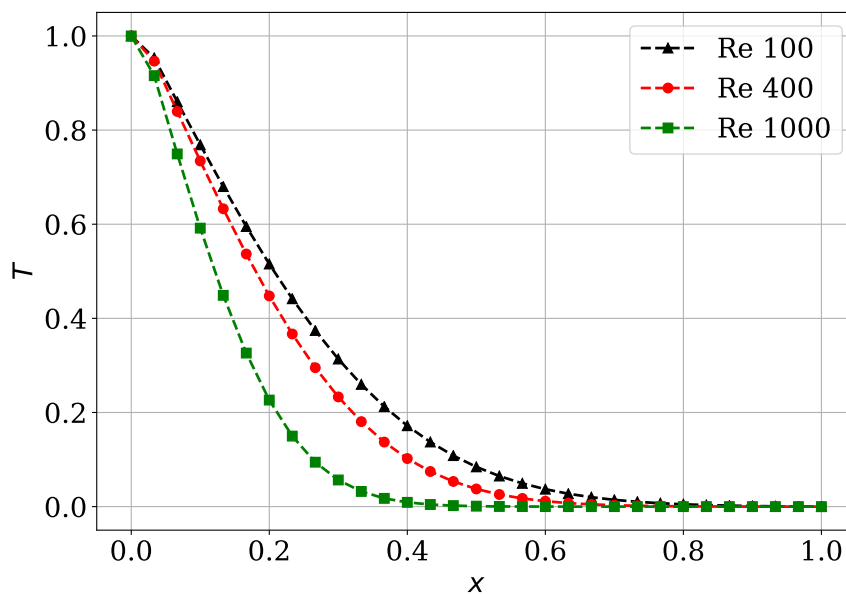
Figure 22 – Temperature distributing for Re 400.



Source – Prepared by author.

In order to verify the temperature stabilization behavior with the increase in the Reynolds number, the central temperature distributions for the Reynolds of 100, 400 and 1000 were simulated and compared, obtaining the Figure 23.

Figure 23 – Temperature distribution in the central plane for different Reynolds.



Source – Prepared by author.

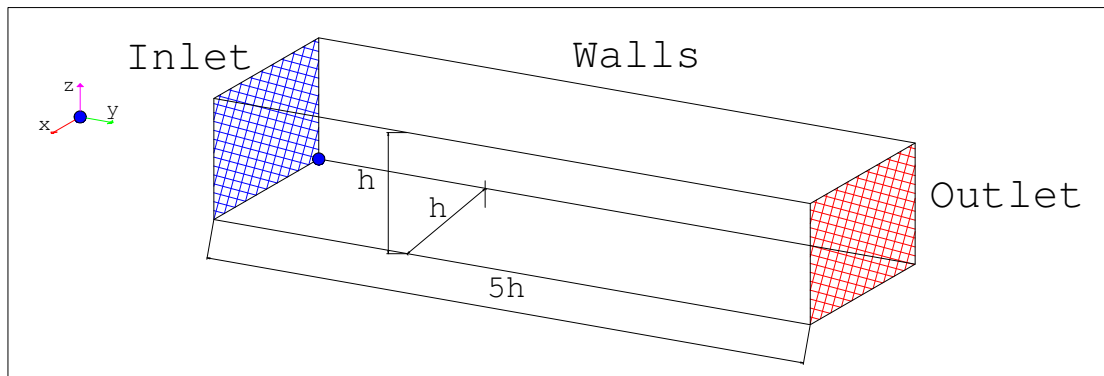
Figure 23 represents a faithful phenomenon of forced convection, which with the increase in the number of Reynolds there is a stabilization of temperature over shorter distances.

Finally, for Reynolds 100 and 400, the discrepancies regarding the results of Ansys simulatons were small, which "validates" in some sort the methodology and the program developed by the author.

5.4 Flow in Channel of Square Cross Section

The analysis of Channel Flow of square cross section aims to verify the behaviour of an isothermal incompressible flow internally in a duct. For this, the geometric conditions are presented in Figure 24.

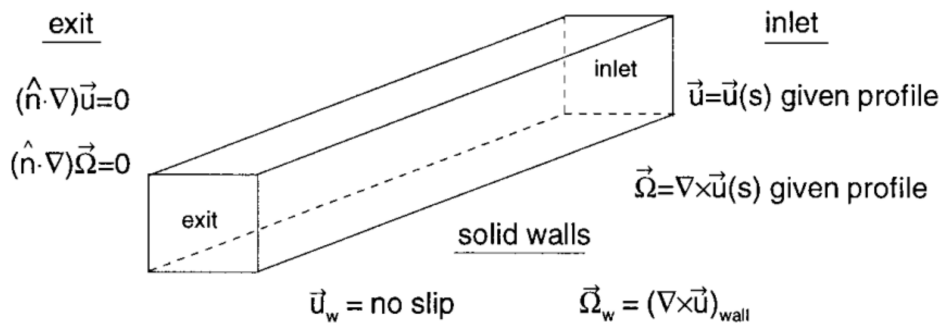
Figure 24 – Geometry of square channel.



Source – Prepared by author.

The boundary and initial conditions were the same as those applied by WONG and BAKER (2002) as explained in Figure 25.

Figure 25 – Boundary conditions for straight channel flow.



Source – WONG and BAKER (2002).

An analytical solution for this flow in a permanent pipeline is presented by WHITE (1974), it is given by

$$u = \frac{48}{\pi^3} \frac{\xi_u(y, z, h^*)}{\varphi} \tag{77a}$$

$$\xi_u(y, z, h^*) = \sum_{n=1,3,5}^N (-1)^{\frac{(n-1)}{2}} \left[1 - \frac{\cosh\left(\frac{n\pi y}{2h^*}\right)}{\cosh\left(\frac{n\pi}{2}\right)} \right] \frac{\cos(n\pi z)}{n^3} \quad (77b)$$

$$\varphi = 1 - \frac{192}{\pi^5} \sum_{n=1,3,5}^N \frac{\tanh\left(\frac{n\pi}{2}\right)}{n^5} \quad (77c)$$

where h^* is the half height of the duct and N is a large integer, for example, $N = 300$ is used.

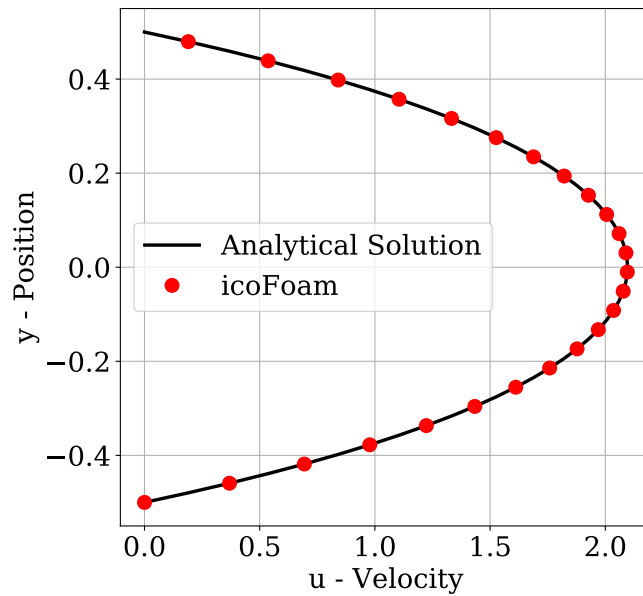
Thus, the simulation has been done for the given boundary conditions presented in Figure 25, for the Square Channel flow to verify the error in relation to the analytical model. For this, a structured, homogeneous and non-uniform mesh was used, applying an arrangement of 30 elements in the main flow direction and 150x30 in the cross section, resulting in 135000 hexahedral elements and 145111 nodes. For mesh non-uniformity, the conditions presented in Table 4 were applied in *simpleGrading*, OpenFOAM toolbox of mesh manipulation.

Table 4 – Parameters of mesh non-uniformity.

	x-direction expansion ratio		
	% - x direction	% - y direction	% - z direction
% - x direction	0.200	0.333	8
% - y direction	0.600	0.333	1
% - z direction	0.200	0.334	0.125
	z-direction expansion ratio		
	% - x direction	% - y direction	% - z direction
% - x direction	0.200	0.333	8
% - y direction	0.600	0.333	1
% - z direction	0.200	0.334	0.125

In the y direction, a uniform distribution of the mesh elements was applied, the ?? shows the non-uniform mesh distribution. Thereby, obtain Figure 26 for condition of $Re = 100$.

Figure 26 – Velocity profile in steady state center plane 3D fully developed channel flow for $Re = 100$.



Source – Prepared by author.

A comparison of the analytical and numerical results, Figure 26, resulted in a relative error of 0.15%, obtaining almost an exact solution for the analyzed conditions.

5.5 Combustion Chamber

The underlying geometry directly influences the mathematical model, with respect to the choice of the coordinate system that will be used for the discretization of the equations.

The central coaxial injector used by MAESTRO et al. (2016) results in an essentially non-premixed combustion, which contrasts with this work proposal. As an alternative, a simpler injector was proposed in order to assure premixed combustion. Table 5 displays the geometrical dimensions of the combustion chamber and the injector.

Table 5 – Characteristic combustion chamber and injector dimensions.

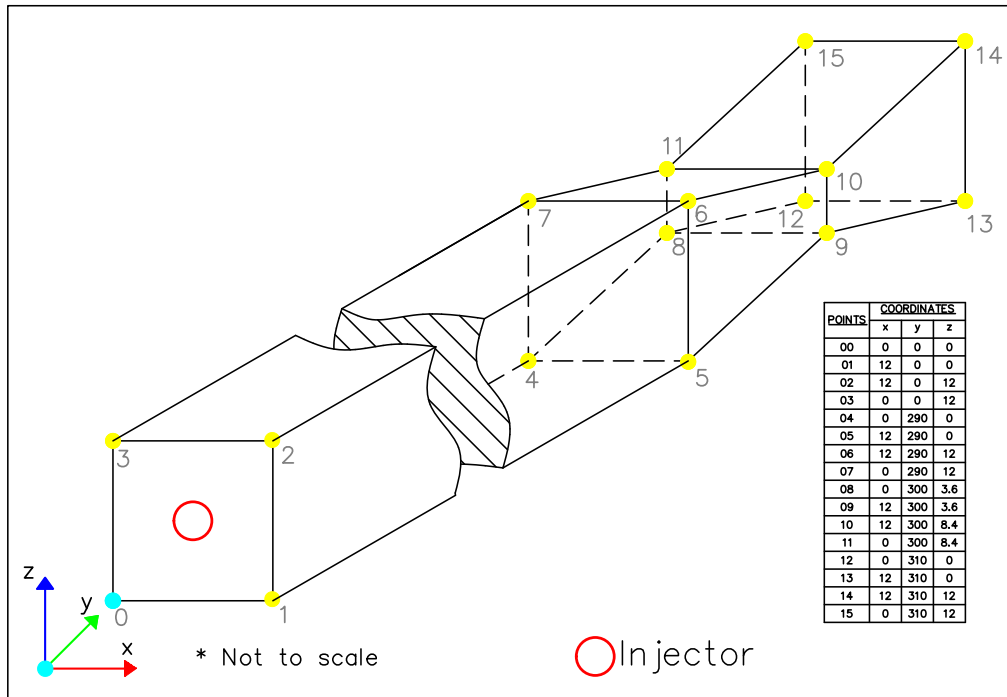
Combustion chamber			Injector	
Chamber length	[mm]	290	GCH_4/GOx diameter	[mm] 5
Chamber width	[mm]	12	GCH_4/GOx post recess*	[mm] 0
Chamber height	[mm]	12		
Throat height	[mm]	4.8		
Contraction ratio A_{cc}/A_{th}	[-]	2.5		

*Post recess is the distance from the front of the injector to the installation wall.

Source – Prepared by author adapted from MAESTRO et al. (2016).

For better characterization of the geometry Figure 27 is presented.

Figure 27 – Combustion chamber, injector and nozzle geometries.



Source – Prepared by author.

The nominal operating conditions in the present study are similar to those applied by MAESTRO et al. (2016) and are represented in Table 6.

Table 6 – Nominal conditions operating.

Temperature*	Methane	269	[K]
	Oxygen	278	[K]
Chamber Pressure		20	[bar]
Mass flow rates	Methane	0.0017	[kg/s]
	Oxygen	0.0045	[kg/s]

*Gaseous

Source – MAESTRO et al. (2016).

For the boundary conditions, those presented in the work of FERZIGER and PERIĆ (2002) for compressible flows were employed.

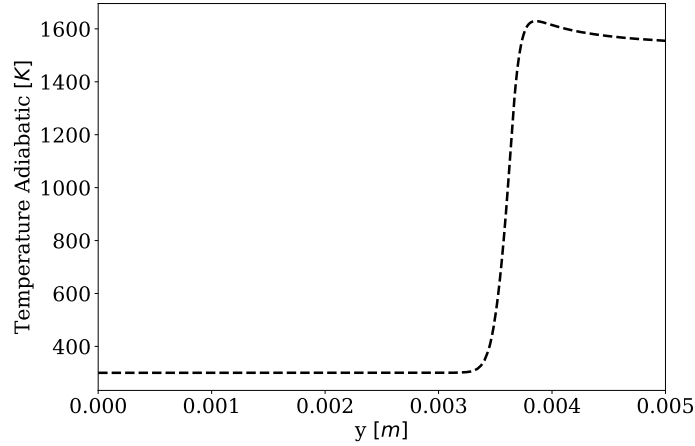
5.5.1 Combustion

Still with the objective of aligning the studies with the work of MAESTRO et al. (2016), the behavior of premixed combustion with homogeneous charge, for unidimensional flow along the length of the combustion chamber presented in Figure 27 was analyzed. To this, the Cantera library was used, considering that such effects occurred with a fixed flame front at the entrance of the combustion chamber. The analyzed mix was GCH_4/GO_2 , with

the fuel ratio of 2.6 and the pressurized chamber at 20 bar. The mass flow rate of the mixture was $\dot{m} = 0.003 \text{ kg/s}$ applied under a 5mm nozzle, see Table 6.

In order to verify the thickness of the flame front, as shown by BLINT (1986), the behavior for an adiabatic combustion flame of GCH_4/GO_2 was simulated, obtaining the Figure 28.

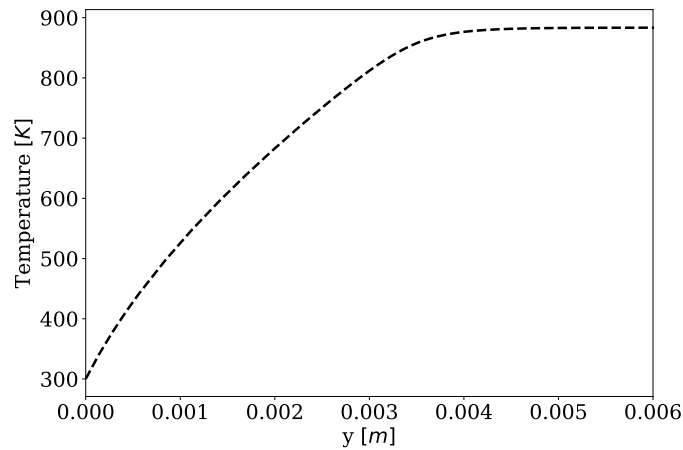
Figure 28 – Release temperature for adiabatic flame.



Source – Prepared by author.

In this way, the code developed to analyze the one-dimensional combustion of the temperature distribution in front of the chemical reaction was obtained, showing the behavior presented in Figure 29.

Figure 29 – Release temperature combustion process.



Source – Prepared by author.

By BLINT (1986) the flame width is

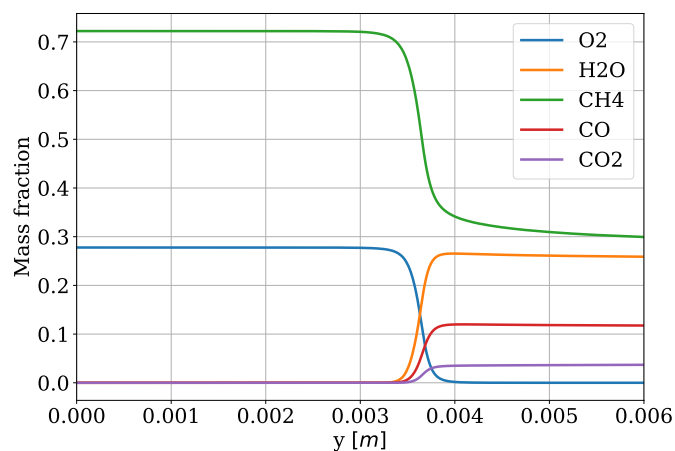
$$\delta T = \frac{T_a - T_u}{\left(\frac{dT}{dx}\right)_{max}} \quad (78)$$

To the conditions analyzed in Figure 28 and Figure 29, and applying the BLINT (1986) method, it was obtained 0.0051 m for the flame width.

Observing the Figure 28 it is noted that during the adiabatic combustion process, there is a region of discontinuity that presents an abrupt release of heat, there is a preheat of the unburned gases due to the diffusion process. The behaviour presented in Figure 29 doesn't present such discontinuity.

Thus, for the established conditions it was possible to verify the mass fractions of 53 chemical species, during the chemical reaction process of combustion. In Figure 30 the most expressive combustion products are presented.

Figure 30 – Mass fraction com conditions of flame fixed.



Source – Prepared by author.

From Figure 30 it is noticed that the limiting of the chemical reaction was oxygen, which, after the flame front, is completely consumed. For the fixed flame condition, it appears that there is the possibility of continuing the combustion process, if the domain is fed with more oxidizer and makes several flame fronts.

5.5.2 Cold Flow in a Chamber Combustion

To analyze the combustion phenomenon in the geometry employed by MAESTRO et al. (2016) it is necessary to evaluate the flow behavior of the homogeneous mixture inside the combustion chamber. This has been done based on the geometry presented in Figure 27, and the same boundary conditions applied for the analysis of one-dimensional combustion. For modeling, incompressible, turbulent and isothermal flow was considered. The turbulence in the flow is due to the discontinuity caused by the injector, which generates low pressure zones in its surrounding regions. The domain discretization was made by a homogeneous and non-uniform structured mesh, composed by 50 divisions in the x-axis, 1200 divisions in the y-axis and 50 divisions in the z-axis, generating 3 millions

hexahedral elements with 3123801 nodes. For non-uniformity, *simpleGrading* was used, with the settings presented in Table 7.

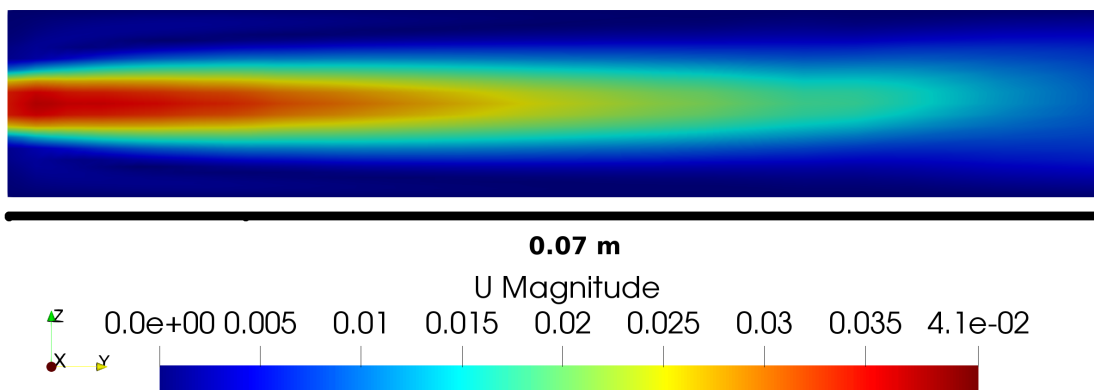
Table 7 – Parameters of mesh non-uniformity for chamber combustion flow with LES.

	x-direction expansion ratio		
	% - x direction	% - y direction	% - z direction
% - x direction	0.200	0.333	4
% - y direction	0.600	0.333	1
% - z direction	0.200	0.334	0.25
	y-direction expansion ratio		
	% - x direction	% - y direction	% - z direction
% - x direction	0.200	0.333	4
% - y direction	0.600	0.333	1
% - z direction	0.200	0.334	0.25
	z-direction expansion ratio		
	% - x direction	% - y direction	% - z direction
% - x direction	0.200	0.333	4
% - y direction	0.600	0.333	1
% - z direction	0.200	0.334	0.25

Source – Prepared by author.

Thus, the domain velocity field was obtained, as a stop criterion was considered when the flow at the exit of the chamber was completely developed, generating the fully developed velocity profile observed by WHITE (1974). In the Figure 31 is shown the magnitude of the velocity field for the region close to the injector.

Figure 31 – Speed field near the injector.



From the velocity field presented by Figure 31, the profiles in the central plane, with normal vector in x-direction, for the y positions at 0.001, 0.01 and 0.03 meters were obtained in order to show the recirculations close to the injector.

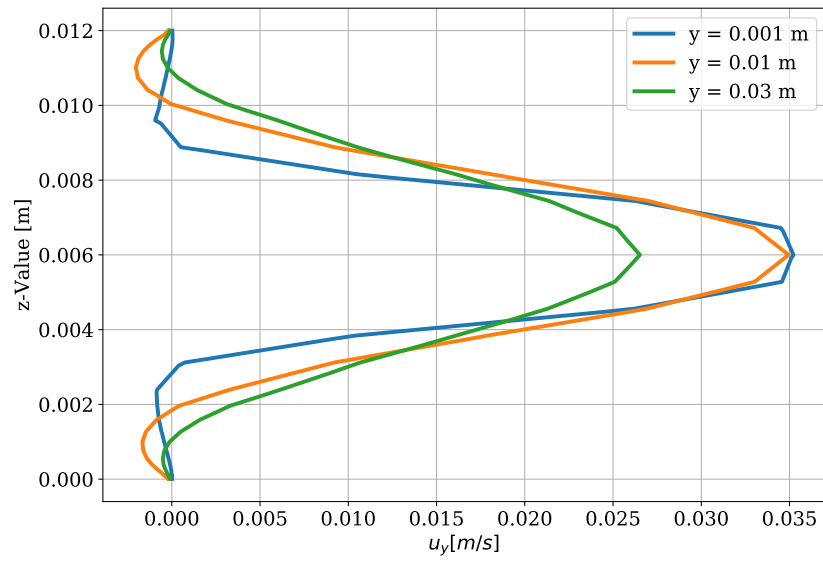


Figure 32 – Profiles for distinct y position near injector.

For more details on the velocity field and the transient behavior of the flow in the combustion chamber see PONCE, 2019.

6 CONCLUSION

From the present work it can be concluded so far, in several aspects analyzed, primarily, that there is great difficulty linked to the reproducibility of the analyzed works, either with regard to the boundary and initial conditions, or even to characterize the discretization method used, whether deliberate or not, resulting in a point for debate by the academic community.

About the discretization method, it is not difficult to manipulate the transport equations to obtain the weak form in preparation to FEM discretization. Associated with isoparametric elements and the corresponding interpolation functions (or shape functions), the Jacobian and its determinant are, as the basis transformation matrices, easily obtained, leading in a natural way to the integration by Gauss rule.

More specifically to the CBS stabilization scheme, the splits proposed by ZIENKIEWICZ, TAYLOR, and NITHIARASU (2014) are developed in Taylor expansion form disregarding the derivatives of third and higher orders. However, if the second order terms were not taken into account, parameters such as shear stress in the context of turbulence modeling would suffer large interference.

Regarding the mathematical model, in this work a novel analytical model for the turbulence equations closure was proposed, in order to lower the computational costs, without loss in the quality of results.

As for the TCI, linked to the turbulence and combustion, the Flamelet/Progress Variable model was employed, causing the addition of dozens of transport equations, further strengthening the idea of analytical models for the closure.

In the aspect of applied programming, the first was the optimization of data processing due to the need for very refined meshes, a fact attributed to LES. To this end, it is proposed to modularize the problem, so, with some independence between modules, there is possible generalizations of program use, and a module can be triggered or not according to the problem to be solved. Another point is that the use of parallel programming, performed on both CPUs and GPUs, optimizes all available tools in the both architectures, reducing computational time, and the need for high processing workstations or even clusters.

Still, regarding the programming, the non utilization of sparse matrices reflected in reductions of up to 70 %, in preliminary tests, together with the necessary RAM reduction, along with a performance improvement of up to 22 times compared to the serial program.

In addition to the focus on validation of numerical and computational aspects, the present work proposes a new mathematical model to address the phenomenon of turbulent flow and turbulent combustion, although the latter has not yet been validated. However, in the invested aspects, the framework proves to be consistent and robust to support several

mesh configurations, obtaining results with low errors.

Regarding the case study, the characterization of the discontinuity generated by the turbulence in the injector was responsible for the use of a more robust computational mesh, in order to meet the criteria of the LES model with the modeling of small scales. However, a difficulty found in the applied numerical method was the Eulerian temporal integration model, which being of first order is easily unstable, requiring the use of Courant numbers (CFL) less than 0.1, which increases the computational time to capture the transient phenomena.

REFERENCES

- SARAIVA, J. F. S., A. C. LESSA, and A. J. R. D. ROCHA (2007). “**História das Relações Internacionais Contemporâneas: da sociedade internacional do século XIX à era da globalização**”, ed. by I. B. de Relações Internacionais. 2ª. AV. Marquês de São Vicente, 1697, Barra Funda, São Paulo: Editora Saraiva.
- CHANG, I.-S. (2000). “**Overview of World Space Launches**”, ed. by T. A. Corporation. Vol. 16. 5. El Segundo, California, U.S.A.: JOURNAL OF PROPULSION and POWER - AIAA.
- ANDERSON JR, J. D. (2015). “**Riding the Crest: A History of Michigan’s Aerospace Engineering Department**”, ed. by N. Air and S. I. Space Museum. Vol. 53. 4. Washington, D.C.: AIAA JOURNAL, p. 12.
- ISECG, I. S. E. C. G. (Aug. 2013). “**The Global Exploration Roadmap**”, International Space Exploration Coordination Group, p. 50.
- HUOT, D. (2017). “**Additional Crew Flights Boost Space Station Science and Research**”, NASA.
- SUTTON, G. P. and O. BIBLARZ (2001). “**Rocket Propulsion Elements**”, 7th ed. 605 Third Avenue, New York, NY: John Wiley & Sons Singapore Pte Ltd, p. 765.
- WANG, Z.-G. (2016). “**Internal Combustion Processes of Liquid Rocket Engines: Modeling and Numerical Simulations**”, ed. by N. D. I. Press. China: John Wiley & Sons Singapore Pte Ltd, p. 395.
- MAESTRO, D., B. CUENOT, L. SELLE, G. FRANK, M. PIFTZNER, Y. DAIMON, R. KELLER, P. GERLINGER, and A. CHEMNITZ (2016). “**Numerical Investigation of Flow and Combustion in a Single-Element GCH_4/GOX Rocket Combustor: Chemistry Modeling and Turbulence-Combustion Interaction**”, ed. by A. I. o. A. a. A. AIAA. Salt Lake City, UT, USA: 52nd AIAA/SAE/ASEE Joint Propulsion Conference, p. 12. DOI: 10.2514/6.2016-4996.
- CHEN, C.-C. and P. M. MATHIAS (2002). “**Applied Thermodynamics for Process Modeling**”, vol. 48. Disponível em: <http://dx.doi.org/10.1002/aic.690480202>: American Institute of Chemical Engineers, pp. 194–200.
- LIANG, P.-Y., S. FISHER, and Y. M. CHANG (1986). “**Comprehensive Modeling of a Liquid Rocket Combustion Chamber**”, vol. 2. 2. Canoga Park, California: Rockwell International, p. 8.
- MÜHLBAUER, B., R. EWERT, O. KORNOW, and B. NOLL (2012). “**Broadband combustion noise simulation of open non-premixed turbulent jet flames**”, vol. 11. 1. International Journal of Aeroacoustics, pp. 1–24. DOI: 10.1260/1475-472X.11.1.1.

- CAO, D., G. HE, F. QIN, X. WEI, and Z. HUANG (2015). “**LES of Turbulent Reacting Flow in a Rocket Based Combined Cycle Combustor**”, ed. by A. I. o. A. a. A. AIAA. 3649. Glasgow, Scotland: 20th AIAA International Space Planes, Hypersonic Systems, and Technologies Conference, p. 15. DOI: 10.2514/6.2015-3649.
- DEKENA, M. and N. PETERS (1999). “**Combustion Modeling with the G-Equation**”, *Oil & Gas Science and Technology*, vol. 54, no. 2, pp. 265–270. DOI: 10.2516/ogst:1999024.
- MARTIN, C. E., L. BENOIT, Y. SOMMERER, F. NICLOUD, and T. POINCOT (2006). “**Large-Eddy Simulation and Acoustic Analysis of a Swirled Staged Turbulent Combustor**”, ed. by A. I. o. A. a. A. AIAA. Vol. 44. 4. AIAA Journal, p. 10. DOI: 10.2514/1.14689.
- BOGER, M., D. VEYNANTE, H. BOUGHANEM, and A. THOUVÉ (1998). “**Direct Numerical Simulation Analysis of Flame Surface Density Comnvept for Large Eddy Simulation od Turbulent Premixed Combustion**”, France: Twenty-Seventh Symposium (International) on Combustion/The Combustion Institute, pp. 917–925. DOI: [https://doi.org/10.1016/S0082-0784\(98\)80489-X](https://doi.org/10.1016/S0082-0784(98)80489-X).
- OEFELEIN, J. C. (2015). “**Analysis of Turbulent Combustion Modeling Approaches for Aero-Propulsion Applications**”, ed. by A. I. o. A. a. A. AIAA. 53rd AIAA Aerospace Sciences Meeting, p. 16. DOI: 10.2514/6.2015-1378.
- ALBAYRAK, A. and W. POLIFKE (2017). “**An analytical model based on the G-equation for the response of technically premixed flames to perturbations of equivalence ratio**”, ed. by SAGE. Vol. 0. 0. International Journal of Spray and Combustion Dynamics, pp. 1–8. DOI: 10.1177/1756827717740776.
- LIU, Y., A. DOWLING, T. DUNSTAN, and N. SWAMINATHAN (Apr. 2012). “**Modeling of combustion noise spectrum from turbulent premixed flames**”. In: *Acoustics 2012*. Ed. by S. F. d’Acoustique. Nantes, France.
- HUO, H. and V. YANG (2017). “**Large-Eddy Simulation of Supercritical Combustion: Model Validation Against Gaseous H₂–O₂ Injector**”, ed. by A. I. o. A. a. A. AIAA. Journal of Propulsion and Power, p. 13. DOI: 10.2514/1.B36368.
- LIPATNIKOV, A. N., J. CHOMIAK, V. A. SABELNIKOV, S. NISHIKI, and T. HASEGAWA (2017). “**A DNS study of the physical mechanisms associated with density ratio influence on turbulent burning velocity in premixed flames**”, ed. by T. bibinitperiod Francis. Combustion Theory and Modelling, pp. 131–155. DOI: 10.1080/13647830.2017.1390265.
- CHUNG, T. J. (2002). “**Computational Fluid Dynamics**”, vol. Only. The Edinburgh Building, Cambridge CB2 2RU, UK: Cambridge University Press, p. 1022.
- HIRSCH, C. (1994). “**Numerical Computation of internal and External Flows: Computational Methods for Inviscid and Viscous Flows**”, vol. 2. John Wiley & Sons Ltd., p. 715.

- FERZIGER, J. H. and M. PERIĆ (2002). “**Computational Methods for Fluid Dynamics**”, 3rd ed. Springer, p. 431.
- CONNOR, J. J. and C. A. BREBBIA (1976). “**Finite Element Techniques for Fluid Flow**”, 3rd ed. London: 88 Kingsway, WC2B 6AB: Newnes-Butterworths, p. 324.
- ZIENKIEWICZ, O. C., R. L. TAYLOR, and P. NITHIARASU (2014). “**The Finite Element Method for Fluid Dynamics**”, 7th ed. ELSEVIER, pp. 1–581.
- SCHLIMPERT, S., S. KOH, K. PAUSCH, M. MEINKE, and W. SCHRÖDER (2016). “**Analysis of combustion noise of a turbulent premixed slot jet flame**”, ed. by Elsevier. Vol. 175. *Combustion and Flame*, pp. 292–306. DOI: 10.1016/j.combustflame.2016.08.001.
- DOMINGO, P., L. VERVISCH, S. PAYET, and R. HAUGUEL (2005). “**DNS of a premixed turbulent V flame and LES of a ducted flame using a FSD-PDF subgrid scale closure with FPI-tabulated chemistry**”, *Combustion and Flame*, vol. 143, pp. 566–586. DOI: 10.1016/j.combustflame.2005.08.023.
- POTTURI, A. S., C. H. PATTON, and J. R. EDWARDS (2017). “**Advanced LES Models for Turbulent Combustion**”, ed. by A. I. o. A. a. A. AIAA. Grapevine, Texas, USA: 55th AIAA Aerospace Sciences Meeting, p. 16. DOI: 10.2514/6.2017-1792.
- NAGHIAN, M., M. LASHKARBOLOK, and E. JABBARI (2017). “**Numerical Simulation of Turbulent Flow Using a Least-Squares Based Meshless Method**”, *International Journal of Civil Engineering*, vol. 15, pp. 77–87. DOI: 10.1007/s40999-016-0087-1.
- DAVIDSON, P. A. (2004). “**Turbulence an Introduction for Scientists and Engineers**”, vol. One. New York: Oxford University Press.
- FRÖHLICH, J. and D. V. TERZI (2008). “**Hybrid LES/RANS Methods for the Simulation of Turbulent Flow**”, *Progress in Aerospace Sciences*, vol. 44, pp. 349–377. DOI: 10.1016/j.paerosci.2008.05.001.
- THAKUR, S., J. WRIGHT, M. IHME, and P. K. TUCKER (2012). “**Simulation of a Shear Coaxial GO₂/GH₂ Rocket Injector with DES and LES Using Flamelet Models**”, ed. by A. I. o. A. a. A. AIAA. 48th AIAA/ASME/SAE/ASEE Joint Propulsion Conference & Exhibit, p. 17. DOI: 10.2514/6.2012-3744.
- NGUYEN, T. M., P. P. POPOV, and W. A. SIRIGNANO (2017). “**Driving Mechanisms of Liquid-Propellant Rocket Longitudinal Combustion Instability**”, ed. by A. I. o. A. a. A. AIAA. Grapevine, Texas, USA: 55th AIAA Aerospace Sciences Meeting, p. 18. DOI: 10.2514/6.2017-0822.
- FOSTER, J. W. and R. S. MILLER (2015). “**Survey of Turbulent Combustion Models for Large Eddy Simulations of Propulsive Flowfields**”, ed. by A. I. o. A. a. A. AIAA. Kissimmee, Florida, USA: 53rd AIAA Aerospace Sciences Meeting, p. 21. DOI: 10.2514/6.2015-1379.

- NOGENMYR, K. J., X. S. BAI, C. FUREBY, and P. PETERSSON (2008). “**A Comparative Study of LES Turbulent Combustion Models Applied to a Low Swirl Lean Premixed Burner**”, ed. by A. I. o. A. a. A. AIAA. Reno, Nevada, USA: 46th AIAA Aerospace Sciences Meeting and Exhibit, p. 14. DOI: 10.2514/6.2008-513.
- LAGENESTE, L. D. D. and H. PITTSCH (2002). “**Comparison of turbulent premixed flames at different turbulence levels**”, ed. by A. R. Briefs. Center for Turbulence Research, pp. 91–102.
- ANGELBERGER, C., D. VEYNANTE, and F. EGOLFOPOULOS (2000). “**LES of Chemical and Acoustic Forcing of a Premixed Dump Combustor**”, ed. by K. A. Publishers. Flow, Turbulence and Combustion, pp. 205–222. DOI: 10.1023/A:1011477030619.
- MERK, M., W. POLIFKE, R. GAUDRON, M. GATTI, C. MIRAT, and T. SCHULLER (2018). “**Measurement and Simulation of Combustion Noise and Dynamics of a Confined Swirl Flame**”, ed. by A. I. o. A. a. A. AIAA. AIAA Journal, pp. 1–13. DOI: 10.2514/1.J056502.
- FLEMMING, F., A. SADIKI, and J. JANICKA (2007). “**Investigation of combustion noise using a LES/CAA hybrid approach**”, *Proceedings of the Combustion Institute*, vol. 31, pp. 3189–3196. DOI: 10.1016/j.proci.2006.07.060.
- BUI, T., W. SCHRÖDER, and M. MEINKE (2008). “**Numerical analysis of the acoustic field of reacting flows via acoustic perturbation equations**”, *Computers & Fluids*, vol. 37, pp. 1157–1169. DOI: 10.1016/j.compfluid.2007.10.014.
- CECERE, D., E. GIACOMAZZI, F. R. PICCHIA, N. ARCIDIACONO, F. DONATO, and R. VERZICCO (Nov. 2011). “**A Non-Adiabatic Flamelet Progress-Variable Approach for LES of Turbulent Premixed Flames**”, *Flow Turbulence Combust*, vol. 86, pp. 667–688. DOI: 10.1007/s10494-010-9319-7.
- LADEINDE, F. and Z. LOU (2017). “**Improved Flamelet Modeling of Supersonic Combustion**”, *Journal of Propulsion and Power*, vol. 34, no. 3, pp. 750–761. DOI: 10.2514/1.B36779.
- FERRARO, F., Y. GE, and M. PFITZNER (2015). “**A consistent hybrid LES-RANS PDF method for non-premixed flames**”, *The 12th International Conference on Combustion & Energy Utilisation*, vol. 66, pp. 317–320. DOI: 10.1016/j.egypro.2015.02.072.
- BILGER, R. W. (2011). “**Turbulent Combustion Modeling: Advances, New Trends e Perspectives**”, ed. by T. Echehki and E. Mastorakos. Vol. 95. Elsevier, pp. 1–495. DOI: 10.1007/978-94-007-0412-1.
- ZONG, N., G. RIBERT, and V. YANG (2008). “**A Flamelet Approach for Modeling of Liquid Oxygen (LOX)/Methane Flames at Supercritical Pressures**”, *46th AIAA Aerospace Sciences Meeting and Exhibit*, pp. 1–16. DOI: 10.2514/6.2008-946.

- PITSCH, H. and M. IHME (2005). “**An Unsteady/Flamelet Progress Variable Method for LES of Nonpremixed Turbulent Combustion**”, *43rd AIAA Aerospace Sciences Meeting*, pp. 1–14. DOI: 10.2514/6.2005-557.
- GLASSMAN, I. and R. A. YETTER (2008). “**Combustion**”, 4th ed. 84 Theobald’s Road, London WC1X 8RR, UK: ELSEVIER.
- POINSOT, T. and D. VEYNANTE (2005). “**Theoretical and Numerical Combustion**”, 2nd ed. Edwards, pp. 1–487.
- WILLIAMS, F. A. (1985). “**Combustion Theory (Combustion science and engineering series)**”, Basic Books.
- DEMIREL, Y. (2007). “**Nonequilibrium Thermodynamics: Transport and Rate Processes in Physical, Chemical and Biological Systems**”, Elsevier Science.
- SCHIESTEL, R. (2008). “**Modeling and Simulation of Turbulent Flows**”, ISTE; Wiley.
- POPE, S. B. (2000). “**Turbulent flows**”, 1st ed. Cambridge University Press.
- KRAICHNAN, R. H. (1976). “**Eddy Viscosity in Two and Three Dimensions**”, *Journal of the Atmospheric Sciences*, vol. 33, no. 8, pp. 1521–1536. DOI: 10.1175/1520-0469(1976)033<1521:EVITAT>2.0.CO;2.
- GÉN, F. (2009). “**Study of Compressible Turbulent Flow in Supersonic Environment by Large-Eddy Simulation**”. PhD thesis. Georgia Institute of Technology, pp. 1–234.
- LIN, W. (2010). “**Large-Eddy Simulation of Premixed Turbulent Combustion Using Flame Surface Density Approach**”. PhD thesis. University of Toronto, pp. 1–181.
- HIRSCH, C. (2007). “**Numerical Computation of Internal and External Flows: Fundamentals of Computational Fluid Dynamics**”, Elsevier.
- LIPATNIKOV, A. (2013). “**Fundamentals of Premixed Turbulent Combustion**”, 6000 Broken Sound Parkway NW, Suite 300: CRC, pp. 97–138.
- GERMANO, M., U. PIOMELLI, P. MOIN, and W. H. CABOT (1991). “**A dynamic subgrid-scale eddy viscosity model**”, *Physics of Fluids A: Fluid Dynamics*, vol. 3, no. 7, pp. 1760–1765. DOI: 10.1063/1.857955.
- VEYNANTE, D. and L. VERVISCH (Oct. 2002). “**Turbulent combustion modeling**”, *Progress in Energy and Combustion Science*, vol. 28, no. 3, pp. 193–266. DOI: 10.1016/S0360-1285(01)00017-X.
- NITHIARASU, P., R. CODINA, and O. C. ZIENKIEWICZ (2006). “**The Characteristic-Based Split (CBS) scheme—a unified approach to fluid dynamics**”, *International Journal for Numerical Methods in Engineering*, vol. 66, pp. 1514–1546. DOI: doi.org/10.1002/nme.1698.
- NITHIARASU, P., R. L. T. BEVAN, and K. MURALI (2012). “**An artificial compressibility based fractional step method for solving time dependent incompressible**

- ible flow equations. Temporal accuracy and similarity with a monolithic method”, *Computational Mechanics*, vol. 51, pp. 255–260. DOI: 10.1007/s00466-012-0719-5.
- GREENSHIELDS, C. J. (2017). *OpenFOAM User Guide, Version 5.0*. Ed. by E. Group.
- GEYZAINE, C. and J.-F. REMACLE (2019). *Gmsh Reference Manual*.
- LANARO, G. (2013). “Python High Performance Programming”, Packt Publishing.
- WONG, K. L. and A. J. BAKER (2002). “A 3D incompressible Navier–Stokes velocity–vorticity weak form finite element algorithm”, *International Journal for Numerical Methods in Fluids*, vol. 38, no. 2, pp. 99–123. DOI: 10.1002/flid.204.
- KIRIS, C., J. HOUSMAN, and D. KWAK (2006). “Comparison of Artificial Compressibility Methods”. In: *Computational Fluid Dynamics 2004*. Ed. by C. Groth and D. W. Zingg. Berlin, Heidelberg: Springer Berlin Heidelberg, pp. 475–480.
- GELFGAT, A. Y. (Feb. 2019). “Linear instability of the lid-driven flow in a cubic cavity”, *Theoretical and Computational Fluid Dynamics*, vol. 33, no. 1, pp. 59–82. DOI: 10.1007/s00162-019-00483-1.
- HACHEM, E., B. RIVAUX, T. KLOCZKO, H. DIGONNET, and T. COUPEZ (2010). “Stabilized finite element method for incompressible flows with high Reynolds number”, *Journal of Computational Physics*, vol. 229, no. 23, pp. 8643–8665. DOI: <https://doi.org/10.1016/j.jcp.2010.07.030>.
- WHITE, F. M. (1974). “Viscous fluid flow”, McGraw-Hill.
- BLINT, R. J. (1986). “The Relationship of the Laminar Flame Width to Flame Speed”, *Combustion Science and Technology*, vol. 49, no. 1-2, pp. 79–92. DOI: 10.1080/00102208608923903.
- PONCE, R. (2019). *Numerical investigation*. English. URL: <https://github.com/ruhanponce/Numerical-Investigation-CBS.git>.
- MARSHALL, W. M., S. PAL, R. D. WOODWARD, and R. J. SANTORO (2005). “Benchmark Wall Heat Flux Data for a G02/GH2 Single Element Combustor”, ed. by A. I. o. A. a. AIAA. Tucson, AZ, USA: 41st AIAA Joint Propulsion Conference, pp. 1–13. DOI: 10.2514/6.2005-3572.
- PANJWANI, B., I. S. ERTESVAG, A. GRUBER, and K. E. RIAN (2010). “Turbulence combustion closure model based on the Eddy dissipation concept for large eddy simulation”, *Advances in Fluid Mechanics VIII*, vol. 69, pp. 1–12. DOI: 10.2495/AFM100031.
- TULLIO, M. D., R. VERZICCO, and G. IACCARINO (2014). *Immersed Boundary Technique for Large–Eddy–Simulation*, pp. 1–97.
- IACCARI, G. (2003). “Immersed boundary technique for turbulent flow simulations”, *The American Society of Mechanical Engineers*, vol. 56, no. 3, pp. 331–347. DOI: 10.1115/1.1563627.

- LIU, S. and C. TONG (2013). “**Subgrid-scale mixing of mixture fraction, temperature, and species mass fractions in turbulent partially premixed flames**”, *Proceedings of the Combustion Institute - ELSEVIER*, vol. 34, pp. 1231–1239. DOI: 10.1016/j.proci.2012.05.017.
- BIRD, R. B., W. E. STEWART, and E. N. LIGHTFOOT (2002). “**Transport Phenomena**”, Second. John Wiley & Sons, Inc., pp. 1–914.
- ARIS, R. (1989). “**Vectors, Tensors, and the Basic Equations of Fluid Mechanics**”, ed. by D. Publications. General Publishing Company, pp. 1–314.
- CHIKITKIN, A., B. ROGOV, G. TIRSKY, and S. UTUZHNIKOV (2015). “**Effect of bulk viscosity in supersonic flow past spacecraft**”, *ELSEVIER - Applied Numerical Mathematics*, vol. 93, pp. 47–60. DOI: 10.1016/j.apnum.2014.01.004.
- NAGNIBEDA, E. and E. KUSTOVA (2009). “**Non-Equilibrium Reacting Gas Flows - Kinetic Theory of Transport and Relaxation Processes**”, Springer - Heat and Mass Transfer. DOI: 10.1007/978-3-642-01390-4.
- BEJAN, A. (2006). “**Advanced Engineering Thermodynamics**”, ed. by D. University. 3rd ed. 111 River Street, Hoboken, NJ 07030, USA: John Wiley & Sons, pp. 1–908.
- BERGMAN, T. L., A. S. LAVINE, F. P. INCROPERA, and D. P. DEWITT (2011). “**Fundamentals of Heat and Mass Transfer**”, 7th ed. 222 Rosewood Drive, Danvers, MA 01923: John Wiley & Sons, pp. 1–1076.
- DONEA, J. (1984). “**A Taylor-Galerkin Method for Convective Transport Problems**”, *International Journal for Numerical Methods in Engineering*, vol. 20, pp. 101–119. DOI: doi.org/10.1002/nme.1620200108.
- ROIG, B. (2007). “**One-step Taylor-Galerkin methods for convection-diffusion problems**”, *Journal of Computational and Applied Mathematics*, vol. 204, pp. 95–101. DOI: doi:10.1016/j.cam.2006.04.031.
- XIKUI, L. and W. WENHUA (1999). “**Characteristic Galerkin Method for Convection-Diffusion Equations and Implicit Algorithm using Precise Integration**”, *Acta Mechanica Sinica*, vol. 15, pp. 371–382. DOI: doi.org/10.1007/BF02487935.
- GATSKI, T. B. and J.-P. BONNET (2009). “**Compressibility, Turbulence and High Speed Flow**”, Elsevier, pp. 1–284.
- POWERS, J. M. (2016). “**LECTURE NOTES ON INTERMEDIATE FLUID MECHANICS**”, Department of Aerospace and Mechanical Engineering University of Notre Dame, pp. 172–174.
- CEBECI, T. (2003). “**Turbulence Models and Their Application**”, Long Beach, California, USA: Springer.
- SAGAUT, P. (2006). “**Large Eddy Simulation for Incompressible Flow: An Introduction**”, ed. by Springer. 3rd ed. Scientific Computation, pp. 1–575.
- SILVA, J. B. C. (Mar. 2017). “**Tópicos em Mecânica dos Fluidos: Turbulência**”.

- PYATNITSKY, L. N. (2009). “**Turbulence Nature and the Inverse Problem**”, vol. 89. 38402 Saint Martin d’Hères Cedex, France: Springer, p. 205.
- POPE, S. B. (1988). “**The evolution of surfaces in turbulence**”, *International Journal for Engineering Science*, vol. 26, pp. 445–469. DOI: 10.1016/0020-7225(88)90004-3.
- BILGER, R. W. (1976). “**The Structure of Diffusion Flames**”, ed. by T. Bibini. Francis. Vol. 13. Combustion Science and Technology 1-6. Department of Mechanical Engineering, The University of Sydney, NSW, Australia: Combustion Science and Technology, pp. 155–170. DOI: 10.1080/00102207608946733.
- OPPENHEIM, A. K. (2008). “**Dynamics of Combustion Systems**”, 2nd ed. 5112 Etcheverry Hall Berkeley, CA 94720-1740, USA: Springer, p. 374.
- RODI, W. and N. FUEYO (2002). “**Engineering Turbulence Modelling and Experiments**”, Mallorca, Spain: Elsevier, p. 1029.
- KERSTEIN, A. R., W. T. ASHURST, and F. A. WILLIAMS (1998). “**Field Equations for Interface Propagation in an Unsteady Homogeneous Flow Field**”, *the American Physical Society*, vol. 37, no. 7. DOI: 10.1103/PhysRevA.37.2728.
- WARNATZ, J., U. MAAS, and R. DIBBLE (2006). “**Combustion: Physical and Chemical Fundamentals, Modeling and Simulation, Experiments, Pollutant Formation**”, 4th ed. Springer, pp. 1–389.
- IM, H. G., T. S. LUND, and J. H. FERZIGER (1997). “**Large eddy simulation of turbulent front propagation with dynamic subgrid models**”, *Physics of Fluids*, pp. 1–9. DOI: 10.1063/1.869517.
- HAWKES, E. R. (2000). “**Large-Eddy Simulation of Premixed Turbulent Combustion**”. PhD thesis. University of Cambridge.
- HAWKES, E. R. and R. S. CANT (2000). “**A flame surface density approach to large-eddy simulation of premixed turbulent combustion**”, *Symposium (International) on Combustion*, vol. 28, pp. 51–58.
- PIERCE, C. D. (June 2001). “**Progress-Variable Approach for Large-Eddy Simulation of Turbulent Combustion**”. PhD thesis. Stanford University, pp. 1–122.
- VERVISCH, L., E. BIDAUX, K. N. C. BRAY, and W. KOLLMANN (1995). “**Surface density function in premixed turbulent combustion modeling, similarities between probability density function and flame surface approaches**”, *Physics of Fluids*, vol. 7, pp. 1–9. DOI: 10.1063/1.868693.
- HINZE, J. O. (1975). “**Turbulence (McGraw-Hill series in mechanical engineering)**”, McGraw-Hill College.
- NITHIARASU, P., O. C. ZIENKIEWICZ, B. V. K. S. SAI, K. MORGAN, R. CODINA, and M. VÁZQUEZ (1998). “**Shock capturing viscosities for the general fluid mechanics algorithm**”, *International Journal for Numerical Methods in Fluids*, vol. 28, no. 9, pp. 1325–1353. DOI: 10.1002/(SICI)1097-0363(19981215)28:9<1325::AID-FLD765>3.0.CO;2-1.

-
- MICHELTSEN, M. L. and J. M. MOLLERUP (2007). “**Thermodynamics Models: Fundamentals & Computational Aspects**”, ed. by E. H. Stenby. 2nd ed. Tie-Line Publications, pp. 1–386.
- ASSAEL, M. J., J. P. M. TRUSLER, and T. F. TSOLAKIS (1998). “**Thermophysical Properties of Fluid: An Introduction to their Prediction**”, 222 Rosewood Drive, Danvers, MA 01923, USA: Imperial College Press, pp. 1–373.

A – STUDY OF ART'S OVERVIEW

Table 8 – Table of study of art's overview.

Author	Year	Turbulence Model	TCI ¹	Combustion Type	Fuel	Mesh	Discretization Model
BOGER et al. (1998)	1998	DNS	Flame Surface Density	Premixed	X	Cartesian structured mesh	FiniNTMIX-3D® (Finite Volume)
DEKENA and PETERS (1999)	1999	LES	G-Equation	Partial premixed	Gasoline	X	CFD FIRE® code (Finite Volume)
ANGELBERGER, VEY- NANTE, and EGOL- FOPOU- LOS (2000)	2000	LES	Thickened Flame	Premixed	$GC_3H_8/GAir$	Structured/Non- Structured Mesh Hybrid	code AVBP® (Finite Volume)

Continued on next page

Table of study of art's overview.

Author	Year	Turbulence Model	TCI ²	Combustion Type	Fuel	Mesh	Discretization Model
LAGENESTE and PITSCH LAGENESTE and PITSCH, 2002	2002	LES	G-Equation	Premixed	$GCH_4/GAir$	Cylindrical Overlapped Mesh	Volume-Finito
PITSCH and IHME (2005)	2005	LES with Dynamic Sub-Grid Scale Models	Unsteady flamelet/progress variable model	Non-Premixed	$GCH_4/GAir$	Structured cylindrical mesh	Second-order finite-volume scheme
MARSHALL et al. (2005)	2005	X	X	X	$GH_2/GAir$	X	Benchmark quality wall heat flux data sets for CFD code validation
DOMINGO et al. (2005)	2005	DNS and LES	Flame Surface Density with GRI	Premixed	$GCH_4/GAir$	Non-Uniform Mesh	Code PREMIX® (Finite Volume)

Continued on next page

Table of study of art's overview.

Author	Year	Turbulence Model	TCI ²	Combustion Type	Fuel	Mesh	Discretization Model
MARTIN et al. (2006)	2006	LES	Thickened Flame	Premixed	$GC_3H_8/GAir$	Structured/Non-Structured Mesh Hybrid	code AVBP® (Finite Volume) e AVSP® (Finite Elemente)
FLEMMING, SADIKI, and JANICKA (2007)	2007	LES/Sub-Grid Scale Models	Flamelet Model	Non-premixed	$GH_2 - N_2/GAir$	Cartesian structured mesh	codes FLOWSI® (LES) e CLAWPACK® (CAA ³) (Finite Volume)
NOGENMYR et al. (2008)	2008	LES/Sub-Grid Scale Models	Flamelet Model, G-Equation and finite rate chemistry models	Premixed	$GCH_4/GAir$	Cartesian grid	4th order central difference scheme (Finite Differences)
ZONG, RIBERT, and YANG (2008)	2008	LES/Sub-Grid Scale Models	Laminar flamelet model and Conserved scalar approach e Direct-closure approach	Non-premixed	$GCH_4/GAir$	Structured mesh	Volume-Finito

Continued on next page

³ Computational Acoustic Analysis

Table of study of art's overview.

Author	Year	Turbulence Model	TCI ²	Combustion Type	Fuel	Mesh	Discretization Model
BUI, SCHRÖDER, and MEINKE (2008)	2008	LES/Sub-Grid Scale Models	Steady flamelet model	Non- premixed	$GH_2 - N_2/GAir$	Cartesian structured mesh	Finite Volume
NOGENMYR et al. (2008)	2008	LES	G-Equation	Premixed	$GCH_4/GAir$	Cartesian structured mesh	Finite Volume
PANJWANI et al. (2010)	2010	LES	Eddy Dissipation Concept (EDC)	Non- Premixed	GH_2/GN_2	Cylindrical grid	Finite Volume

Continued on next page

Table of study of art's overview.

Author	Year	Turbulence Model	TCI ²	Combustion Type	Fuel	Mesh	Discretization Model
CECERE et al. (2011)	2011	LES	Flamelet Progress-Variable	Premixed	GH_2/GN_2	Immersed boundary method with non-uniform cylindrical mesh TULLIO, VERZICCO, and IACCARINO, 2014, IACCARI, 2003	Finite Differences
Y. LIU et al. (2012)	2012	DNS	Two-time correlation	Premixed V flame	$GC_3H_8/GAir$	Cartesian structured and uniform mesh	X
MÜHLBAUER et al. (2012)	2012	Random Particle-Mesh for Combustion Noise (RPM-CN)	Linearized Euler Equations (LEE)	Non- Premixed	nitrogen- diluted methane- hydrogen fuel mixture	Cylindrical unstructured hexahedron mesh	Finite Volume formulation for unstructured grids

Continued on next page

Table of study of art's overview.

Author	Year	Turbulence Model	TCI ²	Combustion Type	Fuel	Mesh	Discretization Model
THAKUR et al. (2012)	2012	Hybrid U/RANS with Detached Eddy Simulation (DES)	Laminar Flamelet Model	Non-Premixed	GH_2/GO_2	X	Finite Volume axisymmetric
S. LIU and TONG (2013)	2013	LES/Sub-Grid Scale Models	Filtred Mass density function (FMDF)	Partial premixed	$GCH_4/GAir$	X	10th-order central finite difference non-dimensionalized by the filtered scalar dissipation rate and the SGS variance

Continued on next page

Table of study of art's overview.

Author	Year	Turbulence Model	TCI ²	Combustion Type	Fuel	Mesh	Discretization Model
OEFELEIN (2015)	2015	LES/SGS turbulence kinetic energy	Laminar Flamelet Model LADEINDE and LOU, 2017, the Transported Probability Density Function Model FERRARO, GE, and PFITZNER, 2015, and the Linear Eddy Model BILGER, 2011	Non-Premixed	X	Adaptative Mesh	Theoretical
CAO et al. (2015)	2015	LES/Dynamic Smagorinsky-Lilly Model	Fluent® ⁴	Premixed	GH_2/GO_2	Structured mesh	Finite Volume

Continued on next page

⁴ No informed the method

Table of study of art's overview.

Author	Year	Turbulence Model	TCI ²	Combustion Type	Fuel	Mesh	Discretization Model
FOSTER and MILLER (2015)	2015	LES	Flamelet models, linear eddy based models (LEM), and transported PDF or filtered density function (FDF) based models	Premixed and non-premixed	X	Unstructured meshes	Finite Volume
MAESTRO et al. (2016)	2016	RANS and LES	Direct integration of chemistry e tabulated flamelets	Premixed	$GCH_4/GAir$	Several	Several
SCHLIMPERT et al. (2016)	2016	RANS/low-dissipation AUSM scheme	G-Equation	Premixed	$GCH_4/GAir$	Cartesian non-structured mesh	Finite Volume
A. N. LIPATNIKOV et al. (2017)	2017	DNS (Statistically Planar Turbulence)	Flame Surface Density	Partial premixed	X	X	X

Continued on next page

Table of study of art's overview.

Author	Year	Turbulence Model	TCI ²	Combustion Type	Fuel	Mesh	Discretization Model
POTTURI, PATTON, and EDWARDS (2017)	2017	LES/RANS hybrid with closure least-squares model NAGHIAN, LASHKAR-BOLOK, and JABBARI, 2017	North Carolina State University's REACTMB with closure Least-squares based model e "laminar chemistry"	Premixed	$GC_3H_8/GAir$	Cartesian Structured Mesh	Finite Volume
ALBAYRAK and POLIFKE (2017)	2017	Laminar	G-Equation	Premixed	X	X	Theoric model
HUO and YANG (2017)	2017	LES/Eddy-viscosity model	Flamelet and flamelet/progress-variable approaches	Non-premixed	$GCH_4/GAir$	Spherical structured mesh	X

Continued on next page

Table of study of art's overview.

Author	Year	Turbulence Model	TCI ²	Combustion Type	Fuel	Mesh	Discretization Model
A. N. LIPAT- NIKOV et al. (2017)	2017	DNS of statistically planar	Unburned Mixture Fingers (UMFs)	Premixed	X	Grid uniform rectangular	X
NGUYEN, POPOV, and SIRIG- NANO (2017)	2017	Hybrid RANS/LES model called Detached Eddy Simulation (DES) Axisymmetric and Multispecies	Flamelet Progress-Variable approach	Liquid-Propellant	$GH_2/GAir$	X	finite-difference variation of the classic Jameson-Schmidt-Turkel (JST) scheme

Source – Prepared by the author.

B – GENERIC MATHEMATICAL MODEL

In this topic, the object of study include: fluid flow, heat and mass transfers in subject of transport phenomena. The fluid flow it is analyzed in fluid mechanics by considering the continuity, linear and angular momentum equations. Transfer of energy, due to temperature gradient, involves heat transfer. In a combustion process, some substancies desapear or are transformed in other substancies. Mas transfer in this process involves conservation of chemical species. A good reference on transport phenomena is BIRD, STEWART, and LIGHTFOOT, 2002.

In this way, the equations for complete analysis, involving the three areas of knowledge, will be presented, from the problem previously proposed in the objectives of the study.

Governing Equations

Constitutive relationships of fluids

The natural independent variable is its velocity field vector \mathbf{u} , which can be represented in indicial notation according to Equation 79 ZIENKIEWICZ, TAYLOR, and NITHIARASU, 2014.

$$u_i, \quad i = 1, 2, 3 \quad \text{or} \quad \mathbf{u} = [u_1, u_2, u_3]^T \quad (79)$$

where the subscripts 1,2,3 represent the orthonormal axes of the analyzed coordinate system.

The deformation rate, \mathbf{S} , is the main cause of the Cauchy tensions, σ_{ij} , defined in a similar way in solid mechanics, Equation 80

$$S_{ij} = \frac{1}{2} \left(\frac{\partial u_i}{\partial x_j} + \frac{\partial u_j}{\partial x_i} \right) - \frac{1}{3} \frac{\partial u_k}{\partial x_k} \delta_{ij} \quad (80)$$

The presentation of Equation 80 is given in tensor index form, however, later for the development of variational forms it is more convenient to write in matrix form for future finite element analysis.

$$\mathbf{S} = [S_{11} \quad S_{22} \quad S_{33} \quad 2S_{12} \quad 2S_{23} \quad 2S_{31}]^T \quad (81a)$$

such that $2S_{ij}$, $i \neq j$ is an engineering shear strain rate represented as

$$2S_{ij} = \dot{\gamma}_{ij} \quad \text{for } i \neq j \quad (81b)$$

Analogously, the stress tensor, σ_{ij} , is expressed in matrix form as

$$\boldsymbol{\sigma} = [\sigma_{11} \quad \sigma_{22} \quad \sigma_{33} \quad \sigma_{12} \quad \sigma_{23} \quad \sigma_{33}]^T \quad (82)$$

The relationship between deviator, or the shear strain tensor, τ_{ij} , and the strain rate have, for Newtonian fluids, a linear relationship characterized in Equation 83 shown by ARIS (1989).

$$\boldsymbol{\tau} = \tau_{ij} \equiv \sigma_{ij} - \frac{1}{3}\delta_{ij}\sigma_{kk} = 2\mu \left(S_{ij} - \frac{1}{3}\delta_{ij}S_{kk} \right) \quad (83)$$

where τ_{ij} is the deviatoric part of the stress tensor and δ_{ij} is the Kronecker delta,

$$\delta_{ij} = \begin{cases} 1, & \text{if } i = j \\ 0, & \text{if } i \neq j \end{cases}$$

and where the repeated subscripts represent the following sum

$$\sigma_{kk} \equiv \sigma_{11} + \sigma_{22} + \sigma_{33} \quad \text{e} \quad S_{kk} \equiv S_{11} + S_{22} + S_{33} \quad (84)$$

The relation between the variation of the average tension and the rate of volumetric deformation defines the average thermodynamic pressure

$$p = -\frac{1}{3}\sigma_{kk} = -\kappa S_{kk} + p_0 \quad (85)$$

where κ is the volumetric viscosity coefficient and p_0 is the initial hydrostatic pressure which is independent of the rate of deformation.

Thus, it has been shown that the ratio of the stresses acting on a fluid is

$$\sigma_{ij} = \tau_{ij} - \delta_{ij}p = 2\mu \left(S_{ij} - \frac{1}{3}\delta_{ij}S_{kk} \right) + \kappa\delta_{ij}S_{kk} - \delta_{ij}p_0 \quad (86a)$$

or

$$\sigma_{ij} = 2\mu S_{ij} + \delta_{ij} \left(\kappa - \frac{2}{3}\mu \right) S_{kk} - \delta_{ij}p_0 \quad (86b)$$

Considering the effects of the very small volumetric viscosity, due to the characteristic of the flow analyzed in the present work, can be neglected

$$\kappa S_{kk} \equiv 0 \quad (87)$$

where, according to CHIKITKIN et al. (2015) κ can be calculated by

$$\kappa = \frac{\pi}{25} \mu Z \quad (88)$$

Z is a general parameter, obtained by

$$Z = \frac{Z_\infty}{1 + \left(\frac{\pi^{\frac{3}{2}}}{2}\right) \left(\frac{T^*}{T}\right)^{\frac{1}{2}} + \left(2 + \frac{\pi^2}{4}\right) \left(\frac{T^*}{T}\right) + \pi^{\frac{3}{2}} \left(\frac{T^*}{T}\right)^{\frac{3}{2}}}$$

where Z_∞ and T^* are values dependent on the chemical species NAGNIBEDA and KUSTOVA, 2009.

In this way it is possible that the relation of the tensions becomes

$$\sigma_{ij} = 2\mu \left(S_{ij} - \frac{1}{3} \delta_{ij} S_{kk} \right) - \delta_{ij} p \equiv \boldsymbol{\tau} - \delta_{ij} p \quad (89a)$$

From above relationship the deviatoric part of the stress tensor is

$$\boldsymbol{\tau} = \tau_{ij} = 2\mu \left(S_{ij} - \frac{1}{3} \delta_{ij} S_{kk} \right) = \mu \left[\left(\frac{\partial u_i}{\partial x_j} + \frac{\partial u_j}{\partial x_i} \right) - \frac{2}{3} \delta_{ij} \frac{\partial u_k}{\partial x_k} \right] \quad (89b)$$

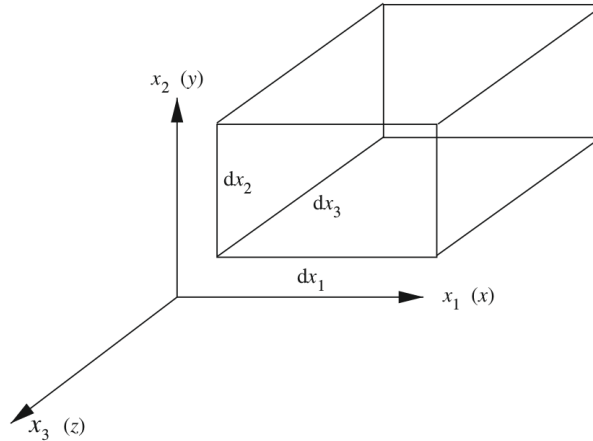
if the flow is incompressible $S_{kk} = 0$.

Mass Conservation

The mass flow balance, ρu_i , entering and leaving an infinitesimal control volume, Figure 33, is equal to the rate of change of the specific mass inside the control volume. The resulting balance equation is:

$$\frac{\partial \rho}{\partial t} + \frac{\partial}{\partial x_i} (\rho u_i) \equiv \frac{\partial \rho}{\partial t} + \nabla^T \cdot (\rho \mathbf{u}) = 0 \quad (90)$$

Figure 33 – Main directions and infinitesimal control volume.



Source – ZIENKIEWICZ, TAYLOR, and NITHIARASU ZIENKIEWICZ, TAYLOR, and NITHIARASU, 2014.

where $\nabla^T = [\partial/\partial x_1, \partial/\partial x_2, \partial/\partial x_3]$ is the nabla operator.

Momentum Conservation

The balance of the linear momentum of the fluid in the direction j , through the control volume of Figure 33, is in dynamic equilibrium with respect to the surface and field (body) forces ZIENKIEWICZ, TAYLOR, and NITHIARASU, 2014. Thereby,

$$\frac{\partial(\rho u_j)}{\partial t} + \frac{\partial}{\partial x_i}[(\rho u_j)u_i] - \frac{\partial}{\partial x_i}(\sigma_{ij}) - \rho g_j = 0, \quad j = 1, 2, 3 \quad (91)$$

Da Equation 89a,

$$\frac{\partial(\rho u_j)}{\partial t} + \frac{\partial}{\partial x_i}[(\rho u_j)u_i] - \frac{\partial \tau_{ij}}{\partial x_i} + \frac{\partial p}{\partial x_j} - \rho g_j = 0, \quad j = 1, 2, 3 \quad (92)$$

From the angular momentum, for a nonpolar flow, results the criterion of symmetry between the components of the stress tensors, i.e.;

$$\sigma_{ij} = \sigma_{ji} \quad ou \quad \tau_{ij} = \tau_{ji}$$

Energy Conservation

In order to analyze energy conservation, one must first introduce the concept of *internal energy per unit mass*, e , it depends directly on the state of the fluid, ie, the pressure p and the temperature T BEJAN, 2006.

$$e = e(T, p) \quad (93)$$

The *total energy per unit mass* (E) will be

$$E = e + \frac{1}{2}u_i u_i \quad (94)$$

Note that Equation 94 includes the contributions of internal and kinetic energies per unit mass.

The *enthalpy per unit mass* is defined as

$$h = e + \frac{p}{\rho} \quad (95)$$

and the *enthalpy of stagnation* is given by

$$H^* = h + \frac{1}{2}u_i u_i = E + \frac{p}{\rho} \quad (96)$$

Energy is transferred by the fluid to the control volume through conduction, advection and radiation, and the radiation usually occurs only at the boundaries. To

exemplify, the heat flow by conduction, q_i given by the Fourier's law, for an isotropic material the heat flux is BERGMAN et al., 2011.

$$q_i = -k_{cond} \frac{\partial T}{\partial x_i} \quad (97)$$

where k_{cond} is the thermal conductivity of the material.

Introducing the terms heat sources such as heat flow per unit volume q_H due to chemical reactions and also including dissipation energy due to internal stresses, i.e., using Equation 89a;

$$\frac{\partial}{\partial x_i}(\sigma_{ij}u_j) = \frac{\partial}{\partial x_i}(\tau_{ij}u_j) - \frac{\partial}{\partial x_j}(pu_j) \quad (98)$$

the energy balance on the control volume of Figure 33 becomes

$$\frac{\partial(\rho E)}{\partial t} + \frac{\partial}{\partial x_i}(\rho u_i E) - \frac{\partial}{\partial x_i} \left(k_{cond} \frac{\partial T}{\partial x_i} \right) + \frac{\partial}{\partial x_i}(pu_i) - \frac{\partial}{\partial x_i}(\tau_{ij}u_j) - \rho g_i u_i - q_H = 0 \quad (99a)$$

Applying the Equation 96, Eq. (85a) can be rewritten

$$\frac{\partial(\rho E)}{\partial t} + \frac{\partial}{\partial x_i}(\rho u_i H^*) - \frac{\partial}{\partial x_i} \left(k_{cond} \frac{\partial T}{\partial x_i} \right) - \frac{\partial}{\partial x_i}(\tau_{ij}u_j) - \rho g_i u_i - q_H = 0 \quad (99b)$$

Incompressible Flow

From the thermodynamics of the simple compressible systems it is shown that the intensive thermodynamic state is defined by only two independent intensive properties, so that:

$$\rho = \rho(T, p) \quad (100)$$

A complete analysis of the major thermodynamic state equations for blends is given in the Appendix G.

Thus, assuming that a flow is incompressible when ρ is constant and uniform in both space and time.

The assumptions of incompressible fluid can be extended to cases of fluids exhibiting very small compressibility in which there are practically no significant variations in density as a consequence of the elastic deformation obtained with the change in pressure. Thereby,

$$d\rho)_s = \frac{\rho}{K} dp)_s \quad (101a)$$

where K is the bulk modulus, by definition,

$$d\rho)_s = \frac{1}{c^2} dp)_s \quad (101b)$$

or

$$\left. \frac{\partial \rho}{\partial t} \right)_s = \frac{1}{c^2} \left. \frac{\partial p}{\partial t} \right)_s \quad (101c)$$

where $c = \sqrt{K/\rho}$ is the velocity of sound in the fluid ZIENKIEWICZ, TAYLOR, and NITHIARASU, 2014.

The transport equations for mass and momentum can be rewritten

$$\frac{1}{c^2} \frac{\partial p}{\partial t} + \rho \frac{\partial u_i}{\partial x_i} = 0 \quad (102a)$$

$$\frac{\partial u_j}{\partial t} + \frac{\partial}{\partial x_i} (u_j u_i) + \frac{1}{\rho} \frac{\partial p}{\partial x_j} - \frac{1}{\rho} \frac{\partial \tau_{ij}}{\partial x_i} - g_j = 0 \quad (102b)$$

For incompressible flows, the deviatoric stress tensor is CHUNG, 2002:

$$\tau_{ij} = \mu \left(\frac{\partial u_i}{\partial x_j} + \frac{\partial u_j}{\partial x_i} \right)$$

Compressible Flow

The governing equations for compressible flows can be expressed in a general conservative manner ZIENKIEWICZ, TAYLOR, and NITHIARASU, 2014.

$$\frac{\partial \Phi}{\partial t} + \frac{\partial F_i}{\partial x_i} + \frac{\partial G_i}{\partial x_i} + Q = 0 \quad (103)$$

The Equation 103 is known as the Navier-Stokes equations for compressible flows. From equations 90, 92, 99b, Φ , F_i , G_i and Q are defined as:

$$\Phi = \begin{Bmatrix} \rho \\ \rho u_1 \\ \rho u_2 \\ \rho u_3 \\ \rho E \end{Bmatrix}; \quad (104a)$$

$$F_i = \begin{Bmatrix} \rho u_i \\ \rho u_1 u_i + p \delta_{1i} \\ \rho u_2 u_i + p \delta_{2i} \\ \rho u_3 u_i + p \delta_{3i} \\ \rho H u_i \end{Bmatrix}; \quad (104b)$$

$$G_i = \left\{ \begin{array}{c} 0 \\ -\tau_{1i} \\ -\tau_{2i} \\ -\tau_{3i} \\ -(\tau_{ij}u_j) - k \frac{\partial T}{\partial x_i} \end{array} \right\}; \quad (104c)$$

and

$$Q = \left\{ \begin{array}{c} 0 \\ -\rho f_1 \\ -\rho f_2 \\ -\rho f_3 \\ -\rho f_i u_i - q_H \end{array} \right\} \quad (104d)$$

where

$$\tau_{ij} = \mu \left[\left(\frac{\partial u_i}{\partial x_j} + \frac{\partial u_j}{\partial x_i} \right) - \frac{2}{3} \delta_{ij} \frac{\partial u_k}{\partial x_k} \right]$$

The Euler equation is a particular case of the Navier-Stokes equation, assuming that the viscosity of the fluid is zero and that there are no heat exchanges. Thus, $\tau_{ij} = 0$ and $q_i = 0$. Applying these conditions to Equation 103 becomes

$$\frac{\partial \Phi}{\partial t} + \frac{\partial F_i}{\partial x_i} + Q = 0 \quad (105)$$

The Finite Element Method Applied to Transport Phenomena

Traditionally applied in structures or in Solid Mechanics, the FEM can also be used with great reliability to analyze the flow of fluids, whether they are viscous or non-viscous, incompressible or compressible CHUNG, 2002. In the case of flows, it is more convenient to use the weak formulation, for spatial discretization of the system of differential equations that model the system. Due to the advective term the equations are not self-adjoint, making necessary the use of some stabilization procedure so that the equation system has stable solutions in both transient and stationary regimes. Because of this, it can be shown that the approach using the conventional Galerkin method does not yield to good results, as ZIENKIEWICZ, TAYLOR, and NITHIARASU (2014). Thus, certain stabilizing methods such as Taylor-Galerkin Method (TGM), Generalized Galerkin Method (GGM), Galerkin Characteristic Method (GCM) and finally the CBS (Characteristic-Based Split) scheme must be applied for stability of solutions.

Weak Formulation

The weak formulation of a partial differential equation is an equivalent way of rewriting it, multiplying by an arbitrary test function, integrating into the problem domain and equating to zero. The mathematical consequences are then analyzed. Consider the general equation of transport:

$$\frac{\partial \phi}{\partial t} + \underbrace{\mathbf{u} \cdot \nabla \phi}_{\text{Advective term}} - \underbrace{\nabla \cdot (k_\phi \nabla \phi)}_{\text{Diffusive term}} = S_\phi \quad \text{in } \Omega \quad (106)$$

The following initial condition, natural and essential boundary conditions for solution of the Equation 106 are prescribed:

$$\phi(\vec{x}, 0) = \phi_0(\vec{x}) \quad (107a)$$

$$\left. \begin{array}{l} \phi = \phi_1 \text{ on } \Gamma_1 \\ k_\phi \frac{\partial \phi}{\partial n} = \phi_2 \text{ on } \Gamma_2 \end{array} \right\} \underbrace{\Gamma_1 \cup \Gamma_2 = \Gamma}_{\text{Arbitrary boundaries of the problem}} \quad (107b)$$

The formulation represented by the equations 106 and 107 is the strong form.

Now multiplying Equation 106 by a weight function W_i and integrating over the Ω domain

$$\int_{\Omega} W_i \frac{\partial \phi}{\partial t} d\Omega + \int_{\Omega} W_i \mathbf{u} \cdot \nabla \phi d\Omega - \underbrace{\int_{\Omega} W_i \nabla \cdot (k_\phi \nabla \phi) d\Omega}_A = \int_{\Omega} W_i S_\phi d\Omega \quad (108)$$

The term A presented in Equation 108, by vector identity, is expressed as:

$$\nabla \cdot (W_i k_\phi \nabla \phi) = \nabla W_i \cdot k_\phi \nabla \phi + W_i \nabla \cdot (k_\phi \nabla \phi) \quad (109)$$

Substituting Equation 109 into Equation 108 results in

$$\int_{\Omega} W_i \frac{\partial \phi}{\partial t} d\Omega + \int_{\Omega} W_i \mathbf{u} \cdot \nabla \phi d\Omega + \int_{\Omega} \nabla W_i \cdot k_\phi \nabla \phi d\Omega - \underbrace{\int_{\Omega} \nabla \cdot (W_i k_\phi \nabla \phi) d\Omega}_B = \int_{\Omega} W_i S_\phi d\Omega \quad (110)$$

Applying the Gaussian Theorem to the term B and introducing the natural boundary conditions, second line of Equation 107, the resulting equation is:

$$\begin{aligned} \int_{\Omega} \nabla \cdot (W_i k_\phi \nabla \phi) d\Omega &= \oint_{\Gamma} \vec{n} \cdot W_i k_\phi \nabla \phi d\Gamma \\ &= \oint_{\Gamma} W_i k_\phi \vec{n} \cdot \nabla \phi d\Gamma \\ &= \int_{\Gamma_1} W_i k_\phi \frac{\partial \phi}{\partial n} d\Gamma + \int_{\Gamma_2} W_i k_\phi \frac{\partial \phi}{\partial n} d\Gamma \end{aligned} \quad (111)$$

In contours in which the ϕ variable is specified, that is, in the contour Γ_1 of the domain, W_i must be null. Thus, the weak formulation of Equation 106 is given by

$$\int_{\Omega} W_i \frac{\partial \phi}{\partial t} d\Omega + \int_{\Omega} W_i \mathbf{u} \cdot \nabla \phi d\Omega + \int_{\Omega} \nabla W_i \cdot k_{\phi} \nabla \phi d\Omega = \int_{\Omega} W_i S_{\phi} d\Omega + \int_{\Gamma_2} W_i k_{\phi} \frac{\partial \phi}{\partial n} d\Gamma \quad (112)$$

The Equation 112 is called weak formulation, since the derivatives of higher orders cease to exist in the ZIENKIEWICZ, TAYLOR, and NITHIARASU, 2014 integration process. The derivatives were re-distributed between the ϕ and W_i functions. The integral in the Γ_2 outline of Equation 112 arises naturally when the weak formulation of the equation is obtained. Therefore, the corresponding boundary conditions presented in autoref subeq: natural_conditions is called the natural contour condition CHUNG, 2002. Finally, by applying the natural boundary conditions, Equation 107b, in Equation 112 we have

$$\int_{\Omega} W_i \frac{\partial \phi}{\partial t} d\Omega + \int_{\Omega} W_i \mathbf{u} \cdot \nabla \phi d\Omega + \int_{\Omega} \nabla W_i \cdot k_{\phi} \nabla \phi d\Omega = \int_{\Omega} W_i S_{\phi} d\Omega + \int_{\Gamma_2} W_i \phi_2 d\Gamma \quad (113)$$

Generalized Galerkin method

Constructing a double residual projection of the system of Navier-Stokes equations in terms of the Jacobians, together with the application of the temporal and spatial test functions ZIENKIEWICZ, TAYLOR, and NITHIARASU, 2014.

$$(W(\xi), (\Theta_{\alpha}, R)) = \int_{\xi} W(\xi) \int_{\Omega} \Theta_{\alpha} \left(\frac{\partial \Phi}{\partial t} + a_i \frac{\partial \Phi}{\partial x_i} + b_i \frac{\partial \Phi}{\partial x_i} + c_{ij} \frac{\partial^2 \Phi}{\partial x_i \partial x_j} - Q \right) d\Omega d\xi = 0 \quad (114)$$

without the Jacobians

$$(W(\xi), (\Theta_{\alpha}, R)) = \int_{\xi} W(\xi) \int_{\Omega} \Theta_{\alpha} \left(\frac{\partial \Phi}{\partial t} + \frac{\partial F_i}{\partial x_i} + \frac{\partial G_i}{\partial x_i} - Q \right) d\Omega d\xi = 0 \quad (115)$$

To simplify the equations 114 and 115, the temporal test function, $W(\xi)$ will be assumed equal to $\delta(\xi - \frac{1}{2})$ or $W(\xi) = 1$.

The finite element equation of GGM is

$$\left[A_{\alpha\beta} \delta_{rs} + \frac{\Delta t}{2} (B_{\alpha\beta rs} + K_{\alpha\beta rs}) \right] \Delta \Phi_{\beta s}^{n+1} = H_{\alpha r}^n + N_{\alpha r}^n \quad (116)$$

where

$$A_{\alpha\beta} = \int_{\Omega} \Theta_{\alpha} \Theta_{\beta} d\Omega$$

$$B_{\alpha\beta rs} = - \int_{\Omega} (a_{irs} + b_{irs}) \Theta_{\alpha, i} \Theta_{\beta} d\Omega$$

$$K_{\alpha\beta rs} = \int_{\Omega} c_{ijrs} \Theta_{\alpha,i} \Theta_{\beta,j} d\Omega$$

$$H_{\alpha r}^n = \Delta t \int_{\Omega} \Theta_{\alpha} \Theta_{\beta} Q_{\beta r} d\Omega$$

$$N_{\alpha r}^n = \Delta t \int_{\Gamma} \Theta_{\alpha}^* (F_{ir}^n + G_{ir}^n) n_i d\Gamma$$

Similarly for Equation 115, you get

$$A_{\alpha\beta} \delta_{rs} \Delta \Phi_{\beta s}^{n+1} = \frac{\Delta t}{2} [E_{\alpha\beta i} (F_{\beta ir}^n + G_{\beta ir}^n)] + \Delta t (H_{\alpha r}^n + N_{\alpha r}^n) \quad (117)$$

where

$$E_{\alpha\beta i} = \int_{\Omega} \Theta_{\alpha,i} \Theta_{\beta} d\Omega$$

Equation 117 is resolved in two steps in the explicit way.

Step 1

$$A_{\alpha\beta} \delta_{rs} \Delta \Phi_{\beta s}^{n+1/2} = \frac{\Delta t}{2} [E_{\alpha\beta i} (F_{\beta ir}^n + G_{\beta ir}^n)] + 2(H_{\alpha r}^n + N_{\alpha r}^n) \quad (118)$$

Step 2

$$A_{\alpha\beta} \delta_{rs} \Delta \Phi_{\beta s}^{n+1} = \frac{\Delta t}{2} [E_{\alpha\beta i} (F_{\beta ir}^{n+1/2} + G_{\beta ir}^{n+1/2})] + 2(H_{\alpha r}^{n+1/2} + N_{\alpha r}^n) \quad (119)$$

The nodal values, $F_{\beta ir}^{n+1/2}$, $G_{\beta ir}^{n+1/2}$ e $H_{\alpha r}^{n+1/2}$ of step 1, are estimated or determined by boundary conditions, and $F_{\beta ir}^{n+1}$, $G_{\beta ir}^{n+1}$ e $H_{\alpha r}^{n+1}$ in step 2 are calculated for $\Phi_{\beta s}^{n+1/2}$ CHUNG, 2002.

Taylor-Galerkin Method

The TGM method is a special case of the generalized Galerkin method (GGM). This is also applied to solve the system of Navier-Stokes equations. In order to deal with the system of Navier-Stokes equations, Equation 103, it is convenient to work with conservation variables transformed from the convection and diffusion flows DONEA, 1984.

$$\frac{\partial F_i}{\partial t} = a_i \frac{\partial \Phi}{\partial t} \quad (120a)$$

$$\frac{\partial G_i}{\partial t} = b_i \frac{\partial \Phi}{\partial t} + c_{ij} \frac{\partial}{\partial t} \left(\frac{\partial \Phi}{\partial x_j} \right) \quad (120b)$$

In Equation 120 it is assumed that both the advective term and the diffusive term are functions of the conservation flow variable, Φ . In addition, the diffusive flow term is a

function of the diffusion gradient of the conservation flow variable. By this we define a_i as convective Jacobian, b_i as diffusive Jacobian, and c_{ij} as the Jacobian of the diffusion gradient. These data are

$$a_i = \frac{\partial F_i}{\partial \Phi}, \quad b_i = \frac{\partial G_i}{\partial \Phi}, \quad c_{ij} = \frac{\partial G_i}{\partial \Phi_{,j}} \quad (121)$$

being $\Phi_{,j} = \frac{\partial \Phi}{\partial x_j}$ the diffusion gradient.

Considering the expansion in Taylor Series of Φ^{n+1} , where the +1 notation represents an analysis in the later time space, in the form,

$$\Phi^{n+1} = \Phi^n + \Delta t \frac{\partial \Phi^n}{\partial t} + \frac{\Delta t^2}{2} \frac{\partial^2 \Phi^{n+1}}{\partial t^2} + O(\Delta t^3) \quad (122)$$

where the second derivative is in the implicit form (n + 1). Replacing Equation 103 in Equation 122 one gets

$$\Delta \Phi^{n+1} = \Delta t \left(-\frac{\partial F_i}{\partial x_i} - \frac{\partial G_i}{\partial x_i} + Q \right)^n + \frac{\Delta t^2}{2} \frac{\partial}{\partial t} \left(-\frac{\partial F_i}{\partial x_i} - \frac{\partial G_i}{\partial x_i} + Q \right)^{n+1} + O(\Delta t^3) \quad (123)$$

From the definition of the Jacobians of convection, diffusion and diffusion gradient, the temporal rate variations of the convection and diffusion variables are;

$$\frac{\partial F_i^n}{\partial t} = \left(a_i \frac{\partial \Phi}{\partial t} \right)^n = \left[a_i \left(-\frac{\partial F_i}{\partial x_i} - \frac{\partial G_i}{\partial x_i} + Q \right) \right]^n \quad (124a)$$

$$\frac{\partial F_i^{n+1}}{\partial t} = a_i \left(-\frac{\partial F_j^{n+1}}{\partial x_i} - \frac{\partial G_j^{n+1}}{\partial x_i} + Q^{n+1} \right)$$

$$\frac{\partial F_i^{n+1}}{\partial t} = a_i \left[-a_j \frac{\partial}{\partial x_j} (\Phi^{n+1} - \Phi^n) - \frac{\partial F_j^n}{\partial x_j} - \frac{\partial G_j^{n+1}}{\partial x_j} + Q^{n+1} \right] \quad (124b)$$

$$\frac{\partial G_i^{n+1}}{\partial t} = \left(b_i \frac{\partial \Phi}{\partial t} \right)^{n+1} + \left[c_{ij} \frac{\partial}{\partial t} \left(\frac{\partial \Phi}{\partial x_j} \right) \right]^{n+1} \quad (125a)$$

or

$$\frac{\partial G_i^{n+1}}{\partial t} = \left(b_i - \frac{\partial c_{ij}}{\partial x_j} \right) \frac{\Delta \Phi^{n+1}}{\Delta t} + \frac{\partial}{\partial x_j} \left(c_{ij} \frac{\Delta \Phi}{\Delta t} \right)^{n+1} \quad (125b)$$

Substituting the equations 124 and 125 into Equation 123:

$$\begin{aligned} \Delta\Phi^{n+1} = & \Delta t \left(-\frac{\partial F_i}{\partial x_i} - \frac{\partial G_i}{\partial x_i} + Q \right)^n \\ & + \frac{\Delta t^2}{2} \left\{ \frac{\partial}{\partial x_i} \left[-a_i \left(-a_j \frac{\partial \Delta\Phi^{n+1}}{\partial x_j} - \frac{\partial F_j^n}{\partial x_j} - \frac{\partial G_j^{n+1}}{\partial x_j} + Q^{n+1} \right) \right. \right. \\ & \left. \left. - \left(e_i + \frac{\partial c_{ij}}{\partial x_j} \right) \frac{\Delta\Phi^{n+1}}{\Delta t} \right] + \frac{\partial Q^{n+1}}{\partial t} \right\} \end{aligned} \quad (126)$$

with

$$e_i = b_i - \frac{\partial c_{ij}}{\partial x_j}$$

Neglecting the temporal and spatial derivatives of Q for flow problems, the above expression will be

$$\left\{ 1 + \frac{\Delta t}{2} \frac{\partial e_i}{\partial x_i} \left(a_i a_j - \frac{c_{ij}}{\Delta t} \right) \frac{\partial}{\partial x_j} \right\} \Delta\Phi^{n+1} = \Delta t \left(-\frac{\partial F_i}{\partial x_i} - \frac{\partial G_i}{\partial x_i} + Q \right)^n + \frac{\Delta t^2}{2} \frac{\partial}{\partial x_i} \left(a_i \frac{\partial F_j}{\partial x_j} \right)^n \quad (127)$$

In this equation, the second derivatives of G_i are neglected and all Jacobians are considered constants within each time interval, being, however, updated at each subsequent time interval. These approximations are direct implications of the method.

In FEM the variables are approximated by the interpolation functions in the form:

$$\Phi = W_\alpha \Phi_\alpha, \quad F_i = W_\alpha F_{\alpha i}, \quad G_i = W_\alpha G_{\alpha i}, \quad Q = W_\alpha Q_\alpha$$

Thus, by applying the approximate functions in Equation 127:

$$(A_{\alpha\beta} \delta_{rs} + B_{\alpha\beta rs}) \Delta\Phi_{\beta s}^{n+1} = H_{\alpha r}^n + N_{\alpha r}^{n+1} + \bar{N}_{\alpha r}^n \quad (128)$$

where

$$\begin{aligned} A_{\alpha\beta} &= \int_{\Omega} W_\alpha W_\beta d\Omega \\ B_{\alpha\beta rs} &= \frac{\Delta t}{2} \int_{\Omega} e_{irs} W_\alpha W_{\beta,i} d\Omega + \frac{\Delta t^2}{2} \int_{\Omega} \left(a_{irq} a_{jq s} - \frac{c_{ijrs}}{\Delta t} \right) W_{\alpha,i} W_{\beta,j} d\Omega \\ H_{\alpha r} &= \Delta t \int_{\Omega} \left[W_{\alpha,i} W_\beta (F_{\beta ir}^n + G_{\beta ir}^n) + W_\alpha W_\beta Q_{\beta r}^n - \frac{\Delta t}{2} a_{irs} W_{\alpha,i} W_{\beta,j} F_{\beta js}^n \right] d\Omega \\ N_{\alpha r}^{n+1} &= \frac{\Delta t^2}{2} \int_{\Gamma} \left(a_{irq} a_{jq s} - \frac{c_{ijrs}}{\Delta t} \right) W_\alpha \Delta\Phi_{s,j}^{n+1} n_i d\Gamma \\ \bar{N}_{\alpha r}^n &= - \int_{\Gamma} \left[\Delta t W_\alpha (F_{ir}^n + G_{ir}^n) - \frac{\Delta t^2}{2} a_{irs} W_\alpha F_{js,i}^n \right] n_i d\Gamma \end{aligned}$$

where the indexes α and β denote the local loop nodes, r and s represent the number of the equation listed in Equation 103, i and j indicate the spatial coordinates CHUNG, 2002.

Instead of evaluating the implicit second-order derivatives, one can maintain the explicit form of the Taylor series. In this way, Equation 122 is rewritten:

$$\Phi^{n+1} = \Phi^n + \Delta t \frac{\partial \Phi^n}{\partial t} + \frac{\Delta t^2}{2} \frac{\partial^2 \Phi^n}{\partial t^2} + \mathbf{O}(\Delta t^3) \quad (129)$$

where

$$\frac{\partial \Phi}{\partial t} = -\frac{\partial F_i}{\partial x_i} - \frac{\partial G_i}{\partial x_i} + Q = -a_i \frac{\partial \Phi}{\partial x_i} - \frac{\partial G_i}{\partial x_i} + Q \quad (130a)$$

$$\frac{\partial^2 \Phi}{\partial t^2} = -\frac{\partial}{\partial t} \left(a_i \frac{\partial \Phi}{\partial x_i} + \frac{\partial G_i}{\partial x_i} - Q \right) \quad (130b)$$

or

$$\frac{\partial^2 \Phi}{\partial t^2} = \frac{\partial}{\partial x_j} \left(a_i a_j \frac{\partial \Phi}{\partial x_i} \right) + \frac{\partial}{\partial x_i} \left(a_i \frac{\partial G_j}{\partial x_j} \right) - \frac{\partial}{\partial x_i} (a_i Q) + \frac{\partial Q}{\partial t} \quad (131)$$

Substituting the Equations 130 and 131 into Equation 129 it is obtained

$$\Delta \Phi^{n+1} = \Delta t \left\{ -\frac{\partial F_i}{\partial x_i} - \frac{\partial G_i}{\partial x_i} + Q + \frac{\Delta t}{2} \left[\frac{\partial}{\partial x_j} \left(a_i a_j \frac{\partial \Phi}{\partial x_i} \right) + \frac{\partial^2 (a_i G_j)}{\partial x_i \partial x_j} - \frac{\partial}{\partial x_i} (a_i Q) + \frac{\partial Q}{\partial t} \right] \right\}^n \quad (132)$$

or

$$\Delta \Phi^{n+1} = \Delta t \left(-\frac{\partial F_i}{\partial x_i} - \frac{\partial G_i}{\partial x_i} + Q \right)^n + \frac{\Delta t^2}{2} \left\{ \frac{\partial}{\partial x_i} \left(a_i a_j \frac{\partial \Delta \Phi^{n+1}}{\partial x_j} + a_i \frac{\partial F_j^n}{\partial x_j} \right) + \frac{\partial^2 (a_i G_j)^{n+1}}{\partial x_i \partial x_j} + \frac{\partial}{\partial x_i} (a_i Q)^{n+1} + \frac{\partial Q^{n+1}}{\partial t} \right\} \quad (133)$$

Rearranging the above equation

$$\left[1 - \frac{\Delta t^2}{2} \frac{\partial}{\partial x_i} \left(a_i a_j - \frac{c_{ij}}{\Delta t} \right) \frac{\partial}{\partial x_j} \right] \Delta \Phi^{n+1} = \Delta t \left(-\frac{\partial F_i}{\partial x_i} - \frac{\partial G_i}{\partial x_i} + Q \right)^n + \frac{\Delta t^2}{2} \left(a_i \frac{\partial F_j^n}{\partial x_j} \right)^n \quad (134)$$

Following the same procedure of neglecting the second derivatives of G_i and further assuming constant Q in space and time, the approximating functions are applied and one obtains:

$$(A_{\alpha\beta} \delta_{rs} + B_{\alpha\beta rs}) \Delta \Phi_{\beta s}^{n+1} = H_{\alpha r}^n + N_{\alpha r}^{n+1} + \bar{N}_{\alpha r}^n$$

where

$$A_{\alpha\beta} = \int_{\Omega} W_{\alpha} W_{\beta} d\Omega$$

$$B_{\alpha\beta rs} = \frac{\Delta t^2}{2} \int_{\Omega} \left(a_{ir} a_{jq} - \frac{c_{ijrs}}{\Delta t} \right) W_{\alpha,i} W_{\beta,j} d\Omega$$

$$H_{\alpha r}^n = \Delta t \int_{\Omega} \left[W_{\alpha,i} W_{\beta} \left(F_{\beta ir}^n + G_{\beta ir}^n \right) - W_{\alpha} W_{\beta} Q_{\beta r}^n - \frac{\Delta t^2}{2} a_{irs} W_{\alpha,i} W_{\beta,j} F_{\beta js}^n \right] d\Omega$$

$$N_{\alpha r}^{n+1} = \frac{\Delta t}{2} \int_{\Gamma} \left(a_{irq} a_{jq s} - \frac{c_{ijrs}}{\Delta t} \right) W_{\alpha} \Delta \Phi_{s,j}^{n+1} n_i d\Gamma$$

$$\bar{N}_{\alpha r}^n = - \int_{\Gamma} \left[\Delta t W_{\alpha} (F_{ir}^n + G_{ir}^n) - \frac{\Delta t^2}{2} a_{irs} W_{\alpha} F_{js,j}^n \right] n_i d\Gamma$$

Taylor-Galerkin Method with the Split Operator

If the source term Q presents very different temporal scales when compared with the time scales of the convection of the fluid, as it happens in chemical reactions, it becomes more advantageous the application of the split of the system of Navier-Stokes equations in two parts, such that the flow can be treated explicitly, whereas the term source in the implicit form ROIG, 2007. In this way, Equation 103 can be rewritten,

$$\frac{\partial \Phi}{\partial t} + \frac{\partial F_i}{\partial x_i} + \frac{\partial G_i}{\partial x_i} = 0 \quad (135a)$$

$$\frac{\partial \Phi}{\partial t} = Q \quad (135b)$$

Applying the split operator to Equation 135 and writing the Taylor-Galerkin method in two steps.

Step 1

$$\Delta \Phi^{n+1/2} = \Phi^{n+1/2} - \Phi^n = \frac{\Delta t}{2} \left(\frac{\partial F_i}{\partial x_i} + \frac{\partial G_i}{\partial x_i} \right)^n, \quad A_{\alpha} \delta_{rs} \Phi_{\beta s}^{n+1/2} = Y_{\alpha r}^n \quad (136a)$$

Step 2

$$\Delta \Phi^{n+1} = -\Delta t \left(\frac{\partial F_i}{\partial x_i} + \frac{\partial G_i}{\partial x_i} \right)^{n+1/2}, \quad A_{\alpha\beta} \delta_{rs} \Phi_{\beta s}^{n+1} = Y_{\alpha r}^{n+1/2} \quad (136b)$$

The Equation 135b is evaluated at an intermediate increment $m+1$ and m between n and $n+1$.

$$\frac{\partial \Phi^{m+1}}{\partial t} = Q^{m+1} \quad (137)$$

being

$$\frac{\partial \Phi^{m+1}}{\partial t} = \frac{\Phi^{m+1} - \Phi^m}{\Delta t} = \frac{\Delta \Phi^{m+1}}{\Delta t} + \frac{\Delta \Phi^m}{\Delta t} \quad (138a)$$

$$Q^{m+1} = Q^m + \frac{\partial Q}{\partial \Phi} \Delta \Phi^{m+1} \quad (138b)$$

with

$$\Delta \Phi^{m+1} = \Phi^{m+1} - \Phi^m, \quad \Delta \Phi^m = \Phi^m - \Phi^n$$

Substituting Equation 138 into Equation 137, **Step 3**

$$\left(I - \Delta t \frac{\partial Q}{\partial \Phi}\right) \Delta \Phi^{m+1} = -\Delta \Phi^m + \Delta t Q^m \quad (139)$$

Using the analogous method for the application of finite elements, through the weak formulation of Galerkin, we have

$$(A_{\alpha\beta} \delta_{rs} - \Delta t B_{\alpha\beta rs}) \Delta \Phi_{\beta s}^{m+1} = -A_{\alpha\beta} \delta_{rs} \Delta \Phi_{\beta s}^m + \Delta t A_{\alpha\beta} \delta_{rs} Q_{rs}^m \quad (140)$$

as

$$A_{\alpha\beta} = \int_{\Omega} W_{\alpha} W_{\beta} d\Omega$$

$$B_{\alpha\beta rs} = \int_{\Omega} f_{rs} W_{\alpha} W_{\beta} d\Omega$$

$$f_{rs} = \frac{\partial Q_{(r)}}{\partial \Phi_{(s)}}$$

Characteristic Galerkin method

The characteristic Galerkin method (CGM) is based on the concept of trajectory or characteristic XIKUI and WENHUA, 1999 with

$$x_i^n = x_i^{n+1} - \Delta t u_i^n \quad (141)$$

Differentiating in relation to time

$$u_i^n = u_i^{n+1} - \Delta t u_j^n \frac{\partial u_i^n}{\partial x_j} \quad (142)$$

Combining the Equations 127 and 128:

$$x_i^{n+1} - x_i^n = \Delta t u_i^n - \frac{\Delta t^2}{2} u_j^n \frac{\partial u_i^n}{\partial x_j} \quad (143)$$

The objective of the CGM is to write the governing equations through the fluid characteristic for the Navier-Stokes equation system in a similar way to that presented in Equation 143. In this way,

$$\Delta \Phi^{n+1} = \Delta t R^n - \frac{\Delta t^2}{2} a_j^n \frac{\partial R^n}{\partial x_j} \quad (144)$$

where R^n is the residue defined as

$$R^n = - \left(\frac{\partial F_i^n}{\partial x_i} + \frac{\partial G_i^n}{\partial x_i} - Q^n \right)$$

According to this method, the momentum equation without the pressure is solved initially, followed by the continuity equation, which takes into account the pressure.

Momentum (initial)

$$\Delta \overline{\rho u_i^n} = \Delta t R_i^n - \frac{\Delta t^2}{2} u_k \frac{\partial \hat{R}_i^n}{\partial x_k} \quad (145)$$

with

$$R_i^n = -\frac{\partial}{\partial x_j} (\rho u_i u_j - \tau_{ij}) + \rho g_i$$

$$\hat{R}_i^n = R_i^n - \frac{\partial p^n}{\partial x_i}$$

Continuity

$$\Delta \rho = -\Delta t \frac{\partial}{\partial x_i} (\rho u_i^n + \theta_1 \Delta \overline{\rho u_i^n}) + \theta_1 \Delta t^2 \frac{\partial^2 p^{n+\theta_2}}{\partial x_i \partial x_i} \quad (146)$$

where $0 \leq \theta_1, \theta_2 \leq 1$

Momentum (actualized)

$$\Delta \rho u_i^n = \Delta \overline{\rho u_i^n} - \Delta t \frac{\partial p^{n+\theta_2}}{\partial x_i} \quad (147)$$

Energy

$$\Delta \rho E^n = \Delta t R^n - \frac{\Delta t^2}{2} u_k \frac{\partial R^n}{\partial x_k} \quad (148)$$

where

$$R^n = -\frac{\partial}{\partial x_i} \left[(\rho E + p) u_i - k \frac{\partial T}{\partial x_i} - \tau_{ij} u_j \right]$$

To exploit the physical effects produced by CGM, Equation 145 is replaced in Equation 147 XIKUI and WENHUA, 1999, then, it is obtained

$$\frac{\partial}{\partial t} (\rho u_i) + \frac{\partial}{\partial x_j} (\rho u_i u_j) + \frac{\partial p}{\partial x_i} - \frac{\partial \tau_{ij}}{\partial x_j} - \rho f_i = S_i(m) \quad (149)$$

where

$$S_i(m) = \frac{\Delta t}{2} \frac{\partial}{\partial x_k} \left\{ u_k \left[\frac{\partial}{\partial x_j} (\rho u_i u_j) + \frac{\partial p}{\partial x_i} - \frac{\partial \tau_{ij}}{\partial x_j} - \rho f_i \right] \right\} \quad (150)$$

Similarly, the continuity equation (Equation 146) and the energy equation (Equation 148) are rewritten as

$$\frac{\partial \rho}{\partial t} + \frac{\partial}{\partial x_j} (\rho u_j) = S(c) \quad (151)$$

being

$$S(c) = \frac{\Delta t}{2} \left[\frac{\partial^2}{\partial x_j \partial x_i} (\rho u_i u_j - \tau_{ij}) + \frac{\partial^2 p}{\partial x_i \partial x_i} - \frac{\partial}{\partial x_i} (\rho f_i) \right] \quad (152)$$

adopting $\theta_1 = 1/2$ and $\theta_2 = 0$ in Equation 146

In this way, the energy equation is in the form,

$$\frac{\partial \rho E}{\partial t} + \frac{\partial}{\partial x_j} \left[(\rho E + p)u_i - k \frac{\partial T}{\partial x_i} - \tau_{ij}u_j \right] = S(e) \quad (153)$$

where

$$S(e) = \frac{\Delta t}{2} u_j \frac{\partial}{\partial x_j} \left[\frac{\partial}{\partial x_i} (\rho E u_i + p u_i - k \frac{\partial T}{\partial x_i} - \tau_{ik} u_k) \right] \quad (154)$$

The terms $S(m)$, $S(c)$ and $S(e)$ in the momentum, continuity and energy squares, respectively, arise as numerical diffusion.

Characteristic-Based Split (CBS)

Methods featuring stabilizers for the matter of the convective term in compressible and incompressible flows need to have sufficient stability to suppress oscillations due to the standard Galerkin discretization of this term. Several stabilization schemes have been introduced in recent years. Among these, CGM and TGM are developed using temporal scaling as a basis. The use of CGM has been demonstrated by several authors for simple convection-diffusion problems, and recently these methods have been employed to deal with the complete equation of fluid dynamics.

Although several versions of CGM are possible, they are all based on a Taylor series expansion and are attractive because of their ease of implementation and versatility. Its equivalence to other standard stabilization schemes can also be demonstrated for convection-diffusion problems if the time step is suitably scaled using an appropriate rate scale and a length scale.

Since its introduction in 1995, as a variant of CGM, the CBS method has been widely employed in problems of fluid dynamics and solids.

The CBS scheme is a variant of the CGM and it was originally introduced for a solution in the fully explicit form. Later, it was extended to the semi-implicit form and can be applied for both compressible and incompressible flows. From the outset, it has been realized that the explicit solution to the fully incompressible fluid dynamics equations using the CBS scheme is possible, provided an artificial compressibility method is employed. The solution of transient problems with CBS was achieved using a two-step time-staging approach. Recently, the method was extended to solve problems of viscoelastic flow NITHIARASU, CODINA, and ZIENKIEWICZ, 2006.

Temporal Discretization

Let be the momentum equation Equation 92, rewritten as

$$\frac{\partial U_i}{\partial t} = - \frac{\partial}{\partial x_j} (u_j U_i) + \frac{\partial \tau_{ij}}{\partial x_j} - \frac{\partial p}{\partial x_i} + \rho g_i \quad (155)$$

where U_i represents the mass flow given by

$$U_i = \rho u_i$$

To apply the split to the equation and introduce the approximations there are two alternatives: Split A and Split B. Assuming in each split a time increment of $\Delta t = t^{n+1} - t^n$,

$$U_i^{n+1} = U_i + \Delta U_i^* + \Delta U_i^{**} \quad (156)$$

For the interval $t^n \leq t \leq t^{n+1}$, the time derivative in Eq. 141 can also be discretized in time as follows:

$$\frac{\partial U_i}{\partial t} = \frac{U_i^{n+1} - U_i^n}{\Delta t} = \frac{\Delta U_i^*}{\Delta t} + \frac{\Delta U_i^{**}}{\Delta t} \quad (157)$$

Thus, from the CGM method we have

$$\begin{aligned} U_i^{n+1} - U_i^n = \Delta t & \left[-\frac{\partial}{\partial x_j} (u_j U_i^n) + \frac{\tau_{ij}^n}{\partial x_j} + (\rho g_i)^n \right] - \Delta t \frac{\partial p^{n+\theta_2}}{\partial x_i} \\ & + \frac{\Delta t^2}{2} u_k \frac{\partial}{\partial x_k} \left[\frac{\partial}{\partial x_j} (u_j U_i) - \frac{\tau_{ij}^n}{\partial x_j} - \rho g_i \right]^n + \frac{\Delta t^2}{2} u_k \frac{\partial}{\partial x_k} \left(\frac{\partial p^{n+\theta_2}}{\partial x_i} \right) \end{aligned} \quad (158)$$

Being

$$\frac{\partial p^{n+\theta_2}}{\partial x_i} = (1 - \theta_2) \frac{\partial p^n}{\partial x_i} + \theta_2 \frac{\partial p^{n+1}}{\partial x_i} \quad (159a)$$

or

$$\frac{\partial p^{n+\theta_2}}{\partial x_i} = \frac{\partial p^n}{\partial x_i} + \theta_2 \frac{\partial \Delta p}{\partial x_i} \quad (159b)$$

where

$$\Delta p = p^{n+1} - p^n \quad (159c)$$

Using the auxiliary variables ΔU_i^* and U_i^{**} , Equation 158 is divided into two parts. In the first part the pressure gradient is removed, while in the second, the pressure gradient corresponding to the beginning of the step, i.e., $\frac{\partial p^n}{\partial x_i}$, is returned. In this way, Split A is recommended for steady-state problems. For transient problems, it is recommended to apply the Split B by adding a pressure stabilizer or the Split A with double time scaling, which presents slightly better results ZIENKIEWICZ, TAYLOR, and NITHIARASU, 2014.

Split A

Introducing the auxiliary variable ΔU_i^* and neglecting the third order terms

$$\Delta U_i^* = \Delta t \left[-\frac{\partial}{\partial x_j} (u_j U_i) + \frac{\partial \tau_{ij}}{\partial x_j} + \frac{\partial (\rho g_i)}{\partial x_i} + \frac{\Delta t}{2} u_k \frac{\partial}{\partial x_k} \left(\frac{\partial}{\partial x_j} (u_j U_i) - \rho g_i \right) \right]^n \quad (160)$$

Thus, the above equation is solved by an explicit time step, making the solution possible. The correction given below is intended to evaluate the pressure increase.

$$\Delta U_i^{**} = -\Delta t \frac{\partial p^{n+\theta_2}}{\partial x_i} + \frac{\Delta t^2}{2} u_k \frac{\partial^2 p^n}{\partial x_k \partial x_i} \quad (161)$$

From the time discretization of the Equation 90 it's obtained:

$$\Delta \rho = -\Delta t \frac{\partial U_i^{n+\theta_1}}{\partial x_i} = -\Delta t \left[\frac{\partial U_i^n}{\partial x_i} + \theta_1 \frac{\partial \Delta U_i}{\partial x_i} \right] \quad (162)$$

Applying the auxiliary variable ΔU_i^* in the above equation,

$$\Delta \rho = -\Delta t \left[\frac{\partial U_i^n}{\partial x_i} + \theta_1 \frac{\partial \Delta U_i^*}{\partial x_i} - \Delta t \theta_1 \left(\frac{\partial^2 p^n}{\partial x_i \partial x_j} + \theta_2 \frac{\partial^2 \Delta p}{\partial x_i \partial x_i} \right) \right] \quad (163)$$

Now, therefore, one can apply the Galerkin method in the above equation. In this way, the governing equations can be solved after the spatial discretization in the following order NITHIARASU, CODINA, and ZIENKIEWICZ, 2006:

- Equation 160 to get at step 1: ΔU_i^*
- Equation 163 to get at step 2: $\Delta \rho$
- Equation 161 to get at step 3: ΔU_i^{**} to establish the values of U_i and p for the energy and gas law at t^{n+1} .

After obtaining ΔU_i and ρ , the energy equation is treated independently and the value of $(\rho E)^{n+1}$ is obtained by the CGM method, given by:

$$\frac{\partial \rho E}{\partial t} = -\frac{\partial}{\partial x_i} (u_i \rho E) + \frac{\partial}{\partial x_i} \left(k \frac{\partial T}{\partial x_i} \right) - \frac{\partial}{\partial x_i} (u_i p) + \frac{\partial}{\partial x_i} (\tau_{ij} u_j) + \rho g_i u_i \quad (164)$$

Split B

In this split, the auxiliary variable ΔU_i^* is also entered, keeping the known values of $\partial p^n / \partial x_i$, i.e.,

$$\Delta U_i^* = \Delta t \left[-\frac{\partial}{\partial x_j} (u_j U_i) + \frac{\partial \tau_{ij}}{\partial x_j} - \frac{\partial p}{\partial x_i} + \rho g_i + \frac{\Delta t}{2} u_k \frac{\partial}{\partial x_k} \left(\frac{\partial}{\partial x_j} (u_j U_i) + \frac{\partial p}{\partial x_i} - \rho g_i \right) \right]^n \quad (165)$$

By including the pressure term, this equation gives a better approximation for U_i^* . Now the correction is given by:

$$\Delta U_i^{**} = -\theta_2 \Delta t \frac{\partial \Delta p}{\partial x_i} \quad (166)$$

Therefore, for $\theta_2 = 0$, no correction (ΔU_i^{**}) will be required. The density variation becomes

$$\Delta \rho = -\Delta t \left[\frac{\partial U_i^n}{\partial x_i} + \theta_1 \frac{\partial \Delta U_i^*}{\partial x_i} - \Delta t \theta_1 \theta_2 \frac{\partial^2 \Delta p}{\partial x_i^2} \right] \quad (167)$$

The solution steps are the same as for Split A.

Space Discretization

Using spatial approximations by finite element definition ZIENKIEWICZ, TAYLOR, and NITHIARASU, 2014:

$$\begin{aligned} U_i &= N_u \hat{U}_i & \Delta U_i &= N_u \Delta \hat{U}_i & \Delta U_i^* &= N_u \Delta \hat{U}_i^* & \Delta U_i^{**} &= N_u \Delta \hat{U}_i^{**} \\ u_i &= N_u \hat{u}_i & p &= N_p \hat{p} & \rho &= N_\rho \hat{\rho} \end{aligned}$$

where the elemental vectors of unknowns and interpolation functions are:

$$\begin{aligned} \hat{U}_i &= [\hat{U}_i^1 \ \hat{U}_i^2 \ \dots \ \hat{U}_i^a \ \dots \ \hat{U}_i^m]^T \\ N &= [N^1 \ N^2 \ \dots \ N^a \ \dots \ N^m] \end{aligned}$$

and a is the identification number of the node, which varies between 1 and m .

Split A

From the weak formulation of the Galerkin method, we have:

$$\begin{aligned} \int_{\Omega} N_u^a \Delta U_i^* d\Omega &= -\Delta t \left[\int_{\Omega} N_u^a \frac{\partial}{\partial x_j} (u_j U_i) d\Omega + \int_{\Omega} \frac{\partial N_u^a}{\partial x_j} \tau_{ij} d\Omega \right. \\ &\quad \left. - \int_{\Omega} N_u^a (\rho g_i) d\Omega \right]^n + \frac{\Delta t^2}{2} \left[\int_{\Omega} \frac{\partial}{\partial x_k} (u_k N_u^a) \left(-\frac{\partial}{\partial x_j} (u_j U_i) \right. \right. \\ &\quad \left. \left. + \rho g_i \right) d\Omega \right]^n + \Delta t \left[\int_{\Gamma} N_u^a \tau_{ij} n_j d\Gamma \right]^n \end{aligned} \quad (168)$$

where the viscous stress tensor is given by

$$\tau_{ij} = 2\mu \left(S_{ij} - \frac{1}{3} \delta_{ij} S_{kk} \right)$$

with the deformation rate given by

$$S_{ij} = \frac{1}{2} \left(\frac{\partial u_i}{\partial x_j} + \frac{\partial u_j}{\partial x_i} \right)$$

and the volumetric deformation given by

$$S_{kk} = \frac{\partial u_k}{\partial x_k}. \quad (169)$$

The six independent components of the deformation rate can be written in matrix form as:

$$\mathbf{S} = [S_{11} \ S_{22} \ S_{33} \ 2S_{12} \ 2S_{23} \ 2S_{31}]^T \quad (170)$$

Defining the matrix

$$m = [1 \ 1 \ 1 \ 0 \ 0 \ 0]^T \quad (171)$$

thus, the rate of volumetric deformation is

$$S_v = S_{ii} = S_{11} + S_{22} + S_{33} = m^T \mathbf{S} \quad (172)$$

The rate of shear strain, then, can be rewritten as:

$$\mathbf{S}^d = \mathbf{S} - \frac{1}{3} m S_v = \left(I - \frac{1}{3} m m^T \right) \mathbf{S} = I_d \mathbf{S} \quad (173)$$

where

$$I_d = \left(I - \frac{1}{3} m m^T \right) \quad (174)$$

Thus

$$I_d = \frac{1}{3} \begin{bmatrix} 2 & -1 & -1 & 0 & 0 & 0 \\ -1 & 2 & -1 & 0 & 0 & 0 \\ -1 & -1 & 2 & 0 & 0 & 0 \\ 0 & 0 & 0 & 3 & 0 & 0 \\ 0 & 0 & 0 & 0 & 3 & 0 \\ 0 & 0 & 0 & 0 & 0 & 3 \end{bmatrix} \quad (175)$$

Similarly, the stress tensor, in matrix form, is:

$$\sigma = [\sigma_{11} \ \sigma_{22} \ \sigma_{33} \ \sigma_{12} \ \sigma_{23} \ \sigma_{31}]^T \quad (176)$$

where, for example,

$$\sigma_{11} = \tau_{11} - p$$

$$\sigma_{12} = \tau_{12}$$

with similar definition for other components.

Once the stress tensor is proportional to the deformation rate, it can be written in the following:

$$\sigma^d = I_d \sigma = \mu I_0 \mathbf{S}^d = \mu \left(I - \frac{1}{3} m m^T \right) \mathbf{S} \quad (177)$$

where I_0 is the following diagonal matrix

$$I_0 = \begin{bmatrix} 2 & & & & & \\ & 2 & & & & \\ & & 2 & & & \\ & & & 1 & & \\ & & & & 1 & \\ & & & & & 1 \end{bmatrix} \quad (178)$$

By introducing the concept of the derivation matrix of the velocities and rates of deformation it is shown that the tensor strain can be defined as:

$$\mathbf{S} = S^* u \quad (179)$$

where

$$u = [u_1 \ u_2 \ u_3]^T$$

and S^* is the derivative operator:

$$S^* = \begin{bmatrix} \frac{\partial}{\partial x_1} & 0 & 0 \\ 0 & \frac{\partial}{\partial x_2} & 0 \\ 0 & 0 & \frac{\partial}{\partial x_3} \\ \frac{\partial}{\partial x_2} & \frac{\partial}{\partial x_1} & 0 \\ 0 & \frac{\partial}{\partial x_3} & \frac{\partial}{\partial x_2} \\ \frac{\partial}{\partial x_3} & 0 & \frac{\partial}{\partial x_1} \end{bmatrix} \quad (180)$$

Defining a matrix B as the S^* operator applied to the interpolation functions results:

$$B = S^* N_u \quad (181)$$

Following, the three steps of solution are described. The solution to ΔU_i^* is:

Step 1

$$\Delta \tilde{U}^* = -M_u^{-1} \Delta t [(C_u \tilde{U} + K_\tau \tilde{u} - f) - \Delta t (K_u \tilde{U} + f_s)]^n \quad (182)$$

Values with notation $\tilde{\cdot}$ represent the nodal values. The mass matrix, convective matrix, diffusive matrix and load vector appearing in Eq. (168) are, respectively, defined as:

$$M_u = \int_{\Omega} N_u^T N_u d\Omega \quad (183a)$$

$$C_u = \int_{\Omega} N_u^T (\nabla(u N_u)) d\Omega \quad (183b)$$

$$K_\tau = \int_{\Omega} B^T \mu \left(I_0 - \frac{2}{3} m m^T \right) B d\Omega \quad (183c)$$

$$f = \int_{\Omega} N_u^T \rho g d\Omega + \int_{\Gamma} N_u^T t^d d\Gamma \quad (183d)$$

where g is $[g_1 \ g_2 \ g_3]^T$ e t^d is the traction corresponding to the shear stress tensor.

In the Equation 182 K_u and f_s are the additional terms originated from the CBS scheme (Taylor serie expansion) and these terms act as stabilizers of the solution. They

are defined as:

$$K_u = -\frac{1}{2} \int_{\Omega} [\nabla^T(uN_u)]^T [\nabla^T(uN_u)] d\Omega \quad (184)$$

and

$$f_s = -\frac{1}{2} \int_{\Omega} [\nabla^T(uN_u)]^T \rho g d\Omega \quad (185)$$

The discretization of the weak formulation of the pressure-density Equation 149 is:

$$\begin{aligned} \int_{\Omega} N_p^a \Delta p d\Omega &= -\Delta t \int_{\Omega} N_p^a \frac{\partial}{\partial x_i} \left(U_i^n + \theta_1 \Delta U_i^* - \theta_1 \Delta t \frac{\partial p^{n+\theta_2}}{\partial x_i} \right) d\Omega \\ &= \Delta t \int_{\Omega} \frac{\partial N_p^a}{\partial x_i} \left[U_i^* + \theta_1 \left(\Delta U_i^* - \Delta t \frac{\partial p^{n+\theta_2}}{\partial x_i} \right) \right] d\Omega \\ &\quad - \Delta t \int_{\Gamma} N_p^a \left[U_i^n + \theta_1 \left(\Delta U_i^* - \Delta t \frac{\partial p^{n+\theta_2}}{\partial x_i} \right) \right] n_i d\Gamma \end{aligned} \quad (186)$$

In addition, one must directly discriminate ρ only in problems of compressible gas flows. However, if p is retained as the main variable, then, for spatial discretization Equation 186 it is obtained at Step 2 of the calculation process:

Step 2

$$(M_p + \Delta t^2 \theta_1 \theta_2 H) \Delta \tilde{p} = \Delta t [G \tilde{U}^n + \theta_1 G \Delta \tilde{U}^* - \Delta t \theta_1 H \tilde{p}^n - f_p] \quad (187)$$

The Equation 187 is solved for $\Delta \tilde{p}$.

The new matrices are:

$$H = \int_{\Omega} (\nabla N_p)^T \nabla N_p d\Omega \quad (188a)$$

$$M_p = \int_{\Omega} N_p^T \left(\frac{1}{c^2} \right)^n N_p d\Omega \quad (188b)$$

$$G = \int_{\Omega} (\nabla N_p)^T N_u d\Omega \quad (188c)$$

$$f_p = \Delta t \int_{\Gamma} N_p^T n^T [\tilde{U}^n + \theta_1 (\Delta \tilde{U}^* - \Delta t \nabla p^{n+\theta_2})] d\Gamma \quad (188d)$$

Applying the weak formulation of the Equation 161:

$$\begin{aligned} \int_{\Omega} N_u^a \Delta U_i^{**} d\Omega &= \int_{\Omega} N_u^a \nabla U_i d\Omega - \int_{\Omega} N_u^a \nabla U_i^* d\Omega \\ &= -\Delta t \int_{\Omega} N_u^a \left(\frac{\partial p^n}{\partial x_i} + \theta_2 \frac{\partial \Delta p}{\partial x_i} \right) d\Omega - \frac{\Delta t^2}{2} \int_{\Omega} \frac{\partial}{\partial x_j} (u_j N_u^a) \frac{\partial p^n}{\partial x_i} d\Omega \end{aligned} \quad (189)$$

Thus, after the calculations of ΔU_i^* and Δp described in steps 1 and 2, respectively, to determine the correction of the mass flow vector, ΔU_i^{**} , Step 3 applies.

Step 3

$$\Delta U^{**} = \Delta \tilde{U} - \Delta \tilde{U}^* = -M_u^{-1} \Delta t \left[G^T (\tilde{p}^n + \theta_2 \Delta \tilde{p} + \frac{\Delta t}{2} P \tilde{p}^n) \right] \quad (190)$$

in which

$$P = \int_{\Omega} (\Delta(uN_u))^T \nabla N_p d\Omega \quad (191)$$

At the end of this step, the values of \tilde{U}^{n+1} and \tilde{p}^{n+1} are determined. The calculation of energy $(\rho E)^{n+1}$ is also required, for compressible flow problems, to obtain density from a thermodynamic state equation involving temperature and pressure. If the density is the variable in Eq. 172, then the pressure can be obtained from a thermodynamic state equation.

Thus, Equation 99b written in the weak form and applying the approximation of the CGM method is:

$$\begin{aligned} \int_{\Omega} N_E^k \Delta(\rho E)^{n+1} d\Omega &= \Delta t \left[- \int_{\Omega} N_E^k \frac{\partial}{\partial x_i} (u_i (\rho E + p)) d\Omega - \int_{\Omega} \frac{\partial N_E^k}{\partial x_i} \left(\tau_{ij} u_j + k \frac{\partial T}{\partial x_i} \right) d\Omega \right]^n \\ &+ \frac{\Delta t^2}{2} \left\{ \int_{\Omega} \frac{\partial}{\partial x_j} (u_j N_E^k) \left[\frac{\partial}{\partial x_i} (-u_i (\rho E + p)) \right] d\Omega \right\}^n \\ &+ \Delta t \left[\int_{\Gamma} N_E^k \left(\tau_{ij} u_j + k \frac{\partial T}{\partial x_i} \right) n_i d\Gamma \right]^n \end{aligned} \quad (192)$$

Using the approximate functions

$$\rho E = N_E \tilde{E} \quad \text{and} \quad T = N_T \tilde{T} \quad (193)$$

results the **Step 4**:

$$\Delta \tilde{E} = -M_E^{-1} \Delta t \left[C_E \tilde{E} + C_p \tilde{p} + K_T \tilde{T} + K_{\tau E} \tilde{u} + f_e - \Delta t (K_{uE} \tilde{E} + K_{up} \tilde{p} + f_{es}) \right]^n \quad (194)$$

where \tilde{E} are the nodal values of ρE and the matrices and vectors are similar to those shown above.

$$\begin{aligned} M_E &= \int_{\Omega} N_E^T N_E d\Omega \\ C_E &= \int_{\Omega} N_E^T \nabla^T (u N_E) d\Omega \\ C_p &= \int_{\Omega} N_E^T \nabla^T (u N_p) d\Omega \\ K_T &= \int_{\Omega} (\nabla N_E)^T k \nabla N_T d\Omega \end{aligned}$$

$$\begin{aligned}
K_{\tau E} &= \int_{\Omega} B^T \mu u_{\alpha v} (I_0 - \frac{2}{3} m m^T) B d\Omega \\
K_{uE} &= -\frac{1}{2} \int_{\Omega} (\nabla^T (u N_E))^T (\nabla N_E) d\Omega \\
f_e &= \int_{\Gamma} N_E^T n^T (t^d u + k \nabla T) d\Gamma \\
K_{up} &= -\frac{1}{2} \int_{\Omega} (\nabla^T N_E)^T (\nabla N_p) d\Omega
\end{aligned}$$

The force term f_{es} contains the source terms.

It is interesting to note that the process of Step 4 may be extended to include any other transport equation describing quantities such as turbulence parameters, chemical concentrations, etc.

For isothermal incompressible flows, the first three steps of the CBS scheme are sufficient. However, for compressible flows, all four steps are necessary and the pressure must be related to density and temperature (energy) by means of a gas law ZIENKIEWICZ, TAYLOR, and NITHIARASU, 2014.

Split B

By applying the Split B, the discretization and solving procedures are very similar those from the Split A. So, applying a discretization procedure identical to the previous one, we have the following solution steps:

Step 1

$$\Delta \tilde{U}_i^* = -M_u^{(-1)} \left[(C_u \tilde{U} + K_{\tau} \tilde{u} + G^T \tilde{p} - f) - \Delta t \left(K_u \tilde{U} + f_s + \frac{\Delta t}{2} P \tilde{p} \right) \right]^n \quad (195)$$

The difference, in relation to Split A, are the additional terms due to the pressure terms included in the Split B.

Step 2

$$(M_p + \Delta t^2 \theta_1 \theta_2 H) \Delta \tilde{p} = \Delta t [G \tilde{U}^n + \theta_1 G \Delta \tilde{U}^* - f_p]^n \quad (196)$$

and

Step 3

$$\Delta \tilde{U}^{**} = -M_u^{-1} \Delta t [\theta_2 G^T \Delta \tilde{p}] \quad (197)$$

Step 4 does not change, it is the same as in Split A.

Diagonalization of the Mass Matrix (*Lumping*)

In steps 1 to 3 of the CBS scheme, the solution requires the inversion of the mass matrices M_u and M_p if a direct method is to be employed. These steps are called explicit or generalized and are used to be approximated in the diagonalized form (*lumped*). Thus, the matrix M_u is rewritten in the lumped form M^L as:

$$M_{ab}^L = \delta_{ab} \int_{\Omega} N_a d\Omega \quad (198)$$

This procedure is applied to transient problems, in which errors occur mainly with mass conservation, thus requiring additional iteration to obtain consistent results.

Interpolation functions

Isoparametric Hexahedral 8 Nodes Definition

Using isoparametric hexahedral eight node elements, the geometry and the unknowns are interpolated by the same interpolation or shape functions. In matrix form, this interpolation can be written as:

$$\begin{bmatrix} x \\ y \\ z \\ u_x \\ u_y \\ u_z \end{bmatrix} = \begin{bmatrix} x_0 & x_1 & x_2 & x_3 & x_4 & x_5 & x_6 & x_7 \\ y_0 & y_1 & y_2 & y_3 & y_4 & y_5 & y_6 & y_7 \\ z_0 & z_1 & z_2 & z_3 & z_4 & z_5 & z_6 & z_7 \\ u_{x_0} & u_{x_1} & u_{x_2} & u_{x_3} & u_{x_4} & u_{x_5} & u_{x_6} & u_{x_7} \\ u_{y_0} & u_{y_1} & u_{y_2} & u_{y_3} & u_{y_4} & u_{y_5} & u_{y_6} & u_{y_7} \\ u_{z_0} & u_{z_1} & u_{z_2} & u_{z_3} & u_{z_4} & u_{z_5} & u_{z_6} & u_{z_7} \end{bmatrix} \begin{bmatrix} N_0^e \\ N_1^e \\ N_2^e \\ N_3^e \\ N_4^e \\ N_5^e \\ N_6^e \\ N_7^e \end{bmatrix} \quad (199)$$

The shape functions in the abstract space of coordinates, ξ , η and ζ ; or reference element are:

$$\begin{aligned} N_0^e &= \frac{1}{8}(1 - \xi)(1 - \eta)(1 - \zeta) & N_4^e &= \frac{1}{8}(1 - \xi)(1 - \eta)(1 + \zeta) \\ N_1^e &= \frac{1}{8}(1 + \xi)(1 - \eta)(1 - \zeta) & N_5^e &= \frac{1}{8}(1 + \xi)(1 - \eta)(1 + \zeta) \\ N_2^e &= \frac{1}{8}(1 + \xi)(1 + \eta)(1 - \zeta) & N_6^e &= \frac{1}{8}(1 + \xi)(1 + \eta)(1 + \zeta) \\ N_3^e &= \frac{1}{8}(1 - \xi)(1 + \eta)(1 - \zeta) & N_7^e &= \frac{1}{8}(1 - \xi)(1 + \eta)(1 + \zeta) \end{aligned} \quad (200)$$

C – TRANSPORT EQUATION AND REYNOLDS DECOMPOSITION

Helmholtz Vorticity Transport Equation

The phenomenon of vorticity presents great importance on the turbulence GATSKI and BONNET, 2009. Thus, a transport equation to vorticity, defined as $\omega = \nabla \times \mathbf{u}$, can be obtained by POWERS, 2016. Consider the momentum equation:

$$\frac{\partial \mathbf{u}}{\partial t} + (\mathbf{u}^T \cdot \nabla) \mathbf{u} = \mathbf{f} - \frac{1}{\rho} \nabla p + \frac{1}{\rho} (\nabla^T \cdot \vec{\tau})^T \quad (201)$$

applying the following vector identities:

$$(\mathbf{u}^T \cdot \nabla) \mathbf{u} = \nabla \left(\frac{\mathbf{u}^T \cdot \mathbf{u}}{2} \right) + \omega \times \mathbf{u}$$

$$\nabla \times (\mathbf{a} \times \mathbf{b}) = (\mathbf{b}^T \cdot \nabla) \mathbf{a} - (\mathbf{a}^T \cdot \nabla) \mathbf{b} + \mathbf{a} (\nabla^T \cdot \mathbf{b}) - \mathbf{b} (\nabla^T \cdot \mathbf{a})$$

$$\nabla \times (\nabla \phi) = 0$$

$$\nabla^T \cdot (\nabla \times \mathbf{u}) = \nabla^T \cdot \omega = 0$$

and applying the curl operator on both sides of the Equation 201 results:

$$\nabla \times \left[\frac{\partial \mathbf{u}}{\partial t} + \nabla \left(\frac{\mathbf{u}^T \cdot \mathbf{u}}{2} \right) + \omega \times \mathbf{u} \right] = \nabla \times \left[\mathbf{f} - \frac{1}{\rho} \nabla p + \frac{1}{\rho} (\nabla^T \cdot \vec{\tau})^T \right] \quad (202)$$

Rearranging,

$$\frac{\partial}{\partial t} (\nabla \times \mathbf{u}) + \nabla \times \left(\nabla \left(\frac{\mathbf{u}^T \cdot \mathbf{u}}{2} \right) \right) + \nabla \times \omega \times \mathbf{u} = \nabla \times \mathbf{f} - \nabla \times \left(\frac{1}{\rho} \Delta p \right) + \nabla \times \left(\frac{1}{\rho} (\nabla^T \cdot \vec{\tau})^T \right) \quad (203)$$

From the conservation of mass and the definition of vorticity, multiplying both sides by density (ρ), we finally have the transport equation to vorticity:

$$\rho \frac{d}{dt} \left(\frac{\omega}{\rho} \right) = \underbrace{(\omega^T \cdot \nabla) \mathbf{u}}_A + \underbrace{\nabla \times \mathbf{f}}_B + \underbrace{\frac{1}{\rho^2} \nabla \rho \times \nabla p}_C + \underbrace{\nabla \times \left(\frac{1}{\rho} (\nabla^T \cdot \vec{\tau})^T \right)}_D \quad (204)$$

The above equation represents the evolution of vorticity with respect to density relative to four physical effects NITHIARASU, BEVAN, and MURALI, 2012:

- A: bending and elongation of vortex tubes;
- B: Nonconservative body forces;
- C: Non-barotropic effect, also known as baroclinic;
- D: Viscous effects.

Mean Flow Equations

Several kinds of averaging are used to define means in turbulent flows. Due to the random characteristic of turbulence, statistical mean should be the natural way of averaging, once the resulting mean is no more a random variable. However, other average approaches such as *time average*, *ensemble average* or *spatial average* are frequently used. In these three last averages, the means are still random variables. *Average* will be any variable denoted by $\bar{\square}$ and *fluctuation*, by \square' .

Thus, the statistical mean, where $P(\phi)$ is the probability density function of ϕ , is of the form CEBECI, 2003

$$\bar{\phi} = \int_{-\infty}^{+\infty} \phi P(\phi) d\phi \quad (205)$$

The *time average*, usually applied for turbulences characterized by being stationary, in which no variation occurs over time, is obtained by

$$F_T(\bar{x}) = \lim_{\Delta t \rightarrow \infty} \frac{1}{\Delta t} \int_t^{t+\Delta t} f(\bar{x}, t) dt \quad (206)$$

The *spatial mean*, normally applied to homogeneous turbulence, flow in which the mean is uniform in all directions, is defined by

$$F_V(t) = \lim_{V \rightarrow \infty} \frac{1}{V} \int \int \int f(\bar{x}, t) dV \quad (207)$$

The *ensemble mean*, applied for N experiments,

$$F_E(\bar{x}, t) = \lim_{N \rightarrow \infty} \frac{1}{N} \sum_{n=1}^N f_n(\bar{x}, t) \quad (208)$$

The filtering process can be defined as a general operation given by SAGAUT, 2006:

$$\bar{\phi}(\bar{x}, t) = \varphi * \phi = \int \varphi(\bar{x} - x', t - t') \phi(x', t') dx' dt' \quad (209)$$

where φ is the filter applied in the equation.

Reynolds decomposition

For the formulation of the RANS method, any instantaneous variable can be decomposed as a sum of the mean plus a fluctuation around the mean; a process known as Reynolds decomposition, in the form:

$$\phi(\vec{x}, t) = \bar{\phi}(\vec{x}, t) + \phi'(\vec{x}, t) \quad (210)$$

In this way, the velocity field is given by

$$u_i(\vec{x}, t) = \bar{u}_i(\vec{x}, t) + u'_i(\vec{x}, t) \quad (211)$$

Applying the time averaging the velocity field is:

$$u_i(\vec{x}, t) = \bar{u}_i(\vec{x}) + u'_i(\vec{x}, t) \quad (212)$$

on what

$$\bar{u}_i = \lim_{\Delta t \rightarrow \infty} \frac{1}{\Delta t} \int_t^{t+\Delta t} u_i(\vec{x}, t) dt$$

From the definition of average one can observe

$$\overline{\bar{u}_i} = \bar{u}_i \quad \text{e} \quad \overline{u'_i} = 0$$

Applying the concept of mean in time implies that

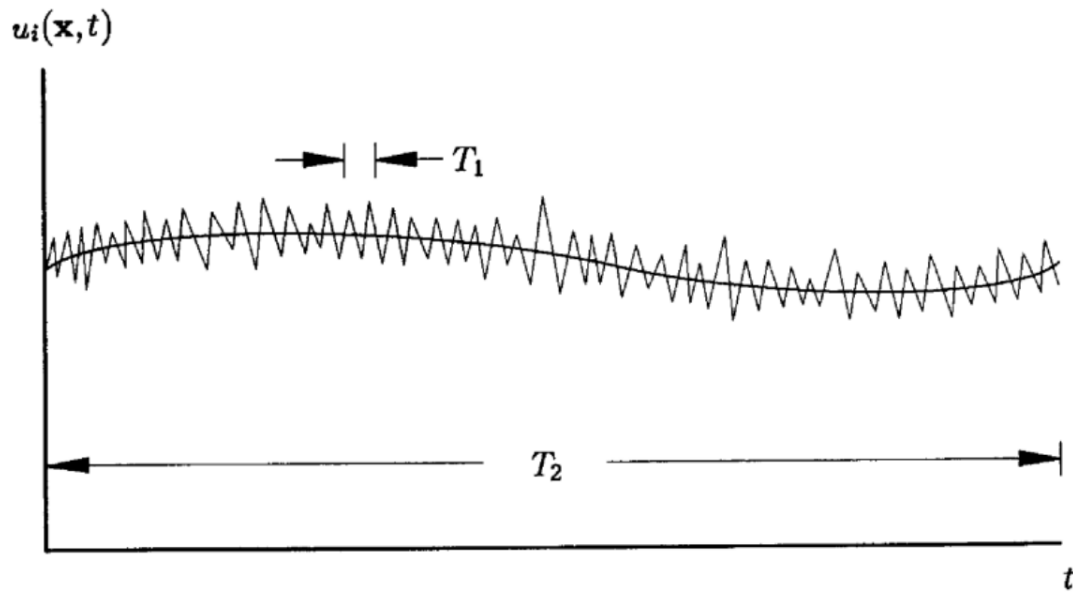
$$\frac{\partial \bar{u}_i}{\partial t} = 0$$

As a result, the system is in a steady state, that is, it presents low variations during the mean flow time. Thus, to analyze the transient process the Reynolds average was defined as:

$$\bar{u}_i(\vec{x}, t) = \lim_{\Delta t \rightarrow \infty} \frac{1}{\Delta t} \int_t^{t+\Delta t} u_i(\vec{x}, t) dt; \quad T_1 \leq \Delta t \leq T_2 \quad (213)$$

Where times T_1 and T_2 are illustrated in Figure 34.

Figure 34 – Characteristic times of turbulent flows.



Source – SILVA SILVA, 2017.

Other ways of considering the transient problem is by applying the concept of set mean and statistics, so the dependence over time is maintained.

From the concept of filter, we have that the filter function is given by SAGAUT, 2006:

$$\begin{aligned}
 \wp(\vec{x} - \vec{x}', t - t') &\equiv \wp_T(\vec{x} - \vec{x}', t - t') \\
 &= G(\vec{x} - \vec{x}')G_T(t - t'; T) \\
 &= \delta(\vec{x} - \vec{x}')\mathcal{H}(t - t')\frac{\mathcal{H}(T - t + t')}{T}
 \end{aligned}
 \tag{214}$$

Thus, another way of expressing the mean through the filter function is:

$$\bar{\phi}_T(\vec{x}, t; T) = \wp_T * \phi = \frac{1}{T} \int_{t-T}^t \phi(\vec{x}, t') dt'
 \tag{215}$$

being the average,

$$\bar{\phi}(\vec{x}) = \lim_{T \rightarrow \infty} \bar{\phi}_T(\vec{x}; T) = \lim_{T \rightarrow \infty} \frac{1}{T} \int_0^T \phi(\vec{x}, t) dt
 \tag{216}$$

Finally, the Reynolds average has as another form of representation,

$$\bar{\phi}(x) = \left(\lim_{T \rightarrow \infty} \wp_T \right) * \phi
 \tag{217}$$

Since $\lim_{T \rightarrow \infty} \wp_T(t) = 0$ can not be interpreted as a convolution filter.

D – TURBULENT COMPRESSIBLE FLOW

As presented by PYATNITSKY (2009), turbulence plays a fundamental role in nature, as in the Earth's atmosphere or in the Sun. Even the air that flows from our lungs is turbulent. Turbulence determines the climate through its influence on large-scale atmospheric and oceanic flows.

"The mathematical description of the turbulence is complex, because of the very difficulty inherent in describing three-dimensional and chaotic processes..." DAVIDSON, 2004. As presented by DAVIDSON (2004), the high complexity of the phenomenon requires modeling by methodologies that are closer to the phenomenon itself such as DNS¹, LES² RANS³. These methods differ in their approximations and accuracy, among which DNS is the one that most closely approximates the real effects, followed by LES, which does not require as much computational power as DNS, but provides excellent results.

Still limited by computational capacity, the most commonly used methods are RANS and LES, or even one of the hybrid or composite methodologies. With these, the equations describing the mean or filtered motions in any of these formulations are invariant in shape, that is, they contain terms in any coordinate referential representing transport, production, redistribution, and diffusion. They are not invariant, since in non-inertial structures or under Euclidean transformations additional terms appear in the general tensor forms of the equations. Also, depending on the filtering process, they differ in relation to the flow field motions being described.

The Helmholtz vorticity transport equation, the basic principle for turbulence, together with the concept of Reynolds decomposition are presented in more detail in Appendix C.

LES methodology

The equations of the Large Eddy Simulation methodology are obtained by means of spatial filters applied to Navier-Stokes equations. The LES methodology assumes the interaction between large and small vortex scales.

Spatial Filter and Favré Mean

The separation between the large and small scales is obtained by applying the spatial filter in the governing equations. According to GÉN (2009), a filtered variable ϕ

¹ Direct Numerical Simulation

² Large Eddy Simulations

³ Reynolds-averaged Navier-Stokes equations

can be obtained by applying a spatial filter as:

$$\bar{\phi} = \int_{\Omega} \phi(\vec{x}', t) \wp(\vec{x}, \vec{x}') d^3 \vec{x}' \quad (218)$$

In the current implementation, the filter used is a kernel top-hat filter. Practically, \wp is the product of three one-dimensional filters:

$$\wp(\vec{x} - \vec{x}') = \prod_{i=1}^3 q_i(x_i - x'_i) \quad (219)$$

where q_i 's is the top-order dimensional filters given by:

$$q_i(x_i - x'_i) = \begin{cases} \frac{1}{\Delta_i}, & |x_i - x'_i| < \frac{\Delta_i}{2} \\ 0, & \text{outros} \end{cases} \quad (220)$$

Δ_i is the width of the one-dimensional local filter in the i direction. The overall filter size, Δ is obtained from the other sizes in the main directions being $\Delta = (\Delta_1 \Delta_2 \Delta_3)^{1/3}$. The dimensions of the one-dimensional filters are based on the spacing of the local mesh, and Δ is a measure of the local mesh.

For compressible flows, the most used filter is based on the mass-weighted variable or density-weighted variable, it is known as Favré filter. Applying this filter to compressible flows significantly reduces the number of unclosed terms that need to be modeled. The filtered Favré variable, denoted by $\tilde{\phi}$, is defined as:

$$\tilde{\phi} = \frac{\overline{\rho\phi}}{\bar{\rho}} \quad (221)$$

Filtered Navier-Stokes Equation

The application of the spatial filter reduces to a function of $\vec{x} - \vec{x}'$, relative to the position in space, and switches the temporal and spatial derivatives, not losing information GÉN, 2009.

→Conservation of Mass

The instantaneous mass conservation is:

$$\frac{\partial \rho}{\partial t} + \frac{\partial(\rho u_i)}{\partial x_i} = 0 \quad (222)$$

Applying the concept of average:

$$\frac{\partial \bar{\rho}}{\partial t} + \frac{\partial(\overline{\rho u_i})}{\partial x_i} = 0 \quad (223)$$

Applying the Favre filter the equation is reduced to

$$\frac{\partial \bar{\rho}}{\partial t} + \frac{\partial(\overline{\rho u_i})}{\partial x_i} = 0 \quad (224)$$

→Conservation of Movement Quantity

Applying the mean concepts and the Favre filter, the momentum equation is given by:

$$\frac{\partial(\bar{\rho}\widetilde{u}_i)}{\partial t} + \frac{\partial}{\partial x_j} [\bar{\rho}\widetilde{u}_i\widetilde{u}_j + \bar{p}^*\delta_{ij} - \bar{\tau}_{ij}] = 0 \quad (225)$$

if

$$\bar{p}^* = \bar{\rho}\widetilde{R}\widetilde{T} + \bar{\rho}R_u T^{sgs} \quad (226)$$

The Eq. 211 can be rewritten as:

$$\frac{\partial(\bar{\rho}\widetilde{u}_i)}{\partial t} + \frac{\partial}{\partial x_j} [\bar{\rho}\widetilde{u}_i\widetilde{u}_j + \bar{p}^*\delta_{ij} + \tau_{ij}^{sgs} - \bar{\tau}_{ij}] = 0 \quad (227)$$

The convective term of the above equation is modeled to be solved by introducing the subgrid stress, τ_{ij}^{sgs} ,

$$\tau_{ij}^{sgs} = \bar{\rho}(\widetilde{u}_i\widetilde{u}_j - \widetilde{u}_i\widetilde{u}_j) \quad (228)$$

τ_{ij}^{sgs} can be related to the correlation of the velocity fluctuations u_i and u_j on the small scales of the (local mesh) filter dimensions.

→Energy Conservation

The energy conservation equation applying the definition of mean flow and filter is given by

$$\frac{\partial(\bar{\rho}\widetilde{E})}{\partial t} + \frac{\partial}{\partial x_j} [\bar{\rho}\widetilde{u}_j\widetilde{E} + \widetilde{u}_j\bar{p}^* + \bar{q}_j - \widetilde{u}_i\bar{\tau}_{ji} + H_j^{sgs} + \sigma_j^{sgs}] = 0 \quad (229)$$

where the subgrid terms originated from the filter process are:

$$H_j^{sgs} = \bar{\rho}(\widetilde{E}u_j - \widetilde{E}u_j) + (\overline{u_j p^*} - \bar{p}^*\overline{u_j}) \quad (230)$$

$$\sigma_j^{sgs} = -(\overline{u_i\tau_{ij}} - \widetilde{u}_i\overline{\tau_{ij}}) \quad (231)$$

→Conservation of Chemical Species

Filtering the conservation equation of species one has

$$\frac{\partial(\bar{\rho}\widetilde{Y}_k)}{\partial t} + \frac{\partial}{\partial x_i} \left[\bar{\rho} \left(\widetilde{Y}_k u_i + \widetilde{Y}_k \widetilde{V}_{i,k} \right) \right] = 0 \quad (232)$$

rearranging in a convenient manner:

$$\frac{\partial(\bar{\rho}\widetilde{Y}_k)}{\partial t} + \frac{\partial}{\partial x_i} \left[\bar{\rho} \left(\widetilde{Y}_k \widetilde{u}_i + \widetilde{Y}_k \widetilde{V}_{i,k} \right) + Y_{i,k}^{sgs} + \theta_{i,k}^{sgs} \right] = 0 \quad (233)$$

the subgrid terms are:

$$Y_{i,k}^{sgs} = \bar{\rho} \left(\widetilde{u_i Y_k} - \widetilde{u_i} \widetilde{Y_k} \right) \quad (234a)$$

$$\theta_{i,k}^{sgs} = \bar{\rho} \left(\widetilde{V_{i,k} Y_k} - \widetilde{V_{i,k}} \widetilde{Y_k} \right) \quad (234b)$$

The subgrid temperature in Eq. 212 is given by

$$T^{sgs} = \sum \frac{\widetilde{Y_k T} - \widetilde{Y_k} \widetilde{T}}{MW_k} \quad (235)$$

Closure Model for the LES Equations

Given the initial conditions and integration time known, the variables $\bar{\rho}$, $\widetilde{u_i}$, \widetilde{E} and $\widetilde{Y_k}$ are known, so the equation of continuity is closed, that is, all variables are completely known. However, the other governing equations have a closure problem, both in terms of subgrid and in terms of the filtered terms, so they require modeling. Thus, from the total energy we have:

$$\begin{aligned} \widetilde{E} &= \tilde{e} + \frac{1}{2} \widetilde{u_k u_k} \\ &= \tilde{e} + \frac{1}{2} \widetilde{u_k u_k} + \frac{1}{2} (\widetilde{u_k u_k} - \widetilde{u_k} \widetilde{u_k}) \\ &= \tilde{e} + \frac{1}{2} \widetilde{u_k u_k} + k^{sgs} \end{aligned} \quad (236)$$

where k^{sgs} represents the subgrid portion of the kinetic energy. Relying only on internal energy,

$$\tilde{e} = \sum_{k=1}^{N_s} \widetilde{Y_k} e_{f,k}^0 + \sum_{k=1}^{N_s} \widetilde{Y_k} \int_{T_0}^{\widetilde{T}} C_{V,k}(T) dT + \sum_{k=1}^{N_s} E_k^{sgs} \quad (237)$$

Applying the Favré filter on the stress tensor of the momentum equation and analogously for the Navier-Stokes equation:

$$\overline{\tau_{ij}} = 2\mu(\widetilde{T}) \left(\widetilde{S_{ij}} - \frac{1}{3} \widetilde{S_{kk}} \delta_{ij} \right) \quad (238)$$

The heat flux, q_i , and the rate of diffusion of species, $V_{i,k}$ are given by:

$$\overline{q_j} = -\kappa(\widetilde{T}) \frac{\partial \widetilde{T}}{\partial x_j} + \bar{\rho} \sum \widetilde{Y_k} h_k(\widetilde{T}) \widetilde{V_{i,k}} + q_j^{sgs} \quad (239)$$

$$\widetilde{V_{i,k}} = -\frac{D_k}{\widetilde{Y_k}} \frac{\partial \widetilde{Y_k}}{\partial x_i} \quad (240)$$

The terms subgrid are not closed, which requires modeling. These terms are:

$$\tau_{ij}^{sgs} = \bar{\rho} (\widetilde{u_i u_j} - \widetilde{u_i} \widetilde{u_j}) \quad (241a)$$

$$H_i^{sgs} = \bar{\rho} \left(\widetilde{E u_i} - \widetilde{E} \widetilde{u_i} \right) + \left(\overline{u_i p} - \widetilde{u_i} \widetilde{p} \right) \quad (241b)$$

$$\sigma_i^{sgs} = \left(\overline{u_j \tau_{ij}} - \widetilde{u_j} \widetilde{\tau_{ij}} \right) \quad (241c)$$

$$Y_{i,k}^{sgs} = \bar{\rho} \left(\widetilde{u_i Y_k} - \widetilde{u_i} \widetilde{Y_k} \right) \quad (241d)$$

$$\theta_{i,k}^{sgs} = \bar{\rho} \left(\widetilde{V_{i,k} Y_k} - \widetilde{V_{i,k}} \widetilde{Y_k} \right) \quad (241e)$$

$$q_{i,k}^{sgs} = \bar{\rho} \left(h_k \widetilde{Y_k V_{i,k}} - \widetilde{h_k} \widetilde{Y_k} \widetilde{V_{i,k}} \right) \quad (241f)$$

$$T^{sgs} = \sum_{k=1}^{N_s} \frac{\left(\widetilde{Y_k T} - \widetilde{Y_k} \widetilde{T} \right)}{MW_k} \quad (241g)$$

$$E_k^{sgs} = Y_k \widetilde{e_k}(T) - \widetilde{Y_k} e_k(\widetilde{T}) \quad (241h)$$

To close the equations, it is employed the concept of turbulent viscosity, ν_t , which is evaluated using the characteristic scale length obtained by the mesh length ($\bar{\Delta}$) and the characteristic velocity based on the subgrid kinetic energy (k^{sgs}). Thus, the turbulent viscosity, GÉN, 2009, is calculated by

$$\nu_t = c_\nu \bar{\Delta} \sqrt{k^{sgs}} \quad (242)$$

Thus, the subgrid stress tensor is modeled as

$$\tau_{ij}^{sgs} = -2\bar{\rho}\nu_t \left(\widetilde{S_{ij}} - \frac{1}{3} \widetilde{S_{kk}} \delta_{ij} \right) + \frac{2}{3} k^{sgs} \delta_{ij} \quad (243)$$

The terms of the energy equation, H_i^{sgs} and σ_i^{sgs} are modeled together. Thus,

$$H_i^{sgs} + \sigma_i^{sgs} = -(\bar{\rho}\nu_t + \mu) \frac{\partial k^{sgs}}{\partial x_i} - \frac{\bar{\rho}\nu_t c_p}{Pr_t} \frac{\partial \widetilde{T}}{\partial x_i} + \widetilde{u_j} \tau_{ij}^{sgs} \quad (244)$$

The subgrid mass fraction of the diffusion of species is modeled in the form:

$$Y_{i,k}^{sgs} = -\frac{\bar{\rho}\nu_t}{Sc_t} \frac{\partial \widetilde{Y_k}}{\partial x_i} \quad (245)$$

An equation to the subgrid kinetic energy can be obtained. The closure model of the type using subgrid kinetic energy k^{sgs} is given by:

$$\begin{aligned} \frac{\partial}{\partial t} (\bar{\rho} k^{sgs}) + \frac{\partial}{\partial x_i} (\overline{\rho u_i k^{sgs}}) &= \frac{\partial}{\partial x_i} \left[(\bar{\rho} \nu_t + \mu) \frac{\partial k^{sgs}}{\partial x_i} + \frac{\bar{\rho} \nu_t \tilde{R}}{Pr_t} \frac{\partial \tilde{T}}{\partial x_i} \right] - \left[1 \right. \\ &\quad \left. + \alpha_{pd} M_t^{sgs^2} \left(\frac{\bar{\rho} \tilde{\epsilon} k^{sgs}}{D_{k^{sgs}}} \right)^2 \right] \left(\tau_{ij}^{sgs} \frac{\partial \tilde{u}_j}{\partial x_i} + \bar{\rho} c_\epsilon \frac{(k^{sgs})^{3/2}}{\Delta} \right) \end{aligned} \quad (246)$$

where by the Kolmogorov cascade energy concept, the kinetic energy of dissipation correlates with the turbulent characteristic velocity scale and the characteristic length of the scale (local mesh size) given by GÉN (2009):

$$D_{k^{sgs}} = \frac{\bar{\rho} c_\epsilon (k^{sgs})^{3/2}}{\Delta} \quad (247)$$

By analyzing the energy of the flow in the spectrum of the frequency, we have that the distribution of the spectrum of energy is given by:

$$E^*(\kappa) = \alpha \epsilon^{2/3} \kappa^{-5/3} \exp -\frac{3}{2} \alpha (\kappa \eta)^{4/3} \quad (248)$$

being κ the Fourier modes, see POPE (1988), η the Kolmogorov length scales and ($\alpha \approx 1.5$) the Kolmogorov constant, where the minimum Fourier mode for these conditions is found by the cutoff wavenumber, defined by

$$\kappa_c \equiv \pi / \bar{\Delta} \quad (249)$$

Based on the Fourier space, an approximation to k^{sgs} is given by

$$k^{sgs} = \int_{\kappa_c}^{\infty} \alpha \epsilon^{2/3} \kappa^{-5/3} d\kappa = \left(\frac{3\alpha}{2} \right)^{3/2} \frac{\epsilon^{2/3}}{\kappa_c^{2/3}} \quad (250)$$

where the total dissipation rate is obtained by:

$$\epsilon = \left(\frac{3\alpha}{2} \right)^{3/2} (k^{sgs})^{3/2} \kappa_c = 0.931 \frac{(k^{sgs})^{3/2}}{\Delta}. \quad (251)$$

Applying the subgrid model,

$$\epsilon^{sgs} = \epsilon \exp \left[-\frac{3}{2} \alpha (\kappa_c \eta)^{4/3} \right] \quad (252)$$

and considering that the term in the exponential is much less than 1, one can approximate the subgrid dissipation for

$$\epsilon^{sgs} \approx \epsilon = 0.931 \frac{(k^{sgs})^{3/2}}{\Delta} \quad (253)$$

The coefficients c_ν in Eq. 228 is defined as:

$$c_\nu = -\frac{\mathcal{M}_{ij} \mathcal{L}'_{ij}}{2\mathcal{M}_{ij} \mathcal{M}_{ij}} \quad (254)$$

where

$$\mathcal{L}'_{ij} = \mathcal{L}_{ij} - \frac{1}{3}\mathcal{L}_{kk}\delta_{ij} \quad (255)$$

and Leonard's tensor, \mathcal{L}_{ij} , is calculated as:

$$\mathcal{L}_{ij} = \widetilde{\bar{\rho}} \left(\frac{\widetilde{\bar{\rho}u_i u_j}}{\widetilde{\bar{\rho}}} - \frac{\widetilde{\bar{\rho}u_i} \widetilde{\bar{\rho}u_j}}{\widetilde{\bar{\rho}}^2} \right) \quad (256)$$

the notation $\widetilde{\square}$ indicates that an explicit filter was applied.

The operator \mathcal{M}_{ij} is defined as:

$$\mathcal{M}_{ij} = k^{test} \widetilde{\Delta} \left(\widetilde{\bar{\rho}S_{ij}} - \frac{1}{3}\widetilde{\bar{\rho}S_{kk}}\delta_{ij} \right) \quad (257)$$

where

$$k^{test} = \frac{1}{2} \frac{\mathcal{L}_{kk}}{\widetilde{\bar{\rho}}} = \frac{1}{2} \left(\frac{\widetilde{\bar{\rho}u_i u_j}}{\widetilde{\bar{\rho}}} - \frac{\widetilde{\bar{\rho}u_i} \widetilde{\bar{\rho}u_j}}{\widetilde{\bar{\rho}}^2} \right) \quad (258)$$

The dissipation coefficient c_ϵ is given by

$$c_\epsilon = \frac{\widetilde{\Delta}}{\widetilde{\bar{\rho}}(k^{test})^{\frac{3}{2}}} \left[\frac{\mu_{eff}}{\widetilde{\bar{\rho}}} \left(\widetilde{\bar{\rho} \sum_{ij} \frac{\partial \widetilde{u}_j}{\partial x_i}} - \sum_{ij} \widetilde{\bar{\rho}} \frac{\partial \widetilde{u}_j}{\partial x_i} \right) - \frac{2}{3} \left(\widetilde{\bar{\rho}k^{sgs} \frac{\partial \widetilde{u}_k}{\partial x_k}} - \widetilde{\bar{\rho}k^{sgs}} \frac{\partial \widetilde{u}_k}{\partial x_k} \right) \right] \quad (259)$$

where the effective viscosity, μ_{eff} , is:

$$\mu_{eff} = \mu + \mu_t$$

The turbulent Prandtl number is obtained from

$$\frac{1}{Pr_t} = - \frac{d_i n_i}{d_i d_i} \quad (260)$$

where n_i is the correlation between velocity and temperature,

$$n_i = \frac{\widetilde{\bar{\rho}u_i \widetilde{T}}}{\widetilde{\bar{\rho}}} - \frac{\widetilde{\bar{\rho}u_i} \widetilde{\bar{\rho}T}}{\widetilde{\bar{\rho}}^2} \quad (261)$$

and

$$d_i = \frac{c_\nu \sqrt{k^{test}} \widetilde{\Delta}}{\widetilde{\bar{\rho}}} \rho \frac{\partial \widetilde{T}}{\partial x_i} \quad (262)$$

Finally, the closing coefficient α_{pd} is defined by:

$$\alpha_{pd} = \frac{\frac{\widetilde{\bar{p}} \frac{\partial \widetilde{u}_i}{\partial x_i} - \widetilde{\bar{p}} \frac{\partial \widetilde{u}_i}{\partial x_i}}{M_t^{test^2} \left(\frac{\widetilde{\bar{\rho}S_k^{test}}}{D_k^{test}} \right)^2} (p_k^{test} - D_k^{test})}{\left(\frac{\widetilde{\bar{p}} \frac{\partial \widetilde{u}_i}{\partial x_i} - \widetilde{\bar{p}} \frac{\partial \widetilde{u}_i}{\partial x_i} \right)} \quad (263)$$

Assuming that k^{test} has the same formulation as k^{sgs} , we have:

$$D_{k^{test}} = \frac{\tilde{\rho} c_\epsilon (k^{test})^{\frac{3}{2}}}{\tilde{\Delta}} \quad (264)$$

Therefore, the LES equations become closed by determining the six closing coefficients (c_ν , c_ϵ , σ_k , Pr_t , Sc_t , α_{pd}).

E – REACTIVE FLOWS - COMBUSTION

For reactive flows of the combustion type, the governing equations are presented. Before, some concepts on premixed combustion are described.

Premixed Combustion

Combustion of premixed air-fuel is becoming more common in practical energy conversion devices because of the greater emphasis on reducing unwanted emissions. A high degree of premix provides effective control of flame stoichiometry. This provides significant benefits by ensuring that the combustion reaction occurs under conditions favorable to the ideal thermochemical process. As an example, it is possible to use the premix to specify poor fuel-air mixtures that avoid the emission of significant amounts of unburned fuel, CO or particles by virtue of chemistry, and which minimize the formation of NO_x by thermal effect, when limiting the temperature after burning. The use of pre-mixed combustion chambers also helps to reduce emissions of CO_2 , contributing to greater energy efficiency BILGER, 1976.

The premixed combustion has been used in automotive internal combustion engines of spark ignition type, for many years. Often the amount of the air-fuel mixture is controlled by the injection system to ensure that combustion occurs under stoichiometric conditions, resulting in minimal post-combustion waste generation.

The technological issues still pending in the premixed combustion reside in the guarantee of flame stability. The premixed burners must be carefully designed to avoid phenomena such as blow-off and flashback, while premixed flames are notoriously prone to instabilities and acoustically convection coupled BILGER, 1976. Small variations of the air-fuel mixture result in significant effects on the flame dynamics and the distribution of heat, resulting in acoustic phenomena such as instabilities and resonances. In practice, it is seldom possible to ensure that the complete mixing between the fuel and the air before combustion occurs, resulting in partially premixed flames. In some circumstances, these are considered more stable than a flame under ideal premix conditions (under stoichiometric conditions).

Turbulent Premixed Combustion

In both RANS or LES methodologies, it is necessary to close the governing equations, either by applying calculations or filters. After the adoption of a closure model for the momentum equation, only the closure of the thermochemical transport equations remains. In premixed turbulent combustion, it is common practice to define a reaction progress variable ζ which varies from zero in the case of fresh reagents to the unit in the fully

burned products. In simple case, ζ is treated as a staggered mass fraction of one or more product species Y_P OPPENHEIM, 2008:

$$\zeta = \frac{Y_P}{Y_{P\infty}} \quad (265)$$

where $Y_{P\infty}$ is the value of Y_P in complete or equilibrium combustion of the products. The staggered mass fraction of the products can also be rewritten in two other ways, in terms of the mass fraction of fuel, Y_F , or temperature:

$$\zeta = \frac{Y_F - Y_{F0}}{Y_{F\infty} - Y_{F0}} \quad (266a)$$

$$\zeta = \frac{T - T_0}{T_\infty - T_0} \quad (266b)$$

where Y_{F0} is the remaining fraction of fuel mass and $Y_{F\infty}$ is the value of Y_F when total combustion of fuels occurs. With respect to temperature, T_0 and T_∞ are the limiting temperatures of the reactants and products, respectively.

Thus, the equation of transport to chemical species in terms of the reaction progress variable is given by:

$$\frac{\partial(\rho\zeta)}{\partial t} + \frac{\partial}{\partial x_k}(\rho u_k \zeta) = \frac{\partial}{\partial x_k} \left(\rho D_\zeta \frac{\partial \zeta}{\partial x_k} \right) + (\rho \Lambda_i) \quad (267)$$

Applying the RANS methodology, the transport equation of chemical species is expressed using the progress variable and applying the Favré average:

$$\frac{\partial}{\partial t}(\bar{\rho}\bar{\zeta}) + \frac{\partial}{\partial x_k}(\bar{\rho}\bar{u}_k\bar{\zeta}) = \bar{\rho}\bar{\Lambda}_i + \frac{\partial}{\partial x_k} \left(\bar{\rho}D_\zeta \frac{\partial \bar{\zeta}}{\partial x_k} \right) - \frac{\partial}{\partial x_k}(\bar{\rho}\overline{u_k''\zeta''}) \quad (268)$$

For the LES methodology, the transport equation of the equation for ζ is given by:

$$\frac{\partial}{\partial t}(\bar{\rho}\bar{\zeta}) + \frac{\partial}{\partial x_k}(\bar{\rho}\bar{u}_k\bar{\zeta}) = \bar{\rho}\bar{\Lambda}_i + \frac{\partial}{\partial x_k} \left(\overline{\rho D_\zeta \frac{\partial \zeta}{\partial x_k}} \right) - \frac{\partial}{\partial x_k}(\overline{\rho u_k \zeta} - \rho \widetilde{u_k \zeta}) \quad (269)$$

The molecular transport term is usually retained in LES, since the Reynolds number on the mesh scale is not large enough to neglect it in relation to the turbulent transport term. The simplest closure model for this term is based on the assumption that the mass diffusivity ρD_ζ is not correlated with the reaction progress variable:

$$\overline{\rho D_\zeta \frac{\partial \zeta}{\partial x_k}} = \bar{\rho} \bar{D}_\zeta \frac{\partial \bar{\zeta}}{\partial x_k} \quad (270)$$

Flamelets Flame Model - G-Equation

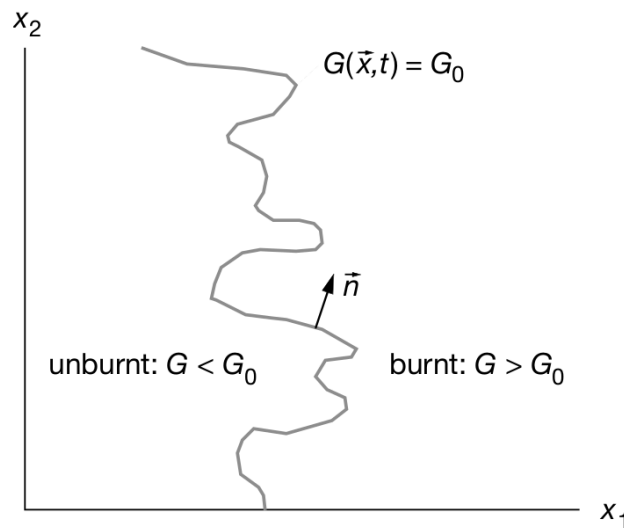
The flamelets hypothesis describes a premixed combustion regime which is often found in practical combustion devices. Within this hypothesis, there is a flame thickness (S_i) which is small when compared to the smaller dynamic scale of turbulence η , Kolmogorov scale RODI and FUEYO, 2002, as well as the characteristic burning time is small compared to the characteristic flow time. As a result, the structure of the flame remains unchanged and the flame may be considered a thin front which propagates at a speed dictated by the properties of the blend which are wrinkled and convected by the flow. A model equation describing the propagation of a thin flame by means of convective transport and normal burning (self-propagation by the Huygens principle) was introduced, called the equation of the field G KERSTEIN, ASHURST, and WILLIAMS, 1998.

The point of analysis is the function of describing the behavior of the flame front (level-set), \mathbb{G} , described by

$$\mathbb{G}(\vec{x}, t) = \mathbb{G}_0 \quad (271)$$

where \mathbb{G}_0 represents the exact location of the flame front. In this way, the characteristic behavior of a turbulent flame front is illustrated in Figure 35.

Figure 35 – Two-dimensional scheme of the function description \mathbb{G} as a function of position.



Source – WARNATZ, MAAS, and DIBBLE, 2006

Thus, the function, already employing the Favré filter (represented by the $\tilde{\square}$), that describes the model is presented as:

$$\frac{\partial \tilde{\mathbb{G}}}{\partial t} + (\tilde{\vec{u}} \cdot \nabla) \tilde{\mathbb{G}} = S_T |\nabla \tilde{\mathbb{G}}| \quad (272)$$

where \mathbb{G} is the variable that defines the location of the flame and S_T is the turbulent velocity of flame. The value of \mathbb{G} is in the interval $[0,1]$ and in the context of the flame front model, \mathbb{G} displays a step function, separating the burned region ($\mathbb{G} < \mathbb{G}_0$) of the unburned region ($\mathbb{G} > \mathbb{G}_0$). The progress variable shows unit value in the unburned region and zero in the burned region of flame propagation that is identified for a fixed value of $0 < \mathbb{G}_0 < 1$.

The closure of the term S_T is based on the subgrid turbulent velocity scale, \tilde{u}' , and the subgrid lamellar scale S_L given by:

$$\frac{S_T}{S_L} = 1 + \alpha \left(\frac{\tilde{u}'}{S_T} \right)^n \quad (273)$$

The constants, α and n , can be specified dynamically a priori as shown in IM, LUND, and FERZIGER (1997).

The subgrid velocity scale, \tilde{u}' , can be estimated as:

$$\tilde{u}' = \Delta \left| \tilde{\varepsilon} \right| = \Delta \sqrt{2\tilde{\varepsilon}_{ij}\tilde{\varepsilon}_{ij}} \quad (274)$$

The G-equation model is based on the flame-forward tracking technique, where the forward displacement of the flame is evaluated in terms of the displacement velocities S_T . As the flame velocity is explicitly included, this leads to an estimate of the volume of flared gases produced along with the release of heat. However, the flame velocity does not present satisfactory results.

Flame Surface Density Model

As another alternative to the turbulence/chemical interaction modeling, the flamelet hypothesis can be used to relate turbulent burning rate to the flame area or surface density. Studies have led to an exact transport equation for the FSD¹ developed by DAVIDSON (2004), considering the application of the LES methodology, which is based on considerations to a propagation surface. The complete study of the application of the FSD model for premixed combustion was developed by HAWKES (2000).

The model of the progress variable and the transport equations applying the FSD method is given by

$$\frac{\partial}{\partial t}(\bar{\rho}\tilde{\zeta}) + \frac{\partial}{\partial x_i}(\bar{\rho}\tilde{u}_i\tilde{\zeta}) = \frac{\partial}{\partial x_i} \left(\frac{\bar{\rho}\nu_i}{Sc_i} \frac{\partial \tilde{\zeta}}{\partial x_i} \right) + \rho_r S_L \bar{\rho} \tilde{\Sigma} \quad (275)$$

and

$$\frac{\partial}{\partial t}(\bar{\rho}\tilde{\Sigma}) + \frac{\partial}{\partial x_i} \left(\bar{\rho}\tilde{\Sigma}\tilde{u}_i \right) = - \frac{\partial}{\partial x_i} \bar{\rho}\tilde{\Sigma} \left[(\bar{u}_i)_s - \tilde{u}_i \right] + S_{\tilde{\Sigma}} + P_{res} + C_{res} + C_{sfs} \quad (276)$$

¹ Flame Surface Density

where

$$S_{\widetilde{\Sigma}} = (S_{res} + S_{hr} + S_{sfs})\widetilde{\rho}\widetilde{\Sigma} \quad (277)$$

The various modeled terms of the transport equation for $\widetilde{\Sigma}$ are defined as:

- **Turbulent surface flotation speed**

$$(\overline{u_i})_s - \widetilde{u}_i = -(\zeta^* - \widetilde{\zeta})\tau S_L N_i - \frac{1}{(\widetilde{\rho}\widetilde{\Sigma})} \frac{\nu_t}{Sc_t} \frac{\partial(\widetilde{\rho}\widetilde{\Sigma})}{\partial x_i} \quad (278)$$

- **Deformation source term solved**

$$S_{res} = (\delta_{ij} - n_{ij}) \frac{\partial \widetilde{u}_i}{\partial x_j} \quad (279)$$

- **Source term of deformation due to heat release**

$$S_{hr} = -(\zeta^* - \widetilde{\zeta})\tau S_L \frac{\partial N_i}{\partial x_i} \quad (280)$$

- **Subgrid source term of deformation**

$$S_{sfs} = \Gamma_k \frac{\widetilde{k}}{\Delta} \quad (281)$$

- **Resolved Term of Propagation**

$$P_{res} = \frac{\partial}{\partial x_i} \left[S_L (1 + \tau \zeta^*) N_i \widetilde{\rho} \widetilde{\Sigma} \right] \quad (282)$$

- **Termination of curvature solved**

$$C_{res} = S_L (1 + \tau \zeta^*) \frac{\partial N_i}{\partial x_i} \widetilde{\rho} \widetilde{\Sigma} \quad (283)$$

- **Subgrid curl term**

$$C_{sfs} = -\alpha \beta S_L \frac{(\widetilde{\rho}\widetilde{\Sigma})^2}{1 - \zeta^*} \quad (284)$$

where $\beta \geq 1$ to satisfy the model show in HAWKES and CANT (2000).

Therefore, the final model of the transport equation by the FSD method is given by

$$\begin{aligned} \frac{\partial}{\partial t} (\widetilde{\rho}\widetilde{\Sigma}) + \frac{\partial}{\partial x_i} (\widetilde{\rho}\widetilde{\Sigma}\widetilde{u}_i) &= \frac{\partial}{\partial x_i} \left(\frac{\widetilde{\rho}\nu_t}{Sc_t} \frac{\partial \widetilde{\Sigma}}{\partial x_i} \right) + (\delta_{ij} - n_{ij}) \frac{\partial \widetilde{u}_i}{\partial x_j} \widetilde{\rho}\widetilde{\Sigma} \\ &\quad - S_L (1 + \tau \widetilde{\zeta}) N_i \frac{\partial}{\partial x_i} (\widetilde{\rho}\widetilde{\Sigma}) - S_L \tau N_i \widetilde{\rho}\widetilde{\Sigma} \frac{\partial \widetilde{c}}{\partial x_i} \\ &\quad + \Gamma_k \frac{\sqrt{\widetilde{k}}}{\Delta} \widetilde{\rho}\widetilde{\Sigma} - \alpha \beta S_L \frac{(\widetilde{\rho}\widetilde{\Sigma})^2}{1 - \widetilde{\zeta}} \end{aligned} \quad (285)$$

Flamelet/Progress-Variable Method

The philosophy underlying chemical models is that the most effective description of turbulent combustion will be able to map details of reaction processes with multicomponent diffusion aiming at a minimal set of tracking scalars. Based on the fact that some models aim at incomplete mixing fractions because the fraction of the mixture contains no intrinsic information on chemical reactions and can not explain chemical variations in directions orthogonal to its gradient. At least one additional scalar is required, and since the mixing fraction is responsible for the transport of conserved scalars, additional scaling scans should not be maintained to be independent of the mixing fraction. A non-conserved tracking scalar is best characterized as a progress variable of the reaction PIERCE, 2001.

In premixed turbulent flames, thickening and blistering of the flame front due to interaction with the subgrid turbulence (*subgrid*), the effect of creating fluctuations that must be taken into account in the closure models of *subgrid*. For this it is necessary to obtain a pre-unidimensional laminar flame database, a presumed probability density function that is used to explain the effect of the *SGS* fluctuations on the chemistry and to construct the database to verify the behavior of the remainder of the spiral. To take into account the fine reaction zones that interact with the turbulence within the subgrade grid, the presumed PDF (Probability Density Function) shape must depend on the local flame surface (FSD) density, which measures the area available per unit volume. In premixed combustion, the flame surface density of any surface *iso* - ζ^* is commonly estimated through the conditional filtered gradient of the progress variable. Finally, this *FSD-PDF* depends on the filtered progress variable, ζ , its variation, ζ_v , and the size of the local filter. A form for closure of the FSD-PDF method is presented by DOMINGO et al. (2005), where it is used an FPI profile of a laminar premixed flame to solve the turbulent field. Within the suggested chemical model, *PDF* taking into account the fluctuations of subgrids of the enthalpy must also be considered. Thus, since the laminar flame database is computed and coupled to the turbulent field by means of the probability density function. Thus the progress variable is obtained by CECERE et al., 2011,

$$\tilde{\mathbb{G}}_i(\vec{x}, t) = \int_0^1 \int_0^1 \tilde{\mathbb{G}}_i^{FPI}(\zeta^*, h) \tilde{P}(\zeta^*; \vec{x}, t) \tilde{P}(h; \vec{x}, t) d\zeta^* dh \quad (286)$$

Since $\tilde{\mathbb{G}}$ is the characterization function of the filtered progress variable. Neglecting the enthalpy fluctuations, the PDF's enthalpy is estimated as:

$$\tilde{P} = \delta(h - \tilde{h}) \quad (287)$$

Thereby,

$$\tilde{\mathbb{G}}_i(\vec{x}, t) = \int_0^1 \int_0^1 \tilde{\mathbb{G}}_i^{FPI}(\zeta^*, h) \tilde{P}(\zeta^*; \vec{x}, t) \delta(h - \tilde{h}) d\zeta^* dh \quad (288)$$

Due to the application of the non-normalized progress variable it is necessary to add two more equations to the governing equations to solve the transport equation. The

progress variable is used to characterize the amount of fuel that is consumed, or the degree of reaction progress, or even to evaluate any amount relevant to the analysis CECERE et al., 2011.

The two equations for the non-normalized progress variable are:

$$\frac{\partial(\bar{\rho}\widetilde{\mathbb{G}}_\zeta)}{\partial t} + \frac{\partial}{\partial x_j}(\bar{\rho}\widetilde{u}_j\widetilde{\mathbb{G}}_\zeta) = \frac{\partial}{\partial x_k}\left(\bar{\rho}\alpha_{\mathbb{G}_\zeta}\frac{\partial\widetilde{\mathbb{G}}_\zeta}{\partial x_k}\right) + \bar{\rho}\widetilde{\omega}_{\mathbb{G}_\zeta} + \frac{\partial f_{\zeta k}}{\partial x_k} \quad (289)$$

and

$$\frac{\partial(\bar{\rho}\widetilde{\mathbb{G}}_\zeta^2)}{\partial t} + \frac{\partial}{\partial x_j}(\bar{\rho}\widetilde{u}_j\widetilde{\mathbb{G}}_\zeta^2) = \frac{\partial}{\partial x_k}(\bar{\rho}\alpha_{\mathbb{G}_\zeta}\widetilde{\mathbb{G}}_\zeta^2) + \frac{\partial f_{\zeta^2 k}}{\partial x_k} - 2\bar{\rho}\widetilde{X}_{\mathbb{G}_\zeta} + 2\bar{\rho}\widetilde{\omega}_{\mathbb{G}_\zeta}\widetilde{\mathbb{G}}_\zeta \quad (290)$$

In this way, the behavior of the effects of flame fluctuations can be obtained. α_{Y_ζ} is the diffusive progress variable, $f_{\zeta k} = -\bar{\rho}\widetilde{u}_k\widetilde{\mathbb{G}}_\zeta + \bar{\rho}\widetilde{u}_k\widetilde{\mathbb{G}}_\zeta$ in terms of the subgrid, with the source terms of the chemical model being filtered and presented in the variables $\omega_{\mathbb{G}_\zeta}$ and $\widetilde{\omega}_{\mathbb{G}_\zeta}\widetilde{\mathbb{G}}_\zeta$ and the dissipation rate scaling of the progress variable $\bar{\rho}\widetilde{X}_{\mathbb{G}_\zeta}$ is modeled as:

$$f_{\zeta k} = \bar{\rho}\alpha_{\mathbb{G}_\zeta}^t \frac{\partial\widetilde{\mathbb{G}}_\zeta}{\partial x_k} \quad (291)$$

where $\alpha_{\mathbb{G}_\zeta}^t$ is turbulent diffusivity:

$$\alpha_{\mathbb{G}_\zeta}^t = C_{\mathbb{G}_\zeta}\bar{\Delta}^2|\bar{\epsilon}|\bar{\epsilon} \quad (292)$$

The constant $C_{\mathbb{G}_\zeta}$ is dynamically calculated for channel flow. It is to be obtained using a characteristic dimension (considered the width). (GERMANO et al., 1991) suggest the following approach for obtaining this constant:

$$\epsilon^{sgs} = m_{ij}\bar{\epsilon} \quad (293)$$

where m_{ij} is the anisotropic parts of the subgrid stress tensor τ_{ij}^{sgs} ,

$$m_{ij} = -2C_{\mathbb{G}_\zeta}\bar{\Delta}^2|\bar{\epsilon}|\bar{\epsilon}. \quad (294)$$

In this work, the obtaintion of this constant is no longer dynamically calculated as suggested by GERMANO et al. (1991) and a isotropic flow model for the subgrids is proposed in the present work

Combinig the equations 253 and 293

$$C_{\mathbb{G}_\zeta}(x, t) = -0.4655 \frac{k^{sgs^2}}{\bar{\Delta}^3|\bar{\epsilon}|\bar{\epsilon}^2} \quad (295)$$

the term $f_{\zeta^2 k}$ is:

$$f_{\zeta^2 k} = \bar{\rho}\alpha_{\mathbb{G}_\zeta}^t \frac{\partial\widetilde{\mathbb{G}}_\zeta^2}{\partial x_k} \quad (296)$$

the scalar dissipation rate of the progress variable, $\bar{\rho}\widetilde{X}_{\mathbb{G}_\zeta}$, is modelled as:

$$\bar{\rho}\widetilde{X}_{\mathbb{G}_\zeta} = \bar{\rho}D|\nabla\widetilde{\mathbb{G}}_\zeta|^2 + \bar{s}_{X\mathbb{G}_\zeta} \quad (297)$$

By VEYNANTE and VERVISCH (2002) if a linear relaxation of the fluctuations generated by micromixing is postulated, then, it results:

$$\bar{s}_{X\mathbb{G}_\zeta} = \frac{\bar{\rho}\widetilde{\mathbb{G}}_{\zeta v}}{\tau_t} \quad (298)$$

where $\tau_t \approx \overline{\Delta}^2 S_{c_t}/\nu_t$ is the turbulent time scale and according to DOMINGO et al. (2005), the turbulent Schmidt number assumed to be 0.7.

A more detailed closure of the chemical model and the estimation of transport properties is presented in CECERE et al. (2011), VERVISCH et al. (1995) and POPE (1988).

F – MATHEMATICAL DETAILING

The system of instantaneous transport equations is that one in Equations 10 and rewritten here for convenience. That system of PDE is:

$$\begin{aligned}\frac{\partial \rho}{\partial t} + \frac{\partial(\rho u_i)}{\partial x_i} &= 0 \\ \frac{\partial(\rho u_i)}{\partial t} + \frac{\partial}{\partial x_j} [\rho u_i u_j + p \delta_{ij} - \tau_{ij}] - \rho g_i &= 0 \\ \frac{\partial(\rho Y_k)}{\partial t} + \frac{\partial}{\partial x_i} [(\rho u_i + \rho V_i^c) Y_k + \rho V_{k,i} Y_k] &= \dot{\omega}_k \\ \frac{\partial(\rho E)}{\partial t} + \frac{\partial}{\partial x_j} [\rho u_j E + u_j p \delta_{ij} - u_i \tau_{ij} + q_j] &= \dot{\omega}_T\end{aligned}$$

Applying some average in Equation 10a:

$$\frac{\partial \bar{\rho}}{\partial t} + \frac{\partial(\bar{\rho} u_i)}{\partial x_i} = 0$$

applying Favre filter:

$$\frac{\partial \bar{\rho}}{\partial t} + \frac{\partial}{\partial x_i} [\overline{\rho(\tilde{u}_i + u'_i)}] = 0$$

$$\frac{\partial \bar{\rho}}{\partial t} + \frac{\partial}{\partial x_i} [\overline{\rho \tilde{u}_i} + \overline{\rho u'_i}] = 0$$

$$\frac{\partial \bar{\rho}}{\partial t} + \frac{\partial}{\partial x_j} (\overline{\rho \tilde{u}_i}) = 0 \tag{299}$$

Applying some average in Equation 10b:

$$\frac{\partial(\overline{\rho u_i})}{\partial t} + \frac{\partial}{\partial x_j} [\overline{\rho u_i u_j + p \delta_{ij} - \tau_{ij}}] - \overline{\rho g_i} = 0$$

$$\frac{\partial(\overline{\rho u_i})}{\partial t} + \frac{\partial}{\partial x_j} [\overline{\rho u_i u_j} + \overline{p \delta_{ij}} - \overline{\tau_{ij}}] - \overline{\rho g_i} = 0$$

From Favre filter definition:

$$\frac{\partial}{\partial t} [\overline{\rho(\tilde{u}_i + u'_i)}] + \frac{\partial}{\partial x_j} [\overline{\rho(\tilde{u}_i + u'_i)(\tilde{u}_j + u'_j)} + \overline{p \delta_{ij}} - \overline{\tau_{ij}}] - \overline{\rho g_i} = 0$$

$$\frac{\partial}{\partial t} \left[\overline{\rho \tilde{u}_i} + \overline{\rho u'_i} \right] = \frac{\partial}{\partial x_j} [\overline{\rho \tilde{u}_i \tilde{u}_j} + \overline{\rho \tilde{u}_i u'_j} + \overline{\rho u'_i \tilde{u}_j} + \overline{\rho u'_i u'_j} + \overline{p \delta_{ij}} - \overline{\tau_{ij}}] - \overline{\rho g_i} = 0$$

$$\frac{\partial}{\partial t} (\overline{\rho \tilde{u}_i}) + \frac{\partial}{\partial x_j} \left[\overline{\rho \frac{\rho u_i}{\bar{\rho}} \frac{\rho u_j}{\bar{\rho}}} + \overline{\rho \frac{\rho u_i}{\bar{\rho}} u'_j} + \overline{\rho u'_i \frac{\rho u_j}{\bar{\rho}}} + \overline{\rho u'_i u'_j} + \overline{p \delta_{ij}} - \overline{\tau_{ij}} \right] - \overline{\rho g_i} = 0$$

$$\frac{\partial}{\partial t} (\overline{\rho u_i}) + \frac{\partial}{\partial x_j} \left[\overline{\frac{\rho u_i \rho u_j}{\rho}} + \overline{\frac{\rho u_i}{\rho}} + \overline{\frac{\rho u_j}{\rho}} + \overline{\rho u'_i u'_j} + \overline{p} \delta_{ij} - \overline{\tau}_{ij} \right] - \overline{\rho g_i} = 0$$

$$\frac{\partial}{\partial t} (\overline{\rho u_i}) + \frac{\partial}{\partial x_j} \left[\overline{\rho u_i u_j} + \overline{\rho u'_i u'_j} + \overline{p} \delta_{ij} - \overline{\tau}_{ij} \right] - \overline{\rho g_i} = 0$$

where $u'_i = (u_i - \widetilde{u}_i)$

$$\frac{\partial}{\partial t} (\overline{\rho u_i}) + \frac{\partial}{\partial x_j} \left[\overline{\rho u_i u_j} + \overline{\rho (u_i - \widetilde{u}_i)(u_j - \widetilde{u}_i)} + \overline{p} \delta_{ij} - \overline{\tau}_{ij} \right] - \overline{\rho g_i} = 0$$

$$\frac{\partial}{\partial t} (\overline{\rho u_i}) + \frac{\partial}{\partial x_j} \left[\overline{\rho u_i u_j} + \overline{\rho u_i u_j} - \overline{\rho u_i u_j} - \overline{\rho u_i u_j} + \overline{\rho u_i u_j} + \overline{p} \delta_{ij} - \overline{\tau}_{ij} \right] - \overline{\rho g_i} = 0$$

$$\frac{\partial}{\partial t} (\overline{\rho u_i}) + \frac{\partial}{\partial x_j} \left[\overline{\rho u_i u_j} + \overline{\rho u_i u_j} - \overline{\rho u_i u_j} - \overline{\rho u_j u_i} + \overline{\rho u_i u_j} + \overline{p} \delta_{ij} - \overline{\tau}_{ij} \right] - \overline{\rho g_i} = 0$$

where $\overline{\rho u_i} = \overline{\rho \widetilde{u}_i}$

$$\frac{\partial}{\partial t} (\overline{\rho u_i}) + \frac{\partial}{\partial x_j} \left[\overline{\rho u_i u_j} + \underbrace{\overline{\rho u_i u_j} - \overline{\rho u_i u_j}}_{\tau_{ij}^{sgs}} - \overline{\rho u_i u_j} + \overline{\rho u_i u_j} + \overline{p} \delta_{ij} - \overline{\tau}_{ij} \right] - \overline{\rho g_i} = 0$$

Thus,

$$\frac{\partial}{\partial t} (\overline{\rho u_i}) + \frac{\partial}{\partial x_j} \left[\overline{\rho u_i u_j} + \tau_{ij}^{sgs} + \overline{p} \delta_{ij} - \overline{\tau}_{ij} \right] - \overline{\rho g_i} = 0 \quad (300)$$

where,

$$\overline{\tau}_{ij} = 2\mu(\widetilde{T}) \left(\widetilde{S}_{ij} - \frac{1}{3} \widetilde{S}_{kk} \delta_{ij} \right)$$

From the Boussinesq's hypothesis for turbulent viscosity, HINZE, 1975, for Newtonian fluids, the subgrid stress tensor is:

$$\tau_{ij}^{sgs} = -2\overline{\rho} \nu_t \left(\widetilde{S}_{ij} - \frac{1}{3} \widetilde{S}_{kk} \delta_{ij} \right) + \frac{2}{3} \overline{\rho} k^{sgs} \delta_{ij}$$

According to Smagorinsky, the turbulent viscosity, ν_t , is model as SCHIESTEL, 2008

$$\nu_t = C_\nu \overline{\Delta}^2 |\overline{\mathbf{S}}| \quad (301)$$

Thus, the conditions of high Reynolds number, isotropic flow and considering that $\overline{\Delta}/\eta \gg 1$, where the cutoff wavenumber - κ_c - is defined by $\kappa_c = \pi/\overline{\Delta}$ POPE, 2000, result in $\kappa_c \eta \ll 1$. In this way, since the exponential of the spectral distribution of the flow can be ignored,

$$E^*(\kappa) = \alpha \epsilon^{\frac{2}{3}} \kappa^{-\frac{5}{3}} \quad (302)$$

The turbulent viscosity can be obtained by applying the closure by spectral theory of KRAICHNAN (1976) applied to isotropic flows:

$$\nu_t = 0.441\alpha^{\frac{3}{2}}\sqrt{\frac{E^*(\kappa_c)}{\kappa_c}} \quad (303)$$

where α is Kolmogorov constant ($\alpha \approx 1.5$).

The subgrid dissipation rate can be approximated by $\epsilon^{sgs} \approx \epsilon = 0.931\frac{(k^{sgs})^{3/2}}{\Delta}$ GÉN, 2009. Therefore, from equations 301 and 303, the subgrid kinetic energy becomes

$$\kappa^{sgs} = 22.5523|\mathbf{S}|^2C_\nu^2\Delta^2 \quad (304)$$

For pressure term,

$$\begin{aligned} \bar{p} &= \overline{\rho RT} \\ \bar{p} &= \overline{\rho(\tilde{R} + R')(\tilde{T} + T')} \\ \bar{p} &= \overline{\rho\tilde{R}\tilde{T}} + \overline{\rho\tilde{R}T'} + \overline{\rho R'\tilde{T}} + \overline{\rho R'T'} \\ \bar{p} &= \overline{\rho\tilde{R}\tilde{T}} + \overline{\rho\tilde{R}(T - \tilde{T})} + \overline{\rho(R - \tilde{R})\tilde{T}} + \overline{\rho R'T'} \\ \bar{p} &= \overline{\rho\tilde{R}\tilde{T}} + \overline{\rho\tilde{R}T} - \overline{\rho\tilde{R}\tilde{T}} + \overline{\rho R'\tilde{T}} - \overline{\rho\tilde{R}\tilde{T}} + \overline{\rho R'T'} \\ \bar{p} &= \overline{\rho\tilde{R}\tilde{T}} + \overline{\rho R'T'} = \overline{\rho\tilde{R}\tilde{T}} + \overline{\rho(R - \tilde{R})(T - \tilde{T})} \\ \bar{p} &= \overline{\rho\tilde{R}\tilde{T}} + \overline{\rho RT} - \overline{\rho\tilde{R}\tilde{T}} - \overline{\rho T\tilde{R}} + \overline{\rho\tilde{R}\tilde{T}} \\ \bar{p} &= \overline{\rho\tilde{R}\tilde{T}} + \underbrace{\overline{\rho RT} - \overline{\rho\tilde{R}\tilde{T}}}_{\bar{\rho}R_uT^{sgs}} - \overline{\rho\tilde{R}\tilde{T}} + \overline{\rho\tilde{R}\tilde{T}} \end{aligned}$$

Thus, the mean pressure term is obtained by:

$$\bar{p} = \overline{\rho\tilde{R}\tilde{T}} + \bar{\rho}R_uT^{sgs} \quad (305)$$

where

$$T^{sgs} = \sum_{k=1}^{N_s} \frac{(\tilde{Y}_k\tilde{T} - \tilde{Y}'_k\tilde{T})}{W_k}$$

Applying some average in Equation 10c:

$$\frac{\partial(\overline{\rho Y_k})}{\partial t} + \frac{\partial}{\partial x_i} [\overline{\rho(u_i + V_i^c)Y_k} + \overline{\rho V_{k,i}Y_k}] = \bar{\omega}_k$$

From the Favre filter definition

$$\begin{aligned} \frac{\partial}{\partial t} [\overline{\rho(\tilde{Y}_k + Y'_k)}] + \frac{\partial}{\partial x_i} \left\{ \overline{\rho[(\tilde{u}_i + u'_i) + (\tilde{V}_i^c + V_i^c)](\tilde{Y}_k + Y'_k)} + \right. \\ \left. + \overline{\rho(\tilde{V}_{k,i}\tilde{Y}_k + V_{k,i}Y'_k)} \right\} = \bar{\omega}_k \end{aligned}$$

$$\frac{\partial}{\partial t} \left[\overline{\rho \widetilde{Y}_k} + \overline{\rho \widetilde{Y}'_k} \right] + \frac{\partial}{\partial x_i} \left\{ \overline{\rho \widetilde{u}_i \widetilde{Y}_k} + \overline{\rho \widetilde{u}_i \widetilde{Y}'_k} + \overline{\rho \widetilde{u}'_i \widetilde{Y}_k} + \overline{\rho \widetilde{u}'_i \widetilde{Y}'_k} + \overline{\rho \widetilde{V}_i^c \widetilde{Y}_k} + \right. \\ \left. + \overline{\rho \widetilde{V}_i^c \widetilde{Y}'_k} + \overline{\rho \widetilde{V}_i^c \widetilde{Y}_k} + \overline{\rho \widetilde{V}_i^c \widetilde{Y}'_k} + \overline{\rho \widetilde{V}_{k,i} \widetilde{Y}_k} + \overline{\rho \widetilde{V}_{k,i} \widetilde{Y}'_k} \right\} = \bar{\omega}_k$$

$$\frac{\partial (\overline{\rho \widetilde{Y}_k})}{\partial t} + \frac{\partial}{\partial x_i} \left\{ \overline{\rho \widetilde{u}_i \widetilde{Y}_k} + \overline{\rho \widetilde{Y}'_k \widetilde{u}_i} + \overline{\rho \widetilde{u}'_i \widetilde{Y}_k} + \overline{\rho \widetilde{u}'_i \widetilde{Y}'_k} + \overline{\rho \widetilde{V}_i^c \widetilde{Y}_k} + \right. \\ \left. + \overline{\rho \widetilde{Y}'_k \widetilde{V}_i^c} + \overline{\rho \widetilde{V}_i^c \widetilde{Y}'_k} + \overline{\rho \widetilde{V}_i^c \widetilde{Y}'_k} + \overline{\rho \widetilde{V}_{k,i} \widetilde{Y}_k} \right\} = \bar{\omega}_k$$

$$\frac{\partial (\overline{\rho \widetilde{Y}_k})}{\partial t} + \frac{\partial}{\partial x_i} \left\{ \overline{\rho \widetilde{u}_i \widetilde{Y}_k} + \overline{\rho \widetilde{V}_i^c \widetilde{Y}_k} + \overline{\rho \widetilde{V}_{k,i} \widetilde{Y}_k} + \overline{\rho \widetilde{u}'_i \widetilde{Y}'_k} + \overline{\rho \widetilde{V}_i^c \widetilde{Y}'_k} \right\} = \bar{\omega}_k$$

where $f' = f - \widetilde{f}$

$$\frac{\partial (\overline{\rho \widetilde{Y}_k})}{\partial t} + \frac{\partial}{\partial x_i} \left\{ \overline{\rho \widetilde{u}_i \widetilde{Y}_k} + \overline{\rho \widetilde{V}_i^c \widetilde{Y}_k} + \overline{\rho \widetilde{V}_{k,i} \widetilde{Y}_k} + \overline{\rho (u_i - \widetilde{u}_i) (Y_k - \widetilde{Y}_k)} + \right. \\ \left. + \overline{\rho (V_i^c - \widetilde{V}_i^c) (Y_k - \widetilde{Y}_k)} \right\} = \bar{\omega}_k$$

$$\frac{\partial (\overline{\rho \widetilde{Y}_k})}{\partial t} + \frac{\partial}{\partial x_i} \left\{ \overline{\rho (\widetilde{u}_i + \widetilde{V}_i^c) \widetilde{Y}_k} + \overline{\rho \widetilde{V}_{k,i} \widetilde{Y}_k} + \overline{\rho u_i Y_k} - \overline{\rho u_i \widetilde{Y}_k} - \overline{\rho \widetilde{u}_i Y_k} + \right. \\ \left. + \overline{\rho \widetilde{u}_i \widetilde{Y}_k} + \overline{\rho \widetilde{V}_i^c \widetilde{Y}_k} - \overline{\rho \widetilde{V}_i^c \widetilde{Y}_k} - \overline{\rho \widetilde{V}_i^c \widetilde{Y}_k} + \overline{\rho \widetilde{V}_i^c \widetilde{Y}_k} \right\} = \bar{\omega}_k$$

$$\frac{\partial (\overline{\rho \widetilde{Y}_k})}{\partial t} + \frac{\partial}{\partial x_i} \left\{ \overline{\rho (\widetilde{u}_i + \widetilde{V}_i^c) \widetilde{Y}_k} + \overline{\rho \widetilde{V}_{k,i} \widetilde{Y}_k} + \overline{\rho u_i Y_k} - \overline{\rho \widetilde{u}_i \widetilde{Y}_k} - \overline{\rho \widetilde{u}_i \widetilde{Y}_k} + \right. \\ \left. + \overline{\rho \widetilde{u}_i \widetilde{Y}_k} + \overline{\rho \widetilde{V}_i^c \widetilde{Y}_k} - \overline{\rho \widetilde{V}_i^c \widetilde{Y}_k} - \overline{\rho \widetilde{V}_i^c \widetilde{Y}_k} + \overline{\rho \widetilde{V}_i^c \widetilde{Y}_k} \right\} = \bar{\omega}_k$$

$$\frac{\partial (\overline{\rho \widetilde{Y}_k})}{\partial t} + \frac{\partial}{\partial x_i} \left\{ \overline{\rho (\widetilde{u}_i + \widetilde{V}_i^c) \widetilde{Y}_k} + \overline{\rho \widetilde{V}_{k,i} \widetilde{Y}_k} + \underbrace{\overline{\rho [(u_i Y_k - \widetilde{u}_i \widetilde{Y}_k) + (V_i^c Y_k - \widetilde{V}_i^c \widetilde{Y}_k)]}}_{Y_{k,i}^{sgs}} \right\} = \bar{\omega}_k$$

Thus,

$$\frac{\partial (\overline{\rho \widetilde{Y}_k})}{\partial t} + \frac{\partial}{\partial x_i} \left[\overline{\rho (\widetilde{u}_i + \widetilde{V}_i^c) \widetilde{Y}_k} + \overline{\rho \widetilde{V}_{k,i} \widetilde{Y}_k} + Y_{k,i}^{sgs} \right] = \bar{\omega}_k \quad (306)$$

where the terms that need modeling are:

$$Y_{k,i}^{sgs} = -\frac{\bar{\rho} \nu_t}{Sc_{kt}} \frac{\partial \widetilde{Y}_k}{\partial x_i} - \sum_{k=1}^N \frac{\bar{\rho} \nu_t}{Sc_{kt}} \frac{\partial \widetilde{Y}_k}{\partial x_i}$$

$$\widetilde{V}_{k,i} \widetilde{Y}_k = -\rho D_k \frac{\partial \widetilde{Y}_k}{\partial x_i} \approx -\bar{\rho} D_k \frac{\partial \widetilde{Y}_k}{\partial x_i}$$

Finally, by applying some average in the Equation 10d:

$$\frac{\partial (\overline{\rho E})}{\partial t} + \frac{\partial}{\partial x_j} [\overline{\rho u_j E} + \overline{u_j p} \delta_{ij} - \overline{u_i \tau_{ij}} + \overline{q_j}] = \overline{\dot{\omega}_T}$$

The Favre decomposition yields:

$$\frac{\partial}{\partial t} [\overline{\rho (\tilde{E} + E')}] + \frac{\partial}{\partial x_j} [\overline{\rho (\tilde{u}_j + u'_j) (\tilde{E} + E')} + \overline{(\tilde{u}_j + u'_j) p} \delta_{ij} - \overline{(\tilde{u}_j + u'_j) \tau_{ij}} + \overline{q_j}] = \overline{\dot{\omega}_T}$$

$$\frac{\partial}{\partial t} \left(\overline{\rho \tilde{E}} + \overline{\rho \tilde{E}'} \right) + \frac{\partial}{\partial x_j} \left[\overline{\rho \tilde{u}_j \tilde{E}} + \overline{\rho \tilde{u}_j \tilde{E}'} + \overline{\rho u'_j E'} + \overline{\rho u'_j E'} + \overline{u'_j p} \delta_{ij} + \overline{u'_j p} \delta_{ij} - \overline{u_i \tau_{ij}} - \overline{u'_i \tau_{ij}} + \overline{q_j} \right] = \overline{\dot{\omega}_T}$$

$$\frac{\partial (\overline{\rho \tilde{E}})}{\partial t} + \frac{\partial}{\partial x_j} [\overline{\rho \tilde{u}_j \tilde{E}} + \overline{\rho u'_j E'} + \overline{u'_j p} \delta_{ij} + \overline{u'_j p} \delta_{ij} - \overline{u_i \tau_{ij}} - \overline{u'_i \tau_{ij}} + \overline{q_j}] = \overline{\dot{\omega}_T}$$

$$\frac{\partial (\overline{\rho \tilde{E}})}{\partial t} + \frac{\partial}{\partial x_j} [\overline{\rho \tilde{u}_j \tilde{E}} + \overline{u'_j p} \delta_{ij} - \overline{u_i \tau_{ij}} + \overline{\rho (u_j - \tilde{u}_j) (E - \tilde{E})} + \overline{(u_j - \tilde{u}_j) p} \delta_{ij} - \overline{(u_i - \tilde{u}_i) \tau_{ij}} + \overline{q_j}] = \overline{\dot{\omega}_T}$$

$$\frac{\partial (\overline{\rho \tilde{E}})}{\partial t} + \frac{\partial}{\partial x_j} [\overline{\rho \tilde{u}_j \tilde{E}} + \overline{u'_j p} \delta_{ij} - \overline{u_i \tau_{ij}} + \overline{\rho u_j E} - \overline{\rho u_j \tilde{E}} - \overline{\rho \tilde{u}_j \tilde{E}} + \overline{\rho \tilde{u}_j \tilde{E}} + (\overline{u_j p} - \overline{u'_j p}) \delta_{ij} - (\overline{u_i \tau_{ij}} - \overline{u'_i \tau_{ij}}) + \overline{q_j}] = \overline{\dot{\omega}_T}$$

$$\frac{\partial (\overline{\rho \tilde{E}})}{\partial t} + \frac{\partial}{\partial x_j} \left[\overline{\rho \tilde{u}_j \tilde{E}} + \overline{u'_j p} \delta_{ij} - \overline{u_i \tau_{ij}} + \underbrace{(\overline{\rho u_j E} - \overline{\rho \tilde{u}_j \tilde{E}})}_{H_i^{sgs}} + (\overline{u_j p} - \overline{u'_j p}) \delta_{ij} - \underbrace{(\overline{u_i \tau_{ij}} - \overline{u'_i \tau_{ij}})}_{\sigma_i^{sgs}} + \overline{q_j} \right] = \overline{\dot{\omega}_T}$$

Thus,

$$\frac{\partial (\overline{\rho \tilde{E}})}{\partial t} + \frac{\partial}{\partial x_j} [\overline{\rho \tilde{u}_j \tilde{E}} + \overline{u'_j p} \delta_{ij} - \overline{u_i \tau_{ij}} + H_i^{sgs} + \sigma_i^{sgs} + \overline{q_j}] = \overline{\dot{\omega}_T} \quad (307)$$

where the several extra terms from the filtering process are:

$$\begin{aligned} \tilde{E} &= \tilde{e} + \frac{1}{2} \widetilde{u_k u_k} \\ &= \tilde{e} + \frac{1}{2} \widetilde{u_k u_k} + \frac{1}{2} (\widetilde{u_k u_k} - \widetilde{u_k u_k}) \\ &= \tilde{e} + \frac{1}{2} \widetilde{u_k u_k} + k^{sgs} \end{aligned}$$

$$\begin{aligned}\tilde{e} &= \sum_{k=1}^{N_s} \tilde{Y}_k \Delta h_{f,k}^0 + \sum_{k=1}^{N_s} \tilde{Y}_k \int_{T_0}^{\tilde{T}} c_{V,k}(T) dT + \sum_{k=1}^{N_s} E_k^{sgs} \\ H_i^{sgs} + \sigma_i^{sgs} &= -(\bar{\rho}\nu_t + \mu) \frac{\partial k^{sgs}}{\partial x_i} - \frac{\bar{\rho}\nu_t c_p}{Pr_t} \frac{\partial \tilde{T}}{\partial x_i} + \tilde{u}_j \tau_{ij}^{sgs} \\ \bar{q}_j &= -\bar{k} \frac{\partial \tilde{T}}{\partial x_i} + \overline{\sum_k \rho h_k V_{k,i} Y_k} + \overline{RT \sum_k \frac{D_{T,k}}{T} \frac{\partial \tilde{T}}{\partial x_i}} + \bar{q}_{Rj} \\ \bar{q}_j &= -\bar{k} \frac{\partial \tilde{T}}{\partial x_i} + \bar{\rho} \overline{\sum_k h_k V_{k,i} Y_k} + \bar{R} \frac{\partial \tilde{T}}{\partial x_i} \overline{\sum_k D_{T,k}} + \bar{q}_{Rj}\end{aligned}$$

Decomposing the terms in the heat flux:

$$\begin{aligned}\bar{q}_j &= -\bar{k} \frac{\partial \tilde{T}}{\partial x_i} + \bar{\rho} \sum_k \overline{(\tilde{h}_k + \tilde{h}'_k) (\widetilde{V_{k,i} Y_k} + V_{k,i} Y'_k)} + \bar{R} \frac{\partial \tilde{T}}{\partial x_i} \overline{\sum_k D_{T,k}} + \bar{q}_{Rj} \\ \bar{q}_j &= -\bar{k} \frac{\partial \tilde{T}}{\partial x_i} + \bar{\rho} \sum_k \left[\overline{\tilde{h}_k \widetilde{V_{k,i} Y_k}} + \overline{\tilde{h}_k \widetilde{V_{k,i} Y'_k}} + \overline{\tilde{h}'_k \widetilde{V_{k,i} Y_k}} + \overline{\tilde{h}'_k \widetilde{V_{k,i} Y'_k}} \right] + \bar{R} \frac{\partial \tilde{T}}{\partial x_i} \overline{\sum_k D_{T,k}} + \bar{q}_{Rj} \\ \bar{q}_j &= -\bar{k} \frac{\partial \tilde{T}}{\partial x_i} + \bar{\rho} \sum_k \overline{\tilde{h}_k \widetilde{V_{k,i} Y_k}} + \bar{R} \frac{\partial \tilde{T}}{\partial x_i} \overline{\sum_k D_{T,k}} + \bar{q}_{Rj} + \underbrace{\bar{\rho} \sum_k \left(\overline{\tilde{h}_k \widetilde{V_{k,i} Y_k}} - \overline{\tilde{h}_k \widetilde{V_{k,i} Y'_k}} \right)}_{q_{sgs}}\end{aligned}$$

Therefore, the total turbulent heat flux is

$$\bar{q}_j = -\bar{k} \frac{\partial \tilde{T}}{\partial x_i} + \bar{\rho} \sum_k \overline{\tilde{h}_k \widetilde{V_{k,i} Y_k}} + \bar{R} \frac{\partial \tilde{T}}{\partial x_i} \overline{\sum_k D_{T,k}} + \bar{q}_{Rj} + q_{sgs}$$

where

$$q_{sgs} = -\sum_k \overline{\tilde{h}_k} \frac{\bar{\rho} \overline{D_k}}{Sc_t} \frac{\partial^2 \tilde{Y}_k}{\partial x_i^2}$$

CBS Applied to Momentum

Considering that the problem presented takes into account the effects of shock waves that occurred during the processes, in this section, modeling of these effects and obtaining of transport equations applying the CBS scheme ZIENKIEWICZ, TAYLOR, and NITHIARASU, 2014. So, from Equation 300

$$\frac{\partial}{\partial t} (\overline{\rho u_i}) + \frac{\partial}{\partial x_j} \left[\overline{\rho u_i u_j} + \tau_{ij}^{sgs} + \bar{p} \delta_{ij} - \bar{\tau}_{ij} \right] - \bar{\rho} \tilde{g}_i = 0$$

being $\tilde{U} = \overline{\rho u_i}$, the temporal decomposition is defined by

$$\tilde{U}_i^{n+1} = \tilde{U}_i^n + \Delta \tilde{U}_i^* + \Delta \tilde{U}_i^{**} \quad (308)$$

For pure diffusion problems, whose equations are of the self-adjunct type, the approximation of Galerkin is considered to be the best solution method. In the case of the transport equations of the present work, the advection terms remove the self-adjunct character of the differential equations. The advective terms can be initially eliminated from the equations, by rewriting them along the characteristic. However, this introduces a complication by having to work with a mobile coordinate system. In the case of the equation of motion, the operator *split* is proposed in the form for Equation 300 ZIENKIEWICZ, TAYLOR, and NITHIARASU, 2014:

$$\begin{aligned} \frac{\partial \widetilde{U}_i}{\partial t} &= \frac{\widetilde{U}_i^{n+1} - \widetilde{U}_i^n}{\Delta t} = \frac{\Delta \widetilde{U}_i^*}{\Delta t} + \frac{\Delta \widetilde{U}_i^{**}}{\Delta t} = \\ &= \psi \left\{ \frac{\partial}{\partial x_j} \left[-\widetilde{\rho} \widetilde{u}_i \widetilde{u}_j - \tau_{ij}^{sgs} - \bar{p} \delta_{ij} + \bar{\tau}_{ij} \right] + \bar{\rho} \widetilde{g}_i \right\}^{n+1} + \\ &\quad (1 - \psi) \left\{ \frac{\partial}{\partial x_j} \left[-\widetilde{\rho} \widetilde{u}_i \widetilde{u}_j - \tau_{ij}^{sgs} - \bar{p} \delta_{ij} + \bar{\tau}_{ij} \right] + \bar{\rho} \widetilde{g}_i \right\}^n \end{aligned} \quad (309)$$

Considering $\psi = 0.5$ the Equation 309 can be rewritten as:

$$\begin{aligned} \frac{\partial \widetilde{U}_i}{\partial t} &= \frac{\widetilde{U}_i^{n+1} - \widetilde{U}_i^n}{\Delta t} = \frac{\Delta \widetilde{U}_i^*}{\Delta t} + \frac{\Delta \widetilde{U}_i^{**}}{\Delta t} = \\ &= \left\{ \frac{\partial}{\partial x_j} \left[-\widetilde{\rho} \widetilde{u}_i \widetilde{u}_j - \tau_{ij}^{sgs} - \bar{p} \delta_{ij} + \bar{\tau}_{ij} \right] + \bar{\rho} \widetilde{g}_i \right\}^{n+1/2} \end{aligned} \quad (310)$$

When the CBS scheme is applied, a variable at position $x \rightarrow \delta$ and time n can be related to the variable at position x and time n , by a series expansion of Taylor, in the form:

$$\phi^n \Big|_{x-\delta} \approx \phi^n - \delta \frac{\partial \phi^n}{\partial x} + \frac{\delta^2}{2} \frac{\partial^2 \phi^n}{\partial x^2} + O(\Delta t^3)$$

where δ is the distance traveled by a particle in the i -direction

$$\delta = \Delta t u_i$$

To capture the shock wave NITHIARASU, ZIENKIEWICZ, et al. (1998) define

$$\frac{\partial \Phi_s^{n+1}}{\partial t} = \frac{\phi_s^{n+1} - \phi_s^{n+1}}{\Delta t} = \frac{\partial}{\partial x_i} \left[\mu_a \left(\frac{\partial \phi}{\partial x_i} \right) \right]. \quad (311)$$

Note that the effects of the shock are given at $n + 1$. The artificial diffusion coefficient, μ_a , for shock capture can be estimated as:

$$\mu_a = C_e \bar{\Delta}^3 \frac{|\mathbf{u}| + c}{p_a} \left| \frac{\partial^2 p}{\partial x_i \partial x_i} \right|_e \quad (312)$$

where p_a is the average pressure in the element, c is the sound speed and C_e is a dimensionless coefficient.

Knowing that the term for characterizing the shock is $U_{s,i}$, we have

$$U_{s,i}^{n+1} = U_i^{n+1} + \Delta t \underbrace{\frac{\partial}{\partial x_i} \left[\mu_a \left(\frac{\partial U_i}{\partial x_i} \right) \right]}_A \quad (313)$$

applying the product derivative rule in A

$$\frac{\partial}{\partial x_j} \left[\mu_a \left(\frac{\partial U_i}{\partial x_j} \right) \right] = \underbrace{\frac{\partial \mu_a}{\partial x_j} \frac{\partial U_i}{\partial x_j}}_{\text{Termo de } O>3} + \mu_a \frac{\partial^2 U_i}{\partial x_j^2}$$

and returning to Equation 313

$$U_{s,i}^{n+1} = U_i^{n+1} + \Delta t \mu_a \frac{\partial^2 U_i}{\partial x_j^2} \quad (314)$$

Applying the Favré filter, Equation 11, in Equation 314

$$\tilde{U}_{s,i}^{n+1} = \tilde{U}_i^{n+1} + \Delta t \bar{\mu}_a \frac{\partial^2 \tilde{U}_i}{\partial x_j^2} \quad (315)$$

where

$$\bar{\mu}_a = C_e \Delta^3 \frac{|\mathbf{u}| + c}{p_a} \left| \frac{\partial^2 \bar{p}}{\partial x_i \partial x_i} \right|_e \quad (316)$$

Therefore, Equation 300 can be rewritten taking taking into account the effects of the shock.

$$\frac{\partial \tilde{U}_i}{\partial t} + \frac{\partial}{\partial x_j} \left[\tilde{u}_i \tilde{U}_j + \tau_{ij}^{sgs} + \bar{p} \delta_{ij} - \bar{\tau}_{ij} \right] - \bar{\rho} \tilde{g}_i = 0$$

applying the Equation 310 approach, and knowing that of the Taylor-Galerkin method, we have that the term of smoothed, ψ , is only applied to the first derivative of Taylor series. Thereby,

$$\begin{aligned} \frac{\partial \tilde{U}_i}{\partial t} &= \frac{\Delta \tilde{U}_i^* + \Delta \tilde{U}_i^{**}}{\Delta t} = \left\{ \frac{\partial}{\partial x_j} \left[-\tilde{u}_i \tilde{U}_j - \tau_{ij}^{sgs} - \bar{p} \delta_{ij} + \bar{\tau}_{ij} \right] + \bar{\rho} \tilde{g}_i \right\} - \\ &\quad - \Delta t (1 - \psi) u_k \frac{\partial}{\partial x_k} \left\{ \frac{\partial}{\partial x_j} \left[-\tilde{u}_i \tilde{U}_j - \tau_{ij}^{sgs} - \bar{p} \delta_{ij} + \bar{\tau}_{ij} \right] + \bar{\rho} \tilde{g}_i \right\} \end{aligned}$$

of the equations 308 and 315, we obtain that the influence of the shock on the flow and

modifying the pressure

$$\begin{aligned} \frac{\Delta\tilde{U}_i^* + \Delta\tilde{U}_i^{**}}{\Delta t} = & \left\{ \frac{\partial}{\partial x_j} \left[-\tilde{u}_i\tilde{U}_j - \tau_{ij}^{sgs} + \bar{\tau}_{ij} \right] + \bar{\rho}\tilde{g}_i \right\}^n - \frac{\partial\bar{p}^{(n+\theta_2)}}{\partial x_i} \delta_{ij} - \\ & - \frac{\Delta t}{2} u_k \frac{\partial}{\partial x_k} \left\{ \frac{\partial}{\partial x_j} \left[-\tilde{u}_i\tilde{U}_j - \underbrace{\tau_{ij}^{sgs} + \bar{\tau}_{ij}}_{\text{Termos } O>3} \right] + \bar{\rho}\tilde{g}_i \right\}^n + \\ & + \frac{\Delta t}{2} u_j \frac{\partial^2\bar{p}^{(n+\theta_2)}}{\partial x_j\partial x_i} \delta_{ij} + \bar{\mu}_a \frac{\partial^2\tilde{U}_i^n}{\partial x_j^2} \end{aligned} \quad (317)$$

being

$$\frac{\partial\bar{p}^{n+\theta_2}}{\partial x_i} = \frac{\partial\bar{p}^n}{\partial x_i} + \theta_2 \frac{\partial\Delta\bar{p}}{\partial x_i} \quad (318)$$

where

$$\Delta\bar{p} = \bar{p}^{n+1} - \bar{p}^n$$

Applying Split B ZIENKIEWICZ, TAYLOR, and NITHIARASU, 2014 on Equation 317, it is defined that

$$\begin{aligned} \Delta\tilde{U}_i^* = & \Delta t \left[-\frac{\partial}{\partial x_j} (\tilde{u}_i\tilde{U}_j) - \frac{\partial\bar{p}}{\partial x_j} \delta_{ij} + \frac{\partial\bar{\tau}_{ij}}{\partial x_j} + \bar{\rho}\tilde{g}_i - \frac{\partial\tau_{ij}^{sgs}}{\partial x_j} \right]^n + \\ & + \frac{\Delta t^2}{2} u_k \frac{\partial}{\partial x_k} \left[\frac{\partial}{\partial x_j} (\tilde{u}_i\tilde{U}_j) + \frac{\partial\bar{p}}{\partial x_j} - \bar{\rho}\tilde{g}_i \right]^n + \Delta t \bar{\mu}_a \frac{\partial^2\tilde{U}_i^n}{\partial x_j^2} \end{aligned} \quad (319)$$

and

$$\Delta\tilde{U}_i^{**} = -\theta_2 \Delta t \left(\frac{\partial\Delta\bar{p}}{\partial x_i} - \frac{\Delta t}{2} u_j \frac{\partial^2\Delta\bar{p}}{\partial x_j\partial x_i} \right) \quad (320)$$

rearranging the Equation 319

$$\begin{aligned} \Delta\tilde{U}_i^* = & \Delta t \left[-\frac{\partial}{\partial x_j} (\tilde{u}_i\tilde{U}_j) - \frac{\partial\bar{p}}{\partial x_j} \delta_{ij} + \frac{\partial\bar{\tau}_{ij}}{\partial x_j} + \bar{\rho}\tilde{g}_i \right]^n + \frac{\Delta t^2}{2} u_k \frac{\partial}{\partial x_k} \left[\frac{\partial}{\partial x_j} (\tilde{u}_i\tilde{U}_j) + \right. \\ & \left. + \frac{\partial\bar{p}}{\partial x_j} - \bar{\rho}\tilde{g}_i \right]^n - \underbrace{\Delta t \left(\frac{\partial\tau_{ij}^{sgs}}{\partial x_j} \right)^n}_{\text{Turbulence influence}} + \underbrace{\Delta t \bar{\mu}_a \frac{\partial^2\tilde{U}_i^n}{\partial x_j^2}}_{\text{shock influence}} \end{aligned} \quad (321)$$

Multiplying the equations 321 and 320 for a weight function (N_u) and integrating into the domain (Ω) results:

$$\begin{aligned} \int_{\Omega} N_u \Delta\tilde{U}_i^* d\Omega = & \Delta t \left[-\int_{\Omega} N_u \frac{\partial}{\partial x_j} (\tilde{u}_i\tilde{U}_j) d\Omega - \int_{\Omega} N_u \frac{\partial\bar{p}}{\partial x_j} d\Omega \delta_{ij} + \right. \\ & \left. + \int_{\Omega} \underbrace{N_u \frac{\partial\bar{\tau}_{ij}}{\partial x_j}}_I d\Omega + \int_{\Omega} N_u (\bar{\rho}\tilde{g}_i) d\Omega \right]^n + \frac{\Delta t^2}{2} \int_{\Omega} \underbrace{(N_u u_k) \frac{\partial}{\partial x_k} \left[\frac{\partial}{\partial x_j} (\tilde{u}_i\tilde{U}_j) + \frac{\partial\bar{p}}{\partial x_j} - \bar{\rho}\tilde{g}_i \right]^n}_{II} d\Omega - \\ & - \Delta t \int_{\Omega} \underbrace{N_u \left(\frac{\partial\tau_{ij}^{sgs}}{\partial x_j} \right)^n}_{III} d\Omega + \Delta t \int_{\Omega} \underbrace{N_u \bar{\mu}_a \frac{\partial^2\tilde{U}_i^n}{\partial x_j^2}}_{IV} d\Omega \end{aligned}$$

and

$$\int_{\Omega} N_u \Delta \widetilde{U}_i^{**} d\Omega = -\theta_2 \Delta t \left[\int_{\Omega} N_u \frac{\partial \Delta \bar{p}}{\partial x_i} d\Omega - \frac{\Delta t}{2} \int_{\Omega} \underbrace{(N_u u_j) \frac{\partial^2 \Delta \bar{p}}{\partial x_j \partial x_i}}_V d\Omega \right]$$

Applying the product derivative rule, the terms highlighted by I, II, III, IV and V can be rewritten as

$$N_u \frac{\partial \bar{\tau}_{ij}}{\partial x_l} = \frac{\partial}{\partial x_j} (N_u \bar{\tau}_{ij}) - \frac{\partial N_u}{\partial x_j} \bar{\tau}_{ij}$$

$$(N_u u_k) \frac{\partial}{\partial x_k} \left[\frac{\partial}{\partial x_j} (\widetilde{u}_i \widetilde{U}_j) + \frac{\partial \bar{p}}{\partial x_j} - \bar{\rho} \widetilde{g}_i \right] = \frac{\partial}{\partial x_k} \left\{ (N_u u_k) \left[\frac{\partial}{\partial x_j} (\widetilde{u}_i \widetilde{U}_j) + \frac{\partial \bar{p}}{\partial x_j} - \bar{\rho} \widetilde{g}_i \right] \right\} - \frac{\partial (N_u u_k)}{\partial x_k} \left[\frac{\partial}{\partial x_j} (\widetilde{u}_i \widetilde{U}_j) + \frac{\partial \bar{p}}{\partial x_j} - \bar{\rho} \widetilde{g}_i \right]$$

$$N_u \frac{\partial \tau_{ij}^{sgs}}{\partial x_l} = \frac{\partial}{\partial x_j} (N_u \tau_{ij}^{sgs}) - \frac{\partial N_u}{\partial x_j} \tau_{ij}^{sgs}$$

$$N_u \bar{\mu}_a \frac{\partial^2 \widetilde{U}_i^n}{\partial x_j^2} = \bar{\mu}_a \frac{\partial}{\partial x_j} \left[N_u \frac{\partial U_i}{\partial x_j} \right] - \bar{\mu}_a \frac{\partial N_u}{\partial x_j} \frac{\partial U_i}{\partial x_j}$$

$$(N_u u_j) \frac{\partial^2 \Delta \bar{p}}{\partial x_j \partial x_i} = \frac{\partial}{\partial x_j} \left[(N_u u_j) \frac{\partial \Delta \bar{p}}{\partial x_i} \right] - \frac{\partial (N_u u_j)}{\partial x_j} \frac{\partial \Delta \bar{p}}{\partial x_i}$$

Applying the Gauss Divergence theorem, we have

$$\begin{aligned} & \Delta t \left[- \int_{\Omega} N_u \frac{\partial}{\partial x_j} (\widetilde{u}_i \widetilde{U}_j) d\Omega - \int_{\Omega} N_u \frac{\partial \bar{p}}{\partial x_j} d\Omega \delta_{ij} - \int_{\Omega} \frac{\partial N_u}{\partial x_j} \bar{\tau}_{ij} d\Omega + \int_{\Omega} N_u (\bar{\rho} \widetilde{g}_i) d\Omega \right]^n - \frac{\Delta t^2}{2} \int_{\Omega} \frac{\partial (N_u u_k)}{\partial x_k} \left[\frac{\partial}{\partial x_j} (\widetilde{u}_i \widetilde{U}_j) + \frac{\partial \bar{p}}{\partial x_j} - \bar{\rho} \widetilde{g}_i \right]^n + \\ & + \Delta t \int_{\Omega} \frac{\partial N_u}{\partial x_j} [\tau_{ij}^{sgs}]^n d\Omega - \Delta t \int_{\Omega} \frac{\partial N_u}{\partial x_j} \bar{\mu}_a \frac{\partial \widetilde{U}_i^n}{\partial x_j} d\Omega + \Delta t \int_{\Gamma} N_u n_j \bar{\tau}_{ij} d\Gamma \end{aligned}$$

and

$$\int_{\Omega} N_u \Delta \widetilde{U}_i^{**} d\Omega = -\theta_2 \Delta t \left[\int_{\Omega} N_u \frac{\partial \Delta \bar{p}}{\partial x_i} d\Omega + \frac{\Delta t}{2} \int_{\Omega} \frac{\partial (N_u u_j)}{\partial x_j} \frac{\partial \Delta \bar{p}}{\partial x_i} d\Omega \right]$$

Applying Galerkin's spatial approach and taking into account account the same nomenclatures presented by ZIENKIEWICZ, TAYLOR, and NITHIARASU (2014), we have

$$\begin{aligned} \mathbf{M}_u \Delta \widetilde{U}_i^* &= -\Delta t \left[\mathbf{C}_u \widetilde{U}_i + \mathbf{K}_{\tau} \widetilde{u}_i + \mathbf{G}^T \widetilde{p} - \mathbf{f} - \frac{\Delta t}{2} \left(\mathbf{K}_u \widetilde{U}_i + \mathbf{P} \widetilde{p} + \mathbf{f}_s \right) \right]^n + \\ &+ \Delta t \left(\mathbf{K}_{\tau_{sgs}} \widetilde{u}_i + \mathbf{V}_k \right) - \Delta t \bar{C}_e \Delta^{-3} \frac{|\widehat{\mathbf{u}}| + \widehat{c}}{\widehat{p}_a} |\nabla^2 p|_e \mathbf{K}_s \widetilde{U}_i \quad (322) \end{aligned}$$

$\nu_t = C_\nu \bar{\Delta}^2 |\mathbf{S}|$; where the modulus of the strain rate is calculated by

$$|\mathbf{S}| = [2S_{ij}S_{ij}]^{1/2} = \left[2 \left(\mathbf{B} \widetilde{\mathbf{u}}_i \right)^T \left(\mathbf{B} \widetilde{\mathbf{u}}_i \right) \right]^{1/2} \quad (323)$$

Arrays in Equation 322 are defined as

$$\mathbf{M}_u = \int_{\Omega} N_u^T N_u d\Omega \quad (324a)$$

$$\mathbf{C}_u = \int_{\Omega} N_u^T \nabla (\mathbf{u} N_u) d\Omega \quad (324b)$$

$$\mathbf{K}_\tau = \int_{\Omega} \mathbf{B} \mu \left(\mathbf{I}_0 - \frac{2}{3} \mathbf{m} \mathbf{m}^T \right) \mathbf{B} d\Omega \quad (324c)$$

$$\mathbf{G} = \int_{\Omega} (\nabla N_p)^T N_u d\Omega \quad (324d)$$

$$\mathbf{f} = \int_{\Omega} N_u^T \rho \mathbf{g} d\Omega + \int_{\Gamma} N_u \bar{\mathbf{t}} d\Gamma \quad (324e)$$

$$\bar{\mathbf{t}} = (\bar{\tau}_{ij} - \bar{p} \delta_{ij}) n_j \quad (324f)$$

$$\mathbf{K}_u = - \int_{\Omega} [\nabla^T (\mathbf{u} N_u)]^T [\nabla^T (\mathbf{u} N_u)] d\Omega \quad (324g)$$

$$\mathbf{P} = - \int_{\Omega} [\nabla (\mathbf{u} N_u)]^T \nabla N_p d\Omega \quad (324h)$$

$$\mathbf{f}_s = \int_{\Omega} [\nabla^T (\mathbf{u} N_u)]^T \rho \mathbf{g} d\Omega \quad (324i)$$

$$\mathbf{K}_{\tau_{sgs}} = -2\bar{\rho} C_\nu \bar{\Delta}^2 |\mathbf{S}| \int_{\Omega} \mathbf{B}^T \left[\mathbf{I}_0 - \frac{2}{3} \mathbf{m} \mathbf{m}^T \right] \mathbf{B} d\Omega \quad (324j)$$

$$\mathbf{V}_k = 15.03487 C_\nu^2 \bar{\Delta}^2 \int_{\Omega} N_u^T |\mathbf{S}|^2 d\Omega \quad (324k)$$

$$\mathbf{K}_s = \int_{\Omega} [\nabla N_u]^T \nabla N_u d\Omega \quad (324l)$$

Thus,

$$\mathbf{M}_u \Delta \widetilde{\mathbf{U}}_i^{**} = -\Delta t \theta_2 \left[\mathbf{G}^T \Delta \widetilde{\mathbf{p}} - \frac{\Delta t}{2} \mathbf{P} \Delta \widetilde{\mathbf{p}} \right] \quad (325)$$

CBS Continuity

From the Equation 299

$$\frac{\partial \bar{\rho}}{\partial t} + \frac{\partial \widetilde{U}_i}{\partial x_j} = 0$$

Applying the temporal split and ignoring the terms above order 3

$$\Delta \bar{\rho} = -\Delta t \left[\frac{\partial \widetilde{U}_i}{\partial x_i} + \theta_1 \frac{\partial \Delta \widetilde{U}_i^*}{\partial x_i} - \theta_1 \theta_2 \frac{\partial^2 \Delta \bar{p}}{\partial x_i^2} \right]$$

Multiplying by the weight function and integrating into the domain

$$\int_{\Omega} N_{\rho} \Delta \bar{\rho} \, d\Omega = -\Delta t \left[\underbrace{\int_{\Omega} N_{\rho} \frac{\partial \widetilde{U}_i}{\partial x_i} \, d\Omega}_I + \theta_1 \underbrace{\int_{\Omega} N_{\rho} \frac{\partial \Delta \widetilde{U}_i^*}{\partial x_i} \, d\Omega}_{II} - \theta_1 \theta_2 \underbrace{\int_{\Omega} N_{\rho} \frac{\partial^2 \Delta \bar{p}}{\partial x_i^2} \, d\Omega}_{III} \right]$$

applying the product derivative rule and knowing that I is similar to II,

$$N_{\rho} \frac{\partial \widetilde{U}_i}{\partial x_i} = \frac{\partial}{\partial x_i} (N_{\rho} \widetilde{U}_i) - \frac{\partial N_{\rho}}{\partial x_i} \widetilde{U}_i$$

and

$$N_{\rho} \frac{\partial^2 \Delta \bar{p}}{\partial x_i^2} = \frac{\partial}{\partial x_i} \left(N_{\rho} \frac{\partial \Delta \bar{p}}{\partial x_i} \right) - \frac{\partial N_{\rho}}{\partial x_i} \frac{\partial \Delta \bar{p}}{\partial x_i}$$

Applying Gauss's Divergence Theorem

$$\begin{aligned} \int_{\Omega} N_{\rho} \Delta \bar{\rho} \, d\Omega &= \Delta t \left[\int_{\Omega} \frac{\partial N_{\rho}}{\partial x_i} \widetilde{U}_i \, d\Omega + \theta_1 \int_{\Omega} \frac{\partial N_{\rho}}{\partial x_i} \Delta \widetilde{U}_i^* \, d\Omega - \theta_1 \theta_2 \int_{\Omega} \frac{\partial N_{\rho}}{\partial x_i} \frac{\partial \Delta \bar{p}}{\partial x_i} \, d\Omega \right] - \\ &\quad - \Delta t \int_{\Gamma} N_{\rho} n_i \left[\widetilde{U}_i + \theta_1 \Delta \widetilde{U}_i^* - \theta_1 \theta_2 \frac{\partial \Delta \bar{p}}{\partial x_i} \right] \, d\Gamma \end{aligned}$$

being $N_{\rho} = N_p$ and applying the Galerkin approximation the discretized equation is obtained

$$\mathbf{M}_{\rho} \Delta \bar{\rho} = \Delta t \left[\mathbf{G} \widetilde{U}_i + \theta_1 \mathbf{G} \Delta \widetilde{U}_i^* - \theta_1 \theta_2 \mathbf{H} \Delta \bar{p} \right] - \mathbf{f}_{\rho} \quad (326)$$

where the matrices that have not yet been defined are

$$\mathbf{M}_{\rho} = \int_{\Omega} N_{\rho}^T N_{\rho} \, d\Omega \quad (327a)$$

$$\mathbf{H} = \int_{\Omega} (\nabla N_{\rho})^T \nabla N_{\rho} \, d\Omega \quad (327b)$$

$$\mathbf{f}_{\rho} = \Delta t \int_{\Gamma} N_{\rho} \mathbf{n}^T \left[\widetilde{U}_i + \theta_1 \Delta \widetilde{U}_i^* - \theta_1 \theta_2 \nabla (\Delta \bar{p}) \right] \, d\Gamma \quad (327c)$$

CBS for Transporting Conservation of Species

From the Equation 306

$$\frac{\partial (\bar{\rho}\tilde{Y}_k)}{\partial t} + \frac{\partial}{\partial x_i} \left[\bar{\rho} (\tilde{u}_i + \tilde{V}_i^c) \tilde{Y}_k + \bar{\rho}\widetilde{V_{k,i}Y_k} + Y_{k,i}^{sgs} \right] = \bar{\omega}_k$$

applying the temporal split

$$\frac{\Delta (\bar{\rho}\tilde{Y}_k)}{\Delta t} = -(1 - \psi) \left\{ \frac{\partial}{\partial x_i} \left[\bar{\rho} (\tilde{u}_i + \tilde{V}_i^c) \tilde{Y}_k + \bar{\rho}\widetilde{V_{k,i}Y_k} + Y_{k,i}^{sgs} \right] - \bar{\omega}_k \right\}^n \quad (328)$$

expanding on Taylor series and following the feature with the smoothed effects, $\psi = 0.5$, applying only to the term of first derivative of the series, we have

$$\begin{aligned} \frac{\Delta (\bar{\rho}\tilde{Y}_k)}{\Delta t} = & - \left\{ \frac{\partial}{\partial x_i} \left[\bar{\rho} (\tilde{u}_i + \tilde{V}_i^c) \tilde{Y}_k + \bar{\rho}\widetilde{V_{k,i}Y_k} + Y_{k,i}^{sgs} \right] - \bar{\omega}_k \right\}^n + \\ & + \frac{\Delta t}{2} u_j \frac{\partial}{\partial u_j} \left\{ \frac{\partial}{\partial x_i} \left[\bar{\rho} (\tilde{u}_i + \tilde{V}_i^c) \tilde{Y}_k + \bar{\rho}\widetilde{V_{k,i}Y_k} + Y_{k,i}^{sgs} \right] - \bar{\omega}_k \right\}^n \end{aligned} \quad (329)$$

Multiplying by the weight function and integrating into the domain

$$\begin{aligned} \int_{\Omega} N_Y \Delta (\bar{\rho}\tilde{Y}_k) d\Omega = & -\Delta t \int_{\Omega} N_Y \frac{\partial}{\partial x_i} \left[\bar{\rho} (\tilde{u}_i + \tilde{V}_i^c) \tilde{Y}_k + \bar{\rho}\widetilde{V_{k,i}Y_k} + Y_{k,i}^{sgs} \right]^n d\Omega + \\ & + \Delta t \int_{\Omega} N_Y (\bar{\omega}_k)^n d\Omega + \frac{\Delta t^2}{2} \int_{\Omega} (N_Y u_j) \frac{\partial}{\partial u_j} \left\{ \frac{\partial}{\partial x_i} \left[\bar{\rho} (\tilde{u}_i + \tilde{V}_i^c) \tilde{Y}_k + \right. \right. \\ & \left. \left. + \bar{\rho}\widetilde{V_{k,i}Y_k} + Y_{k,i}^{sgs} \right] - \bar{\omega}_k \right\}^n d\Omega \end{aligned}$$

of a product's derivative rule

$$\begin{aligned} N_Y \frac{\partial}{\partial x_i} \left[\bar{\rho}\widetilde{V_{k,i}Y_k} + Y_{k,i}^{sgs} \right] = & \frac{\partial}{\partial x_i} \left\{ N_Y \left[\bar{\rho}\widetilde{V_{k,i}Y_k} + Y_{k,i}^{sgs} \right] \right\} - \\ & - \frac{\partial N_Y}{\partial x_i} \left[\bar{\rho}\widetilde{V_{k,i}Y_k} + Y_{k,i}^{sgs} \right] \\ (N_Y u_j) \frac{\partial}{\partial u_j} \left\{ \frac{\partial}{\partial x_i} \left[\bar{\rho} (\tilde{u}_i + \tilde{V}_i^c) \tilde{Y}_k + \bar{\rho}\widetilde{V_{k,i}Y_k} + Y_{k,i}^{sgs} \right] - \bar{\omega}_k \right\} = & \\ \frac{\partial}{\partial u_j} \left\{ (N_Y u_j) \frac{\partial}{\partial x_i} \left[\bar{\rho} (\tilde{u}_i + \tilde{V}_i^c) \tilde{Y}_k + \bar{\rho}\widetilde{V_{k,i}Y_k} + Y_{k,i}^{sgs} \right] - \bar{\omega}_k \right\} - & \\ - \frac{\partial (N_Y u_j)}{\partial u_j} \left\{ \frac{\partial}{\partial x_i} \left[\bar{\rho} (\tilde{u}_i + \tilde{V}_i^c) \tilde{Y}_k + \bar{\rho}\widetilde{V_{k,i}Y_k} + Y_{k,i}^{sgs} \right] - \bar{\omega}_k \right\} & \end{aligned}$$

So, applying Gauss's divergence theorem

$$\begin{aligned} \int_{\Omega} N_Y \Delta (\bar{\rho}\tilde{Y}_k) d\Omega = & -\Delta t \int_{\Omega} N_Y \frac{\partial}{\partial x_i} \left[(\tilde{u}_i + \tilde{V}_i^c) \bar{\rho}\tilde{Y}_k \right] d\Omega + \Delta t \int_{\Omega} \frac{\partial N_Y}{\partial x_i} \left[\bar{\rho}\widetilde{V_{k,i}Y_k} + Y_{k,i}^{sgs} \right] d\Omega + \\ & + \Delta t \int_{\Omega} N_Y (\bar{\omega}_k) d\Omega - \frac{\Delta t^2}{2} \int_{\Omega} \frac{\partial N_Y}{\partial u_j} \left\{ \frac{\partial}{\partial x_i} \left[\bar{\rho} (\tilde{u}_i + \tilde{V}_i^c) \tilde{Y}_k + \bar{\rho}\widetilde{V_{k,i}Y_k} + Y_{k,i}^{sgs} \right] - \bar{\omega}_k \right\} - \\ & - \Delta t \int_{\Gamma} \left\{ N_Y \left[\bar{\rho}\widetilde{V_{k,i}Y_k} + Y_{k,i}^{sgs} \right] - \frac{\Delta t}{2} (N_Y u_j) \left[\frac{\partial}{\partial x_i} \left[\bar{\rho} (\tilde{u}_i + \tilde{V}_i^c) \tilde{Y}_k + \bar{\rho}\widetilde{V_{k,i}Y_k} + Y_{k,i}^{sgs} \right] \right] \right\} n_j d\Gamma \end{aligned}$$

of the Galerkin approach

$$\mathbf{M}_Y \left(\bar{\rho} \tilde{Y}_k \right) = \Delta t \left[-\mathbf{C}_{u,y} \left(\bar{\rho} \tilde{Y}_k \right) + \mathbf{K}_{k,i} \left(\bar{\rho} \tilde{Y}_k \right) + \mathbf{K}_{Y_{sgs}} \left(\bar{\rho} \tilde{Y}_k \right) + \mathbf{f}_\omega \right] \quad (330)$$

$$\mathbf{M}_Y = \int_{\Omega} N_Y^T N_Y d\Omega \quad (331a)$$

$$\mathbf{C}_{u,y} = \int_{\Omega} N_Y^T \nabla \cdot \left[\left(\tilde{u}_i + \tilde{V}_i^c \right) N_Y \right] d\Omega \quad (331b)$$

$$\mathbf{K}_{k,i} = - \int_{\Omega} \bar{\rho} \bar{D}_k N_Y^T \nabla N_Y d\Omega \quad (331c)$$

$$\mathbf{K}_{Y_{sgs}} = - \int_{\Omega} \frac{\nu_t}{Sc_{kt}} N_Y^T \nabla N_Y d\Omega - \int_{\Omega} N_Y^T \sum_{k=1}^N \frac{\nu_t}{Sc_{kt}} \nabla N_Y d\Omega \quad (331d)$$

$$\begin{aligned} \mathbf{f}_\omega &= \int_{\Omega} N_Y^T \bar{\omega}_k d\Omega - \int_{\Gamma} \left\{ N_Y \left[\bar{\rho} \widetilde{V_{k,i} Y_k} + Y_{k,i}^{sgs} \right] - \right. \\ &\left. - \frac{\Delta t}{2} (N_Y u_j) \left[\frac{\partial}{\partial x_i} \left[\bar{\rho} \left(\tilde{u}_i + \tilde{V}_i^c \right) \tilde{Y}_k + \bar{\rho} \widetilde{V_{k,i} Y_k} + Y_{k,i}^{sgs} \right] \right] \right\} n_j d\Gamma \end{aligned} \quad (331e)$$

G – THERMODYNAMIC STATE EQUATIONS

State equation models are employed for the prediction of the thermodynamic properties of pure fluids and their mixtures MICHELSEN and MOLLERUP, 2007.

Perfect Gas Model

The behavior of the perfect (or ideal) gases is described by Clapeyron's Law, Equation 332. These types of gases are characterized by the low interaction between the particles, due to the size of the particles becomes less significant compared to the empty space between them.

$$p\bar{V} = mR_{\text{gas}}T \quad \text{or} \quad Pv = R_{\text{gas}}T \quad (332a)$$

where R_{gas} is the specific constant of each gas. In the molar form the expression remains.

$$p\bar{V} = n\bar{R}T \quad \text{or} \quad P\bar{v} = \bar{R}T \quad (332b)$$

where \bar{R} is the universal gas constant, its value being $8.31451 \text{ kJ/kmol K}$ in SI units.

Van der Waals model

The simplest state cubic equation is van der Waals (Equation 333), which, although it does not faithfully represent the behavior of real gases, is based on solid theories, reproduces qualitative physical behaviors and is the point of the other cubic equations.

$$p = \frac{R_{\text{gas}}T}{\bar{v} - b} - \frac{a}{\bar{v}^2} \quad \text{or} \quad \left(p + \frac{a}{\bar{v}^2}\right)(\bar{v} - b) = R_{\text{gas}}T \quad (333)$$

Taking into account that the isotherm passing at the critical point has an inflection at that point:

$$\left(\frac{\partial p}{\partial \bar{v}}\right)_T = 0 \quad \text{and} \quad \left(\frac{\partial^2 p}{\partial \bar{v}^2}\right)_T = 0 \quad (334)$$

from which the critical constants a and b of Equation 333 are obtained:

$$a = \frac{3p^c}{(\bar{v}^c)^2} = \frac{27(R_{\text{gas}}T^c)^2}{64p^c} \quad \text{e} \quad b = \frac{\bar{v}^c}{3} = \frac{R_{\text{gas}}T^c}{8p^c} \quad (335)$$

Rewriting the van der Waals equation for the reduced properties one has

$$p_r = \frac{8T_r}{(3v_r - 1)} - \frac{3}{v_r} \quad (336)$$

where v_r is the reduced volume obtained by the relation $v_r = \frac{v}{v_c}$, at reduced pressure (p_r) given by $p_r = \frac{p}{p_c}$ and T_r is the reduced temperature where $T_r = \frac{T}{T_c}$.

In terms of the compressibility factor (z), Equation 333 becomes

$$z = \frac{\bar{v}}{\bar{v} - b} - \frac{a}{R_{\text{gas}}T\bar{v}} \quad (337)$$

Generalized Cubic State Equations

Other van der Waals-based state equations have been developed, including Redlich-Kwong (RK), Redlich-Kwong-Soave (RKS) and Peng-Robinson (PR). In order to improve the numerical accuracy of the results obtained for the state of the real gases, PR. These are very important tools in engineering modeling as they have been developed to deal particularly with the chemical equilibrium of phases of complex multicomponent mixtures ASSAEL, TRUSLER, and TSOLAKIS, 1998.

In Table 9 it is shown four models of cubic equations.

Table 9 – Cubic equations of state.

van der Waals (vdW), 1873	$p = \frac{R_{\text{gas}}T}{\bar{v} - b} - \frac{a}{\bar{v}^2}$
Redlich-Kwong (RK), 1949	$p = \frac{R_{\text{gas}}T}{\bar{v} - b} - \frac{a}{\bar{v}(\bar{v} + b)\sqrt{T}}$
Soave-Redlich-Kwong (RKS), 1972	$p = \frac{R_{\text{gas}}T}{\bar{v} - b} - \frac{a\alpha(T)}{\bar{v}(\bar{v} + b)}$
Peng-Robinson (PR), 1976	$p = \frac{R_{\text{gas}}T}{\bar{v} - b} - \frac{a\alpha(T)}{\bar{v}(\bar{v} + b) + b(\bar{v} - b)}$

Source – ASSAEL, TRUSLER, and TSOLAKIS ASSAEL, TRUSLER, and TSOLAKIS, 1998.

Redlich-Kwong equation for mixing

The Redlich-Kwong (RK) state equation in addition to the form presented in the Table 9 for a single pure substance, can also, as well as van der Waals, be applied to blends, expressed then in its complete form by the equations 338 and 339 ASSAEL, TRUSLER, and TSOLAKIS, 1998.

$$p = \frac{RT}{\bar{v} - b} - \frac{a}{\bar{v}(\bar{v} + b)\sqrt{T}} \quad (338)$$

or

$$z^3 - z^2 + (A - B^2 - B)z - AB = 0 \quad (339a)$$

where

$$A = \sum_{i=1}^n \sum_{j=1}^n x_i x_j (1 - \delta_{ij}) \sqrt{A_i A_j} \quad (339b)$$

$$B = \sum_{i=1}^n x_i B_i \quad (339c)$$

$$a = \sum_{i=1}^n \sum_{j=1}^n x_i x_j (1 - \delta_{ij}) \sqrt{a_i a_j} \quad (339d)$$

$$b = \sum_{i=1}^n x_i b_i \quad (339e)$$

and

$$\begin{aligned} A_i &= 0.42748 \frac{p_{r_i}}{T_{r_i}^{2.5}} & B_i &= 0.08664 \frac{p_{r_i}}{T_{r_i}} \\ a_i &= 0.42748 \frac{R_{\text{gas}}^2 (T_i^c)^{2.5}}{p_i^c} & b_i &= 0.08664 \frac{R_{\text{gas}} T_i^c}{p_i^c} \end{aligned}$$

Redlich-Kwong-Soave State Equation

The Redlich-Kwong-Soave (*RKS*) state equation, also known as Soave, is a modification of the RK equation, with the introduction of a temperature dependent function, $a\alpha(T)$.

Along with the Peng-Robinson equation, both are the most widely used equations in the world. Due to pressure adjustments and the introduction of the Pitzer $\check{\omega}$ acentric factor, these equations can be employed in the analysis of light hydrocarbons and non-polar molecules. In contrast, they should not be applied in systems with hydrogen bonds or other forms of molecular association. In general with the complete Lee-Kesler model we obtain better results than with the *RKS* and *PR* equations, but these require only a tenth of the processing time and this is important for high complexity ASSAEL, TRUSLER, and TSOLAKIS, 1998.

The acentric factor for a pure substance i was defined by Pitzer in 1955 as

$$\check{\omega}_i = -1 - \log_{10}(p_{r_i}^{\text{sat}}(T_{r_i} = 0, 7)) \quad (340)$$

The equations 341 and 342 represent the two forms of the Soave equation MICHELSEN and MOLLERUP, 2007.

$$p = \frac{R_{\text{gas}} T}{\bar{v} - b} - \frac{a\alpha(T)}{\bar{v}(\bar{v} + b)} \quad (341)$$

or

$$z^3 - (1 - B)z^2 + (A - B^2 - B)z - AB = 0 \quad (342a)$$

where

$$A = \sum_{i=1}^n \sum_{j=1}^n x_i x_j (1 - \delta_{ij}) \sqrt{A_i A_j} \quad (342b)$$

$$B = \sum_{i=1}^n x_i B_i \quad (342c)$$

$$a\alpha = \sum_{i=1}^n \sum_{j=1}^n x_i x_j (1 - \delta_{ij}) \sqrt{(a_i \alpha_i)(a_j \alpha_j)} \quad (342d)$$

$$b = \sum_{i=1}^n x_i b_i \quad (342e)$$

and

$$A_i = 0.42747 \alpha_i \frac{p_{r_i}}{T_{r_i}^{2.5}} \quad B_i = 0.08664 \frac{p_{r_i}}{T_{r_i}}$$

$$a_i = 0.42747 \frac{R_{\text{gas}}^2 (T_i^c)^2}{p_i^c} \quad b_i = 0.08664 \frac{R_{\text{gas}} T_i^c}{p_i^c}$$

$$\alpha_i = \left[1 + n_i \left(1 - \sqrt{T_{r_i}} \right) \right]^2 \quad n_i = 0.48508 + 1.55171 \check{\omega}_i - 0.15613 \check{\omega}_i^2$$

Peng-Robinson Equation of State

The Peng-Robinson state equation (*PR*) is structurally similar to *RKS*, as this requires only the critical constants and the acentric factors for its application to mixtures. The equations 343 and 344 present the two forms of the PR equation.

$$p = \frac{R_{\text{gas}} T}{\bar{v} - b} - \frac{a\alpha(T)}{\bar{v}(\bar{v} + b) + b(\bar{v} - b)} \quad (343)$$

or

$$z^3 - (1 - B)z^2 + (A - 3B^2 - 2B)z - (AB - B^2 - B^3) = 0 \quad (344a)$$

where

$$A = \sum_{i=1}^n \sum_{j=1}^n x_i x_j (1 - \delta_{ij}) \sqrt{A_i A_j} \quad (344b)$$

$$B = \sum_{i=1}^n x_i B_i \quad (344c)$$

$$a\alpha = \sum_{i=1}^n \sum_{j=1}^n x_i x_j (1 - \delta_{ij}) \sqrt{(a_i \alpha_i)(a_j) \alpha_j} \quad (344d)$$

$$b = \sum_{i=1}^n x_i b_i \quad (344e)$$

and

$$A_i = 0.45724 \alpha_i \frac{p_{r,i}}{T_{r,i}^{2.5}} \quad B_i = 0.07780 \frac{p_{r,i}}{T_{r,i}}$$

$$a_i = 0.45724 \frac{R_{\text{gas}}^2 (T_i^c)^2}{p_i^c} \quad b_i = 0.07780 \frac{R_{\text{gas}} T_i^c}{p_i^c}$$

$$\alpha_i = \left[1 + n_i \left(1 - \sqrt{T_{r,i}} \right) \right]^2 \quad n_i = 0.37464 + 1.54226 \check{\omega}_i - 0.26992 \check{\omega}_i^2$$

Lee-Kesler's Equation of State

In terms of the semiempirical non-cubic equations, there are the Benedict-Web-Rubin (*BWR*) and the derivated model, Lee-Kesler (*LK*), for which details will be discussed. With twelve empirical constants (Table 10), the LK model is associated to the principle of the corresponding states in the linear form in $\check{\omega}$:

$$z = z^{(0)}(T_r, p_r) + \check{\omega} z^{(1)}(T_r, p_r) \quad (345)$$

where $z^{(0)}(T_r, p_r)$ is the compressibility factor for the pure substances in which $\check{\omega} = 0$, the simple substances, whereas $z^{(1)}$ is the correction, which depends only on T_r, p_r , to obtain the compressibility factor z for a pure substance whose acentric factor is $\check{\omega}$.

By knowing experimentally $z_{ref}(T_r, p_r)$ for the chosen reference substance and $z^{(0)}(T_r, p_r)$ for the simple substances, the constants of Table 10 are determined. Then, $z(T_r, p_r)$ can be obtained as follows:

$$z = z_{ref} + \left(\frac{\check{\omega}}{\check{\omega}_{ref}} - 1 \right) (z_{ref} - z^{(0)}) \quad (346)$$

In any case, be $z^{(0)}$ or z_{ref} , the compressibility factor, according to LK, will be given by:

$$z = \left(\frac{p_r v_r'}{T_r} \right) = 1 + \frac{B}{v_r'} + \frac{C}{v_r'^2} + \frac{D}{v_r'^5} + \frac{c_4}{T_r^3 v_r'^2} \left(\beta + \frac{\gamma}{v_r'^2} \right) \exp \left(-\frac{\gamma}{v_r'^2} \right) \quad (347)$$

where

$$v'_r = \frac{zT_r}{p_r}$$

$$B = b_1 - \frac{b_2}{T_r} - \frac{b_3}{T_r^2} - \frac{b_4}{T_r^3}$$

$$C = c_1 - \frac{c_2}{T_r} + \frac{c_3}{T_r^3}$$

$$D = d_1 + \frac{d_2}{T_r}$$

Table 10 – Constants of the Lee-Kesler model.

Constants	Simple Substance
b_1	0.118193
b_2	0.265728
b_3	0.154790
b_4	0.030323
c_1	0.0236744
c_2	0.0186984
c_3	0.0
c_4	0.042724
$d_1 \times 10^4$	0.155488
$d_2 \times 10^4$	0.623689
β	0.65392
γ	0.060167

Source – ASSAEL, TRUSLER, and TSOLAKIS ASSAEL, TRUSLER, and TSOLAKIS, 1998.

For the mixtures, according to the model *LK*:

$$\bar{v}_c = \sum_j \sum_k x_j x_k \bar{v}_{cjk} \quad (348)$$

$$(\bar{v}_c T_c) = \sum_j \sum_k x_j x_k \bar{v}_{cjk} T_{cjk} \quad (349)$$

$$\bar{v}_{cjk} = \frac{1}{8} (\bar{v}_{cj}^{-1/3} + \bar{v}_{ck}^{-1/3})^3 \quad T_{cjk} = (T_{cj} T_{ck})^{1/2} \quad (350)$$

$$\check{\omega} = \sum_j x_j \check{\omega}_j \quad (351)$$

$$z_c = 0.2905 - 0.085\check{\omega} \quad (352)$$

$$p_c = z_c \bar{R} \frac{T_c}{v_c} \quad (353)$$